Touch Lab Report 3

Determination of Mechanical Properties of the Human Fingerpad In Vivo Using a Tactile Stimulator

Rogeve J. Gulati and Mandayam A. Srinivasan

RLE Technical Report No. 605

January 1997

The Research Laboratory of Electronics
MASSACHUSETTS INSTITUTE OF TECHNOLOGY
CAMBRIDGE, MASSACHUSETTS 02139-4307

Report Documentation Page		

1. REPORT DATE **JAN 1997**	2. REPORT TYPE	3. DATES COVERED **00-01-1997 to 00-01-1997**

4. TITLE AND SUBTITLE **Determination of Mechanical Properties of the Human Fingerpad In Vivo Using a Tactile Stimulator**	5a. CONTRACT NUMBER
	5b. GRANT NUMBER
	5c. PROGRAM ELEMENT NUMBER
6. AUTHOR(S)	5d. PROJECT NUMBER
	5e. TASK NUMBER
	5f. WORK UNIT NUMBER

7. PERFORMING ORGANIZATION NAME(S) AND ADDRESS(ES) **Massachusetts Institute of Technology,The Research Laboratory of Electronics,77 Massachusetts Avenue,Cambridge,MA,02139-4307**	8. PERFORMING ORGANIZATION REPORT NUMBER

9. SPONSORING/MONITORING AGENCY NAME(S) AND ADDRESS(ES)	10. SPONSOR/MONITOR'S ACRONYM(S)
	11. SPONSOR/MONITOR'S REPORT NUMBER(S)

12. DISTRIBUTION/AVAILABILITY STATEMENT **Approved for public release; distribution unlimited**

13. SUPPLEMENTARY NOTES

14. ABSTRACT

15. SUBJECT TERMS

16. SECURITY CLASSIFICATION OF:			17. LIMITATION OF ABSTRACT	18. NUMBER OF PAGES **270**	19a. NAME OF RESPONSIBLE PERSON
a. REPORT **unclassified**	b. ABSTRACT **unclassified**	c. THIS PAGE **unclassified**			

Determination of Mechanical Properties of the Human Fingerpad, *In Vivo*, Using a Tactile Stimulator

Rogeve J. Gulati

Mandayam A. Srinivasan | Principal Research Scientist
Department of Mechanical Engineering
Research Laboratory of Electronics
Massachusetts Institute of Technology

H. Steve Colburn | Professor of Biomedical Engineering
Boston University

Abstract

A desire to better understand the mechanics of the human fingerpad, *in vivo*, as related to haptic performance and tactual perception prompted an investigation of the fingerpad's characteristic force response to indentation. A computer-controlled, high-precision tactile stimulator was constructed to deliver a combination of uniaxial static, ramp and sinusoidal indentations normal a specific region of the stationary and passive fingerpads of five different subjects. Both input indentation depth and fingerpad force response were recorded as a function of time to capture transients and steady state features. Three aluminum indentors, a point, a 6.35 mm diameter circular probe and a flat plate, were used for indentation to represent three general classes of loading profiles encountered in manual exploration and manipulation. With each shape, repeatability of the response was tested and the effects of varying amplitude, velocity and frequency of indentation were investigated.

The experiments revealed that the force response of the fingerpad is both nonlinear and viscoelastic with respect to indentation depth and velocity. A clear variation was present in the force response among the five subjects tested and across the three different indentors. This variation was minimized partly by determining a subject specific parameter with which to normalize the force response data. A nonlinear Kelvin model was then proposed to mathematically represent this characteristic force response of the fingerpad to indentation as a function of indentor and subject. However, in implementation, the nonlinear model was approximated by a lumped parameter model composed of a piecewise linear set of springs in parallel with series spring-dashpots. Parameters were estimated for the model for each subject and indentor given the experimental input and normalized output data. These "individual" models were able to predict data for that particular subject and indentor very well ($R^2 > 0.96$) but not as well for others. The means of the parameters across subjects were further utilized to construct more general, indentor specific versions of the model, which were only slightly worse at predicting force response to some given indentation.

Table of Contents

Chapter 1

Introduction

1.1 The Mechanics of Touch

The mechanical behavior of the fingerpad tissues plays an important role in the perception of physical properties (e.g. shape and texture) and in control of contact conditions during tactual exploration or object manipulation. Mechanical behavior refers simply to the force response characteristics of the fingerpad as a material to deformation. And "fingerpad" refers to a specific region of complex, nonhomogeneous, anisotropic soft tissue on the palmar side of the distal phalanx, its surface distinguished by concentric ridges that form unique fingerprint patterns. Distributed within the distinct layers of hairless, palmar skin and underlying subcutaneous tissues are the sensory nerve endings called mechanoreceptors that respond to the spatial and temporal properties of loading on the fingerpad. Each type of receptor is sensitive to particular features of the contact conditions (e.g. vibration, fluttery motions) and transmits information to regions of the brain such as the sensorimotor cortex where a "tactile image" can be formed. In the absence of auditory and visual sensory cues or inputs, many object properties can be determined based on the tactile sense alone. This thesis focuses on the simplest, one-

dimensional case of relating loads on the fingerpad at the contact interface to the associated fingertip deformation.

Modeling the mechanical behavior of the fingerpad has impact in both understanding all of the physical mechanisms involved in human tactile sensing as well as the improvement of contact interactions with haptic tools and devices. Because the basic, characteristic response of fingerpad affects first the stress/strain distribution in the skin and subcutaneous layers and subsequently the intensity of tactile receptor response, simple mechanical models lay foundations for more advanced research of touch biomechanics and neurophysiology. During manual interactions with devices (e.g. robots, virtual environment haptic interfaces, prosthetics and tactile aids for the blind), the mechanical behavior of the fingerpad also influences the perception and control of parameters such as slip, compliance, grip force and viscosity at the contact interface.

Whenever we touch an object, the source of all tactile information is the spatio-temporal distribution of mechanical loads on the fingertip skin at the contact interface. (Srinivasan, 1992). The loads or pressure distributions along the palmar surface of "fingerprint" skin create time varying stress and strain densities within the skin and subcutaneous layers. Rapidly adapting and slowly adapting receptors, well-placed and oriented within the fingerpads, relay this stress/strain information to the brain, where a tactile image is formed that describes shape, texture, temperature, etc. of the object or material being explored. At the neurophysiological level, studies are being conducted on the afferent neural response to static and dynamic loadings (e.g. Johnson and Hsaio, 1992; Srinivasan and LaMotte, 1987). *Direct* measurement of stress/strain rates and densities at receptor sites, though, is not presently possible (Srinivasan, 1992). This information can be provided instead by three-dimensional computer based finite element models (FEM) of the fingertip which match its material and mechanical behavior. In practice, an FEM of a fingerpad indentation response can be verified against real *in vivo*

biomechanical data. This effort requires extensive investigation of the characteristic mechanical response of the fingertip and the acquisition of real-time data on subjects who vary in size, shape, stiffness, etc.

Modeling the fingertip's mechanical behavior is also a strong asset to better understanding haptic control and improving the design and development of haptic interfaces. Contact conditions during manual manipulation and exploration are inherently affected by the mechanical properties of both the object(s) in contact and the soft tissues of the fingerpads. Perception of slip and control of grip force are two examples where the mechanics of the fingerpad plays a direct physical role in haptic performance. By modeling the force response under deformation, we begin to better comprehend the mechanisms involved in controlling and perceiving those contact conditions.

In summary, it can be said that a thesis of this kind will provide a valuable and necessary building block for the understanding of the human sense of touch. It will perhaps see direct application in the design of simple haptic interfaces that simulate mechanical behavior of objects (e.g. various types of switches and buttons). The next few chapters present some anatomical and physiological background and the development of an experimental device, "tactile stimulator." Its implementation in recording the *in vivo* force response of the human fingerpad to precise deformations under three different indentor shapes is discussed next. Based on this data for several subjects, a sequence of linear and nonlinear models that fit the characteristic response with increasing precision are proposed, discussed, and refined to produce the most generalized model that appears reasonably valid for all the subjects tested.

1.2 Previous Research

The mechanics of the human fingerpad and the properties of skin and soft tissues, *in vitro*, have been topics of investigation for many years, but it is apparent that only in the last few decades have major steps been taken to focus the study *in vivo*. An extensive search of literature established the dominance of *in vitro* research on tissue mechanics. This is likely due to the greater ease of material tests, *in vitro*, on an isolated and separated skin or tissue sample. Interest in the sense of touch, though, requires understanding of the bulk material properties of the fingerpad as a whole. *In vivo* study of any anatomical and physiological properties of the body certainly provide much greater challenges. The noninvasive data that is available on skin in combination with its attached underlying tissues has been focused more on sections of the body such as the thigh and forearm, as opposed to the fingerpad "pulp." These experiments are often limited to high frequency response and skin impedance. Consequently, the lack of *in vivo* data on the mechanical properties of the passive human fingerpad prompted study of its characteristic force response to deformation.

Several papers represent the pool of *in vivo* studies performed. Finlay (1970) "glued" probes to skin at several locations on the body and imposed rotational vibrations at 1 Hz in an effort to characterize impedance of the skin. However, in his experiments, sinusoidal stimuli were given to hairy (dorsal) regions of skin not inclusive of the fingerpad, and he was concerned with the response to skin "stretch" as opposed to indentation. The results demonstrated a nonlinear response to dynamic, torsional skin stretch in the human forearm and thigh. But, Finlay himself makes the important observation relevant to this study that "if...a surgeon wishes to have information on the mechanical properties of skin in a given area, then he must conduct specific tests in that

area." Lanir (1990) performed indentation experiments on human forehead skin to show the effects of aging. Indenting from 0.2 to 1 mm with a circular Teflon probe of 0.2 cm^2, he discovered that indentation increases exponentially with loading pressure from 0 to 5 kPa. Though the forehead tissues are structurally distinct from the fingerpad, the findings were indicative of a nonlinear indentation response in the skin and its underlying tissues. Other papers explore mechanical impedance (Franke, 1950; Von Gierke *et al.*, 1951), shear wave propagation (Pereira *et al.*, 1989; 1991) and dynamic *in vitro* testing of skin (Veronda and Westmann, 1968; Pereira *et al.*, 1990). *In vitro* and *in vivo* tests for compressibility have implied that human skin is incompressible (e.g. North and Gibson, 1978), however, the MIT Touch Laboratory's *in vivo* tests for compressibility on the human fingerpad have yielded results that imply the fingertip is compressible to some degree (Srinivasan *et al.*, 1992). Petit and Galifret explored force versus indentation in the rat and man, including the human fingerpad in their investigation (Petit and Galifret, 1978). For indentations up to 1 mm, they presented an exponential relationship between deformation and loads (up to 0.04 N). Also noted were (1) periodic "tremors" in the skin due to respiration and proximity to blood vessels and (2) a relaxed rate of reformation to the original shape after indentor removal (viscoelasticity). The investigation was limited in scope with respect to specific fingerpad mechanics and did not provide enough data for the modeling proposed in this paper. Moore and Mundie (1972) performed another study on the static force of the skin-tissue system relating to the tactile regime, but the data is also of limited extent and makes few specific claims about the characteristic mechanical response of the fingerpad. Reactance as a function of probe area and static pressure is discussed and analyzed over a range of frequencies from 10-750 Hz, but the little data shown does not appear to be leading toward mechanistic models. In fact, it can be confidently stated that all of these studies and others like them are concerned with areas of the primate or animal body other than the fingertip, are far from conclusive about

characterizing force as a function of loading or are *in vitro*, which, at best, serve only as a foundation for additional research.

Reliable, repeatable data on the force response of the human fingerpad to various types of static and dynamic stimuli is not yet available *en masse* to provide for viscoelastic linear or nonlinear modeling of the fingertip. The next chapter offers a short description of the fingerpad, leading into a discussion of the "tactile stimulator," experiments performed and a presentation and analysis of data, as well as models of the force response to indentation with three separate probes.

Chapter 2

Structure of the Fingertip

2.1 The Fingertip

The hand is one of the most complex structures of the human body in terms of both sensory acquisition and motor control. Close to a quarter of the sensorimotor cortex is dedicated to its control and to tactile processing (McMahon, 1984). And the fingertips, the primary source of tactile information, contain the mechanoreceptors that facilitate touch. A finger is represented in Figure 2-1, showing its macroscopic features--the outline of the skin, bone and nail.
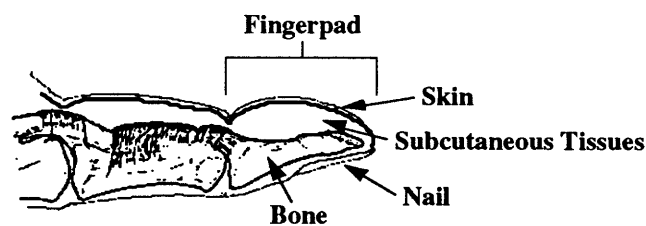
Figure 2-1: Cross-section of the human finger.

The bone and nail can be assumed to be completely rigid, relative to the softness of the bulbous fingerpad and the magnitude of forces involved in typical manual interactions .

Thus, this study focuses only on the skin and subcutaneous tissues that comprise the "pulp" (Thomine, 1981). In general, skin is a complex, multilayered organ composed of the epidermis and dermis (Lanir, 1989). The skin of the fingertip is thick, the epidermis being close to 1.0 mm (Quilliam, 1978). The dermis is rich in nerve endings and uniquely organized with features such as the dermal papillae, tendrils of tissue that push up into pockets of the epidermis (Quilliam, 1978). A schematic of skin is shown in Figure 2-2.
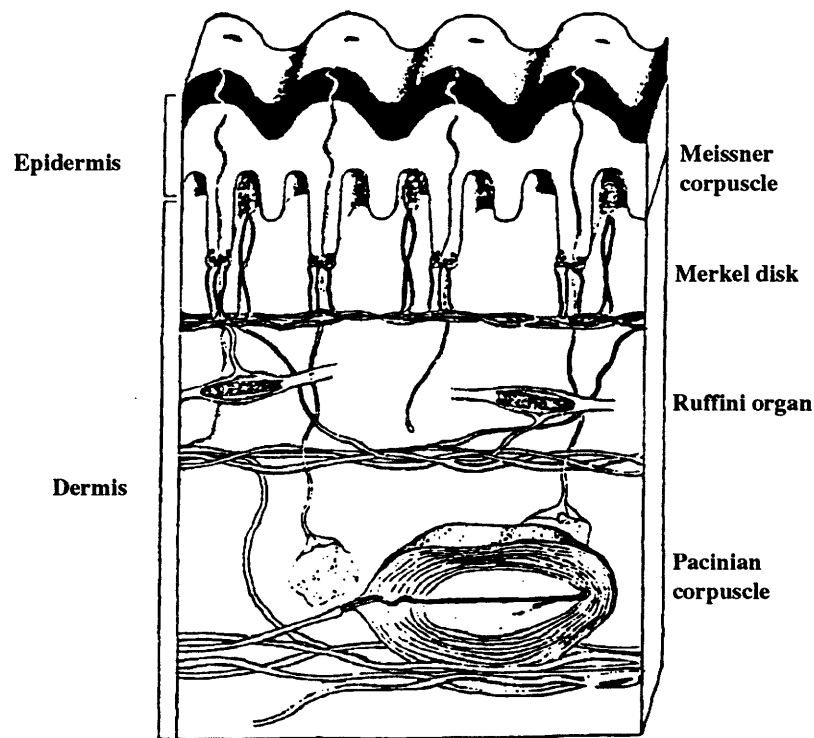
Figure 2-2: Cross-sectional view of fingertip skin, showing papillary ridges and the embedded receptors (Darian-Smith, 1984).

The underlying subcutaneous tissue is composed primarily of fat cells that are enmeshed to give the finger its firm, rounded outline. They also contribute to the fingertip's elastic,

cushion like ability to adapt to the shape of an object snugly and to reform easily from such deformations (Quilliam, 1978).

2.2 The Pulp

In studying the mechanical properties of the fingertip as they relate to tactile sense, a specific focus is made on the *pulp*, the palmar region of the distal phalanx (Thomine, 1981). The pulp of the fingertip is bordered by the edges of the nail, the junction of palmar and dorsal skin and the distal interphalangeal groove. Its composition includes hairless palmar skin and underlying fatty tissue, described briefly above. Palmar skin is distinctly characterized from the more prevalent dorsal skin by a thick epidermal layer and the dermal papillae, as shown below in Figure 2-3.
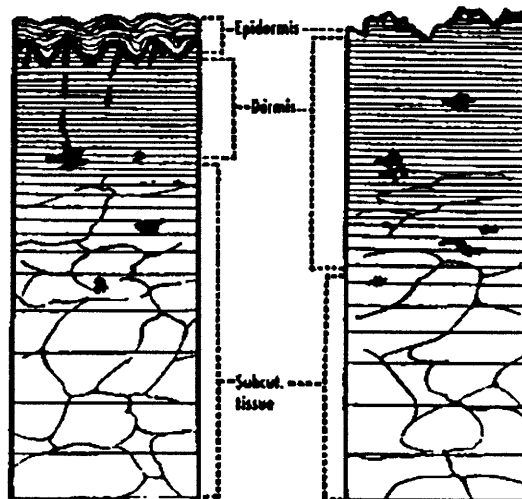
Figure 2-3: A comparison of palmar (left) and dorsal skin (Quillam, 1978).

The epidermis of the palmar, fingertip skin is notably thick. It is composed of four distinct layers. Deepest is the basal layer, formed of basal cells, melanocytes and

9

collagen or reticular fibrils, which fasten the epidermis to the dermal layer below. Next is the malphigian, a thick multicellular layer responsible for skin regeneration and cellular multiplication. Above that is the granular layer, which is only 2-3 cells thick and is enhanced by active keratinization, or the buildup of keratin within the cell walls as cell death occurs. The horny layer is the most superficial, composed of highly compressed, flattened cells. Also present in the palmar epidermis is the stratum lucidum, a thin oil-rich layer between the granular and horny layers. Skin regeneration occurs continuously, as cells migrate from deeper layers to the most superficial where they eventually die and "flake off."

The dermis is made up of connective tissue with intertwining collagen, elastin and reticular fibers, as well as some cells, blood vessels and nerve endings. A notable feature of the palmar dermis is the presence of papillary ridges, seen previously in Figure 2-2, which push up into and help shape the epidermal layers. In the fingerpad, the ridges formed by the epidermal and dermal layers take a concentric pattern to form the fingerprints. Within the folds of the ridges can be found the Merkel's Discs and Meissner's Corpuscles, tactile receptors that respond to light touch and fluttery motions, respectively. The subpapillary dermis contains the larger Ruffini's Corpuscles, which respond to skin stretch.

Below the dermis lies a thick, cushion-like layer of fatty tissue or subdermal adipose. The Pacinian Corpuscles, large, rapidly adapting receptors that respond to high frequency vibration (greater than 200 hz) reside here.

In summary, the pulp is multilayered and nonhomogeneous, and all aspects of its structure can play an crucial role in tactile sense. For instance, the arrangement of receptors within the papillary ridges allow finer touch discrimination when stroking an object. Similarly, the thick, cushiony subdermal adipose layer's tendency to conform to the object allows improved discrimination of shape. Each of these physical features in

turn affects the distributions of stresses and strains during loading due to a deformation. The pulp's mechanical properties are, therefore, a critical feature of the sense of touch and haptic control. For purposes of this research, the entire pulp is viewed as a nonlinear, nonhomogeneous block of material whose mechanical properties as a whole need to be identified quantitatively.

Chapter 3

Initial Design Considerations

The primary goals of this project were (1) to acquire *in vivo* data on the force response of the fingerpad to diverse displacement-controlled, static and dynamic indentation profiles and (2) to characterize this data with a model normalized to fit the mechanical response of any given finger. To realize these goals, it was important to understand both the basic features of the response of the "pulp" to indentation and aspects of the models that would be used to simulate those responses. The fingerpad, a 4-5 mm thick region of tissue, blood vessels and receptors, has been shown to be comprised of several distinct layers, each with unique properties--from the hard, flaky outer epidermal layers to the cushion-like subdermal adipose. Under *in vivo* conditions, the pulp exhibits properties during and after indentation that clearly characterize its viscoelastic nature. If indented, the fingertip responds with force that increases monotonically to indentation depth like a stiff spring element. However, when unloaded (indentor removed), the viscous nature of the fingerpad becomes obvious. The pulp relaxes to its original shape at some rate slower than the initial deformation. It was inferred from these features that models of the fingertip will include "springs" and "dashpots", elements which produce forces in response to deformations and deformation rates, respectively.

The extent of modeling performed before the construction of a tactile stimulation device to conduct experiments was limited primarily by the lack of real, *in vivo* data on the mechanics of the fingerpad. However, as noted above, it was reasonable to propose a model combining spring (elastic) and dashpot (viscous) elements. Three basic, viscoelastic spring-dashpot models that are common to the study of biological tissues are shown in Figure 3-1. These models do not attempt to account for effects of the inertia of the tissue mass. However, because the tissue mass is relatively small, there was no preliminary indications that it would play a significant role in the force response characteristics.
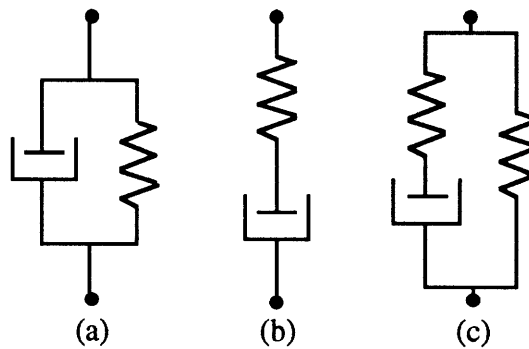
Figure 3-1: (a) Voigt model, (b) Maxwell model, (c) Kelvin model

Previous researchers of biological tissues have found that the Kelvin model is the lowest order model to match well the mechanical properties of living tissues (Fung, 1990). These issues are discussed in much greater detail after an analysis of experimental results (Chapter 7), where nonlinear elements and the contribution of mass are also investigated. It was enough at this stage to state that experimental, displacement-controlled inputs had to be varied in terms of both depth and velocity to best characterize all the features of fingerpad mechanics.

The resultant force response of the fingerpad will also be influenced by the shape and associated contact area of the probe providing indentation. To elaborate, this is treated as a basic problem in mechanics. The fingerpad, a "block" of viscoelastic material, is viewed most simply as a "bed of springs." If the total area of contact at the probe-skin interface is increased, the number of springs compressed increases as well. Similarly, if one thinks of the finger as a compressible fluid-filled membrane or balloon (Srinivasan, 1989) there is a significant difference between the profile of indentation with a point as opposed to a plane. In both situations, total resultant force of the fingerpad is dependent upon both size (contact area) and shape of the indentor. The conclusion was that indentor shapes would have to be varied sufficiently in order to completely characterize the general force response to deformation.

With some basic goals for experiments laid out, the requirements for an experimental device were determined in terms of the approximate ranges and accuracies of position and force control. It was decided that a device capable of providing displacement input and measuring force output was necessary. The range of motion was determined to be more than half a centimeter (the thickness of the pulp) with at least 50 microns of accuracy (10%, assuming increments of indentation of 0.5 mm). The velocity range was estimated to be 0-80 mm/sec, allowing inputs from slow ramps to an approximate step. And, for periodic waveform inputs, a range of 0-20 Hz was chosen for the current study. One justification for this is that during active exploration or manipulation of objects, humans can control their actions to at most 10 Hz (Brooks, 1990), which makes this a limited but practical range for investigation. In all, this covered a wide range of velocities, accelerations, and frequencies. Expected traces of indentation inputs as functions of time are shown in Figure 3-2, where ramp velocity and depth and sinusoid starting depth, frequency and amplitude could be varied sufficiently to produce enough data for modeling.
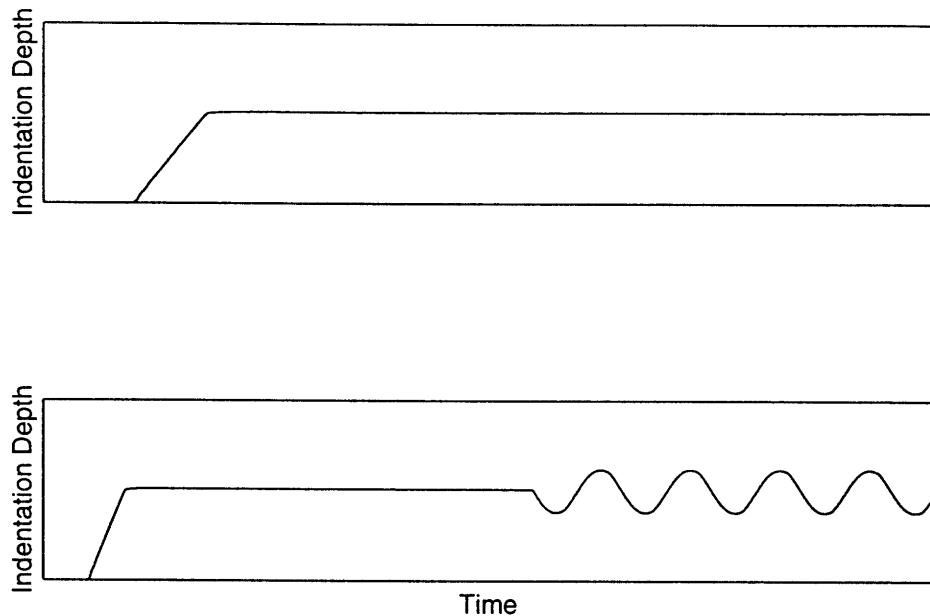
Figure 3-2: Graphical representation of typical (a) ramp/hold and (b) sinusoid displacement inputs along a single axis.

In addition to its precision and dynamic requirements, the device also needed to be capable of delivering (and measuring) adequate forces to indent the finger "smoothly" over the full span of velocities, from a slow ramp to a pseudo-step. The range of "normal" forces were quantified experimentally with a multiple axis strain gage force sensor. For indentations of 4 mm with circular probes of 6.35 mm diameter, forces up to 3 Newtons were measured at the indentor-skin interface. Similar preliminary tests at various depths indicated that a resolution on the order of 0.01 N was necessary to capture fine differences between varied loading conditions. In the following section(s), several types of motion actuators and position encoders are discussed. Following that, additional force sensor requirements are briefly described.

3.1 Linear Actuation and Position Encoders

The first choice made in selecting actuators was to use direct-current motors over alternating-current to produce precisely controlled input indentations. AC motors are more efficient in terms of power consumption and can offer higher speed characteristics. However, they are also designed for single, synchronous speed, high horsepower operations. Variable speed performance can be achieved by alternating the frequency of the power supply or varying the pole and winding architecture. Controlling frequency modulation, though, becomes significantly complicated in high speed motor applications, and there are practical limits to the number of speeds that can be obtained by modifying the ratio of poles and windings. Additionally, AC motors experience a torque ripple that is not easily accounted for by controllers. The device used for the experiments discussed in this thesis needed to be capable of easily varied speed and fast braking accelerations and decelerations. Some of this was shown in the proposed stimuli plotted in Figure 3-2. In its primary mode of indentation, high torque to inertial ratios and low torque ripple or cogging were also required to accentuate the smoothness of motion against higher resisting forces of the finger. DC actuators were the best apparent solution, and are well-accepted practice in small robotics applications such as this one. Some DC actuators are discussed in the rest of this section.

The first type of actuator considered was a DC linear lead screw stepper motor. These actuators have the advantage of higher position resolution and noncumulative error in *real* accuracy. However, stepper motors in general experience vibration and/or cogging during the actual phase of motion, especially at lower velocities. An inherent mechanical vibration can be expected with any type of lead screw mechanism, which by definition involves contact (and friction) of moving and static metal components. In

addition, their highest load performance is inversely proportional to the velocity of motion. Stepper motors are, however, efficient at accelerating a load and have high braking torques when continuously energized. Some of the basic problems can be diminished by operating with a microstepping controller, which effectively decreases step size by an order of magnitude or more. This has the effect of eliminating some degree of the vibrations during motion and greatly improving position accuracy. In addition, microsteppers improve torque vs. speed performance. The extent to which vibrations can be decreased or filtered out at low velocities, however, did not seem sufficient for performing smooth, continuous sinusoidal inputs (refer again to Figure 3-2) over the full range of frequencies and amplitudes.

Brushless linear DC motors were a more viable option for the smooth type of control desired along one axis. As stated in *Machine Design's* Annual 1991 index, these motors can be "extremely stiff, fast and efficient" with very high position accuracy that will not deteriorate over time. In fact, high-performance brushless, linear actuators are available from companies such as Anorad™ which can provide relatively smooth motion with adequate load performance at high velocities. However, these packages tend to be very expensive (over $20,000 for 2 to 3 DOF), which was not within a reasonable budget set for the first attempt at these experiments. Lower cost linear motors have cogging problems, which affects smoothness of motion in a manner similar to the vibrations that would be experienced by lead screw steppers or brushed motors. Cost, unfortunately, became the determining factor in not exploring these motors further.

What was also seen during this investigation is that there are many more rotary types of motors than linear on the market, and it became apparent that a multi-joint linkage, actuated by rotary motors could be a better solution than higher cost linear motors. This option has all of the general benefits of DC motors (e.g. variable speed, fast braking, high accelerations), and rotary type motors tend to be available in a wider variety

of torque characteristics at much lower prices. Conveniently, a device designed and built by Professor Robert Howe at Harvard University for use in teleoperation research was available for this project, saving some of the additional time required for design and development. It utilizes a linkage mechanism, operated by two brushed DC motors that allows smooth motion in two axes (Howe, 1992). Though it was obvious that some modifications would have to be made to adapt the device to the needs of these experiments, it seemed an easily realizable and inexpensive a solution to creating the experimental apparatus, since the motors were capable of reasonably high velocities and good power characteristics (torque vs. speed).

Complementary to the search for actuators, several types of the rotary position sensors were investigated as well. These included optical encoders, magnetic encoders, resolvers, potentiometers, and rotary inductosyns. While each was found to have its own advantages and disadvantages, potentiometers were already included with the Harvard device, and they seem the simplest to implement for accurate position control (in combination with an A/D board for the actual encoding). Their use in the device is discussed further in the following chapter.

3.2 Force Sensor Requirements

Despite the fact that indentations would be performed along only one axis, it was necessary to impose a two-axis constraint upon the force sensor design--the normal axis and a perpendicular shear axis. Reasoning was based, for one, upon the expectation that shear force could develop in the finger during normal loading due to any asymmetry of tissue properties and imperfections in the finger. This is demonstrated in Figure 3-3, where a cross-section of the finger is viewed in abstract form as a bed of springs and dashpots with a slightly asymmetric distribution of angular orientation.
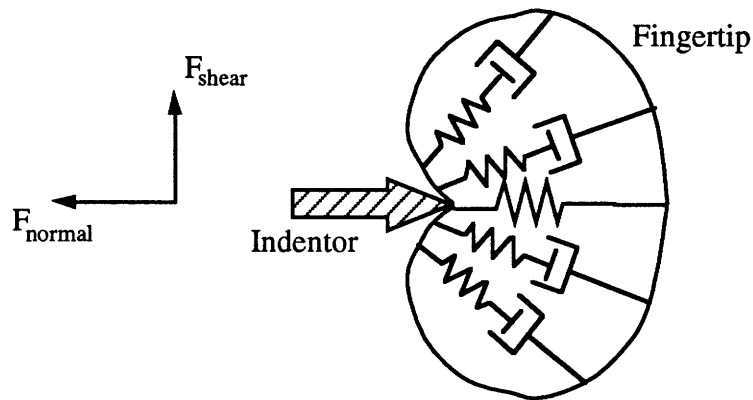
Figure 3-3: Representation of fingertip deformation.

The uppermost and lowest spring dashpots are, in this example, represented as having orientations differing by 10 degrees. Clearly, the force response of such a system to a normal indentation would include a resultant component in the shear direction (i.e. shear components of the spring force responses do not sum to zero). It is necessary to at least check the magnitude of this shear force relative to the normal force. In theory, if the finger is well oriented, the former should be very small. Measuring the second axis of force is also a verification of the quality of the indentation stimulus. If the path of indentation is indeed normal, there should only be a shear contribution due to the characteristics described by Figure 3-3. Gross changes in shear force could indicate some error in the apparatus or experimental design.

A definitive choice was made to rely upon a cantilever beam/strain gage force sensor design. The benefits of such sensors are that they are relatively easy to build, and they can be designed to the specific constraints of the experiment. In this case, the normal force requirements have already been mentioned. The shear force range and accuracy were assumed to be about an order of magnitude smaller. Further, the flexibility

provided by custom designing a sensor was a feature that could be added to allow indentors to be easily changed with minimal disturbance of the entire setup.

Chapter 4

Tactile Stimulator

After careful consideration of the experimental design constraints, the types of actuators and encoders, and a cursory cost analysis of each of those solutions, the decision was made to modify the existing features of Professor Robert Howe's Harvard manipulator to suit the needs of a "tactile stimulator." The Harvard manipulator is designed for "good control of small forces and motions," and the performance of simple manipulation tasks (Howe, 1992). However, the investigation of fingertip mechanics requires a smaller range of motion and much finer precision in control than was attainable from its original design. This chapter discusses the modifications made to the device, including the link construction, sensor design, filtering, and amplification, controller hardware and the design of proportional derivative control software.

4.1 Overview of System Components

An extensive process of design, calibration and improvement of the Harvard manipulator, produced the system shown schematically in Figure 4-1.
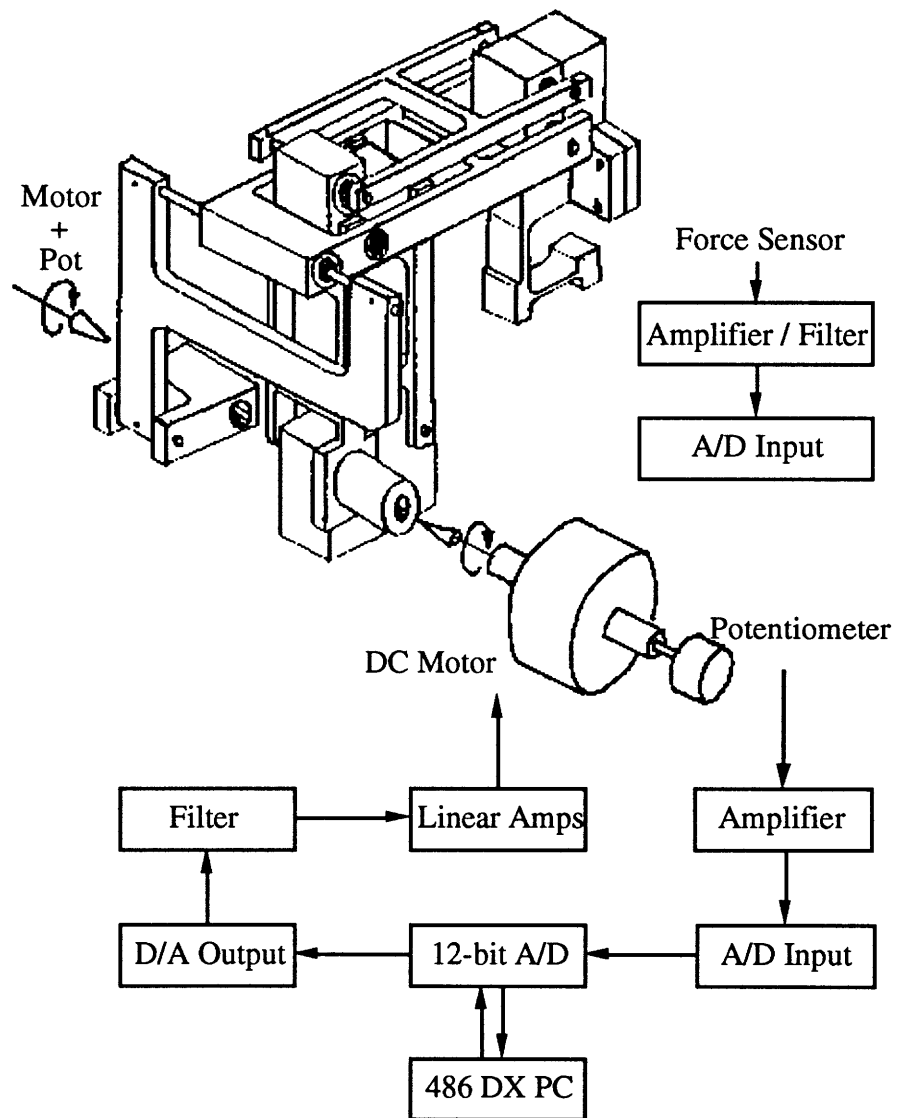
Figure 4-1: The tactile system plus sensors and controller hardware.

The tactile stimulator is a two-link, two degree of freedom robot manipulator with a planar workspace of at least 25 mm square. Brushed DC motors provide joint torque, and hence, input endpoint forces, while contactless potentiometers coupled to the motor shafts provide an encoding of joint position (when used in combination with the A/D board). The schematic also depicts a simple block diagram of the controller hardware, consisting of a 12-bit A/D board used to digitize the analog sensor outputs and a 486 DX computer to process and compute the control signals and to record data. Following is an extended outline of each of the components of the stimulator and, where appropriate, the calibration procedures used to determine sensitivity and resolutions.

4.2 Robot Manipulator Design

The tactile stimulator, as shown in Figure 4-2, is in simplest terms a two-bar linkage. Each linkage is composed of a set of parallel links in a configuration that allows end effector orientation to be preserved.

Motor B
(Upper Linkage)

Motor A
(Lower Linkage)
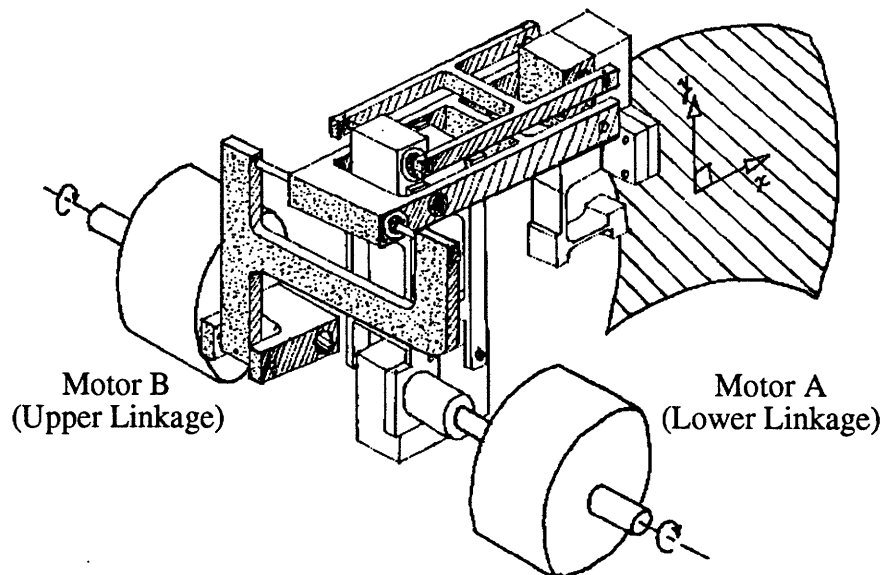
Figure 4-2: Stimulator link assembly.

In the figure, the stimulator has been subdivided into its two bar linkages. The links that compose the upper linkage have been shaded in. And the pivot points of the two linkages that define the relative degrees of freedom are indicated by arrows. Motor A directly drives the lower linkage, whose tip traverses a horizontal arc with respect to ground. Similarly, Motor B controls the vertical arc of the upper linkage, though torque must be transmitted to the pivot point via several intermediate links. With these two distinct degrees of freedom, the stimulator endpoint--where the indentor is fixed--can be moved about the workspace indicated as a hatched region, limited only by the range of the joint angles.

The Harvard manipulator was also specifically designed to preserve end effector orientation during motion in the workspace. As is evident from Figure 4-2, both the upper and lower linkages are composed of sets of parallel links. Viewed in 2-D, the links form two parallelograms, each with a pair of sides that maintain a constant orientation, horizontal and vertical, respectively. Figure 4-3 demonstrates the preserved orientation of the end effector at two stimulator positions.
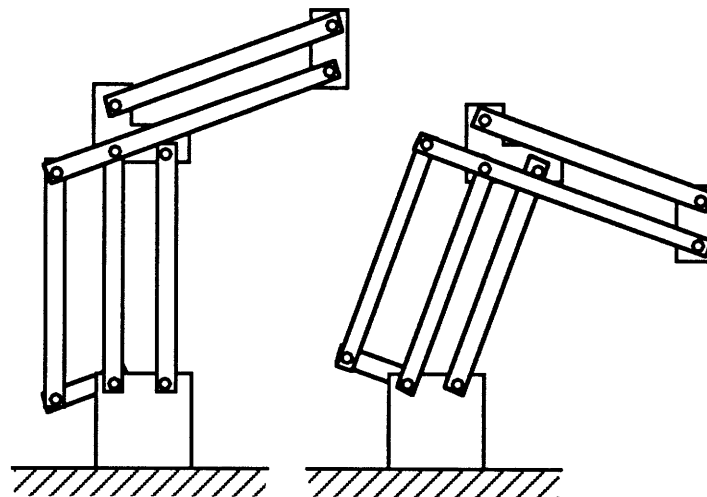
Figure 4-3: 2-D view of the stimulator in two positions.

The original upper linkage of the Harvard manipulator required significant redesign to improve the stability and stiffness of the links for high precision, dynamic control of the stimulator. However, the specifics of this design process will not be detailed in this thesis. A simple assembly drawing of the final "tactile stimulator" design is shown below in Figure 4-4. The links were machined to high tolerance from 2024 aluminum, chosen for its low density (weight) and high vibration stiffness (comparable to steel). The roller bearings shown are SFR2-5 Alpine™ bearings with L-01(5) lube. The shafts were cut from precision ground 1/8" stainless steel rod. The component coupling the links to Motor B utilizes a pair of self-lubricating brass bushings in place of the original design's roller bearings.
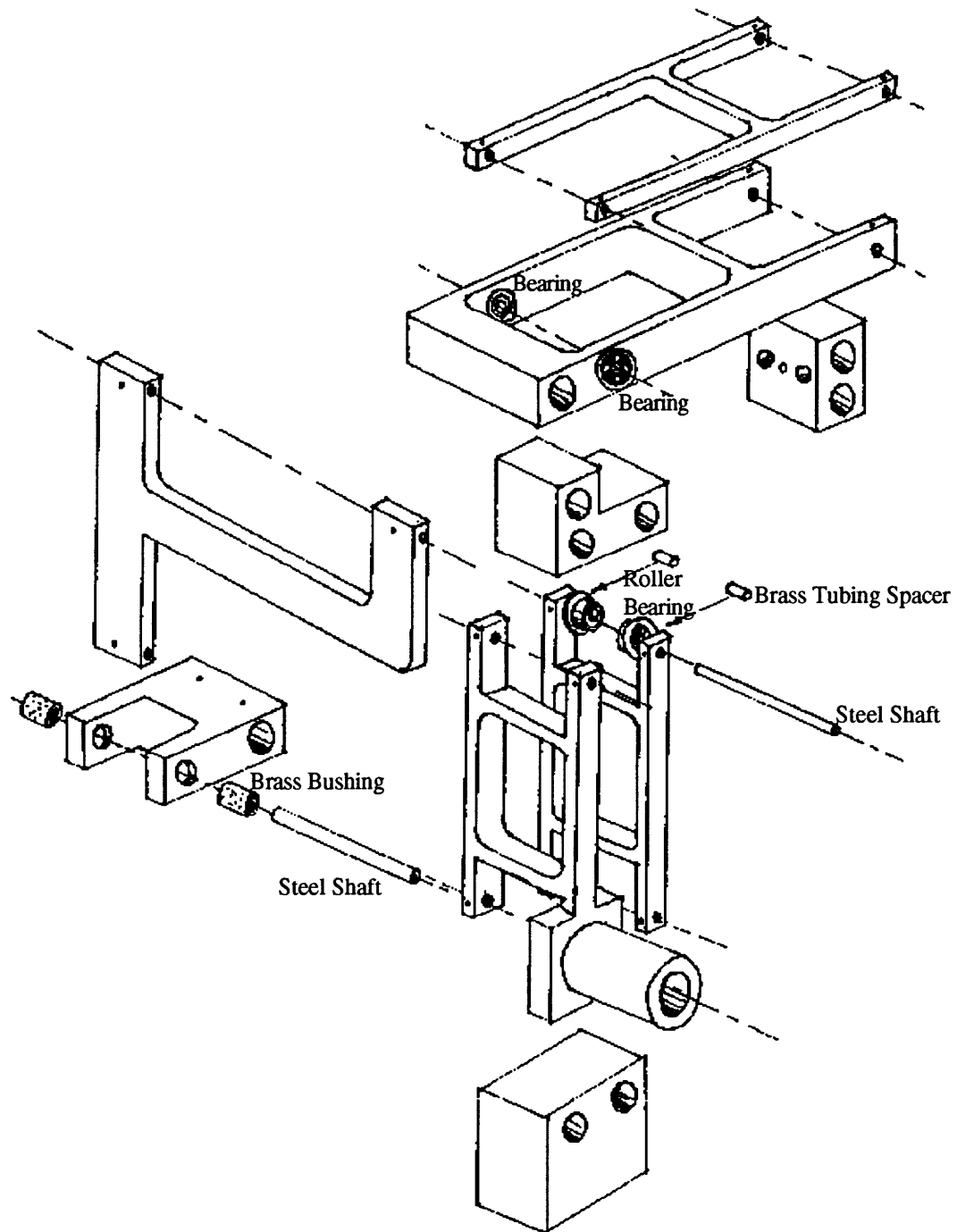
Figure 4-4: Simple assembly drawing of the tactile stimulator.

The labels in the figure read: Bearing, Bearing, Roller Bearing, Brass Tubing Spacer, Steel Shaft, Brass Bushing, Steel Shaft.

4.3 Joint Angle Position Encoders

Each motor has a double ended shaft, coupled at one end to a linkage and at the other to one of the CP-2UT Midori™ contactless, precision rotary potentiometers. The configuration of the coupling between the motor and potentiometer is depicted in Figure 4-5.
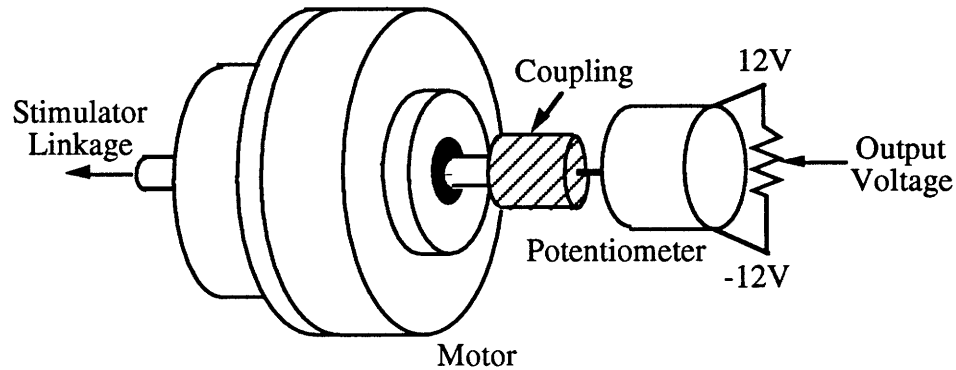
Figure 4-5: Motor shaft coupled to potentiometer.

To form a voltage divider for angle encoding, a ±12 volt supply is applied across the potentiometer, and the output is wired to a separate differential input channel on a Data Translations 2811 A/D board. These particular potentiometers provide a linear change in resistance over two 90° arcs out of the full 360° rotation. The shaft-potentiometer coupling was fixed such that the angular motion of each joint was within a linear output range of the corresponding potentiometer (according to their performance characteristics).

Without amplification of output signal, the resolution of angle encoding (over the 90° linear range) was not sufficient for high precision endpoint control. This resolution was fixed by the A/D board to 12-bits over a bipolar 10 volt range. However, the only problem lay in that the initial range of motion was much larger than was required. The Cartesian endpoint accuracy of the pots was approximated by measuring the arc length traversed at the end of each link and determining the smallest possible change that could

be registered by the A/D board. The design constraints outlined in the previous chapter called for 20-50 micron resolution in a 1 cm workspace along each axis. Improvement of the accuracy of the sensors was achieved simply by amplifying sensor output. An inverting amplifier was added to each potentiometer circuit such that the required 1 cm arc of motion corresponded to the full 10 volt input range of the A/D board. This gave full 12-bit resolution, as yet not accounting for noise, over the desired range of motion. Assuming perfect accuracy of the A/D board (one count), the accuracy of the potentiometers is under 3 microns at the effective endpoint of each link, where link lengths are as shown in Figure 4-6, representing the simplified stimulator.

Vertical Travel

76.2 mm

Horizontal Travel

76.2 mm
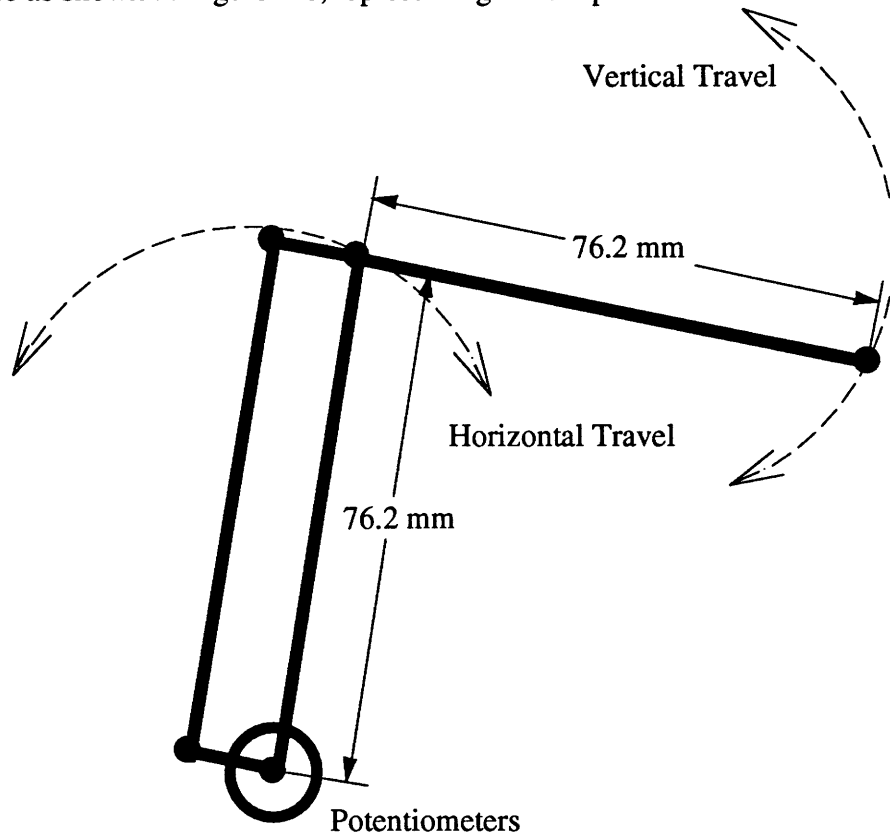
Potentiometers

Figure 4-6: Simplified stimulator and arc lengths.

The amplifier and potentiometer schematics are drawn in Figure 4-7.
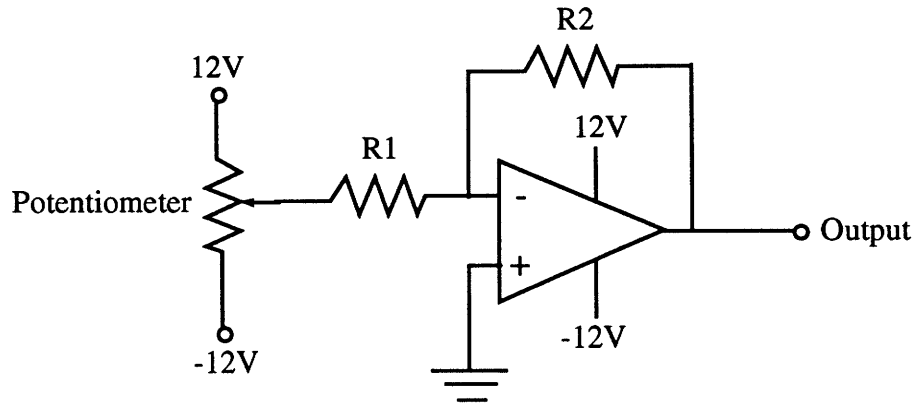
Figure 4-7: Potentiometer and amplifier circuitry.

Eventually, the potentiometers had to be calibrated in terms of volts per degree (angle) to be used for inverse kinematics calculations of endpoint position. This calibration was performed by replacing the brushed motor with a rotary stepper motor and measuring the corresponding output of the sensor at steps of 0.9 ±0.05 degrees. The calibration constants were:

Top Link: 618 counts / degree

Bottom Link: 589 counts / degree

where a "count" on the 12-bit board represents approximately 2.5 mV. The angle accuracy of the potentiometers, again assuming perfect accuracy of the A/D board is better than 0.005 degrees.

4.4 Motors, Amplifiers and DA Output

As shown in Figure 4-2, the motion of the stimulator links is produced by two brushed DC Minertia™ S02A motors, controlled by analog output from the A/D board which is converted to current by a pair of linear amplifiers. The motors have dual-ended shafts, which allowed coupling to both the potentiometers and the joints of the robot. Electro-Craft™ linear amplifiers are used to drive the motors, current-limited to produce a maximum 6 amps at 5 volts (maximum DA output of the DT2811), based on the motor specifications for continuous operation. The maximum torque produced at 6 amps input current limits endpoint force in the stimulator. In the lower linkage (horizontal motion), horizontal force can reach as high as 3 Newtons. In the upper linkage, because the weight of the links and end effector must be supported, the limit of vertical force produced falls below 1 Newton.

To minimize the effects of high frequency noise in the motor control signals, low-pass filters were added to the DA output to the amplifiers. In control of the stimulator, DA output to the motors was based upon position and velocity signals, which were in an inherently noisy environment. Over the course of assembling the hardware, a significant number of preliminary experiments were performed, using control laws and algorithms that will be described in the next few sections. In all such tests, the major frequency content of the generated DA output was measured to be within 0 to 150 Hz, while the rest of the signal was low-magnitude, high frequency white noise. A low-pass Butterworth filter was added to each DA output to cutoff these high frequency noise components. This had the desired effect of improving the stimulator's performance in terms of stability (less vibration) and accuracy. The filter design is shown below in Figure 4-8.
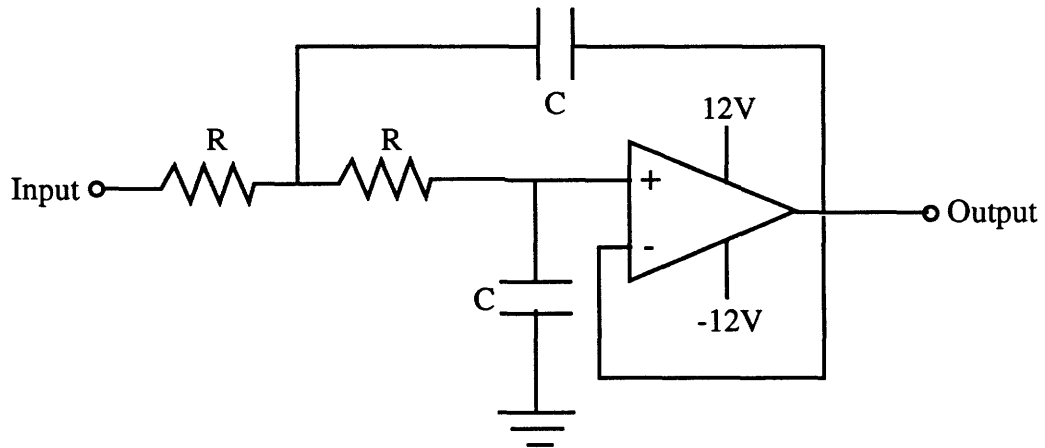
Figure 4-8: Low-pass Butterworth Filter. R = 130 kΩ; C = 8200 pf

4.5 Timer Board and Velocity Measurement

Timing control was developed for the tactile stimulator for two reasons: (1) to allow velocity to be measured discretely from the clean position signals, and (2) for implementation of control during robot position control and sampling frequencies during data acquisition. The anticipated method of dynamic stimulator control was proportional-derivative, which requires as input both velocity and position to calculate motor torque. The most efficient and reliable method chosen to measure joint velocity using the potentiometers was to take the discrete difference in position over known time intervals. A "timer" board with a 1 MHz clock was implemented in the PC to provide time sampling at easily controlled frequencies. Using the counters on the timer board as a time base, measurements of position were taken at known discrete intervals to produce an average discrete velocity profile. The time intervals over which velocity was measured were set large enough to "filter" out the effects of noise (at least 10 control frequency cycles or 10 times the control interval), but small enough to produce the most stable control observed in testing the stimulator. A flexible timing routine included with the

timer board also allows the software to run at a specified control and sampling frequency, programmable up to at least 10 kHz. In this case, control frequency (2 kHz) is the rate at which position measurements are taken and output signals to the motors are produced and sampling frequency (500 Hz) is the rate at which data is recorded (or sampled). The former allows smoother control than simply running "open loop" at an unspecified frequency with random control intervals, which was often the case during preliminary device testing. The latter, sampling frequency, determines the time interval at which data is to be recorded.

4.6 Proportional Derivative Control

As stated in previous sections, a proportional-derivative law was used to control the angular position of each of the two stimulator links. Proportional control, in this application, is characterized by a motor torque proportional to the difference between desired and actual position. As is, though, proportional control does not take into account the velocity of the link. This creates an underdamped system which produces large overshoots and growing instability in link motion. Proportional-derivative control "adds" an anticipatory term, proportional to velocity, that produces much smoother dynamic control. More accurately, velocity is used to provide negative feedback. For the stimulator links, the control law used for the stimulator can be written in equation form as:

$$V = k_p * (p_{des} - p_{actual}) - k_v * (v_{actual}) \qquad \text{(4-1a)}$$

where V is the voltage (proportional to torque) to the motors, p and v are position and velocity, and the k's are fixed gains of the system that had to be determined

32

experimentally. It was discovered later that this is not a traditional PD control law, which should be of the form:

$$V = k_p(p_{des} - p_{act}) + k_v(v_{des} - v_{act})$$ (4-1b)

The equation used (4-1a) may have had the effect of overdamping the stimulator at high prescribed velocities, but that was not readily apparent in the experimental results. Future versions of the stimulator will incorporate (4-1b). Position and velocity of each link were measured in terms of joint angles and angular velocities by the potentiometers, routed through the A/D board. Optimal gains, k_p and k_v, were found by tweaking the values with the appropriate units over a range based upon experience with the system. This was done until gains were found to produce the most stable control. Gains that were too small would not generate sufficient endpoint force, and gains that were excessively large caused the stimulator to become unstable despite the anticipatory aspect of the control. In terms of A/D board counts, the highest stable control gains were $k_p = 5$ and $k_v = 8$ for the bottom link and $k_p = 3$ and $k_v = 4$ for the top link, where position, velocity and voltage output are given in counts as well (e.g. 0 counts = -5 volts; 2048 = 0; 4096 = +5 volts).

Though the experimentally determined gains provided stable control of the stimulator links, the generated endpoint forces were not sufficient to perform all desired fingerpad indentations. It was described above that the gains could not be increased further without introducing instability, at least under "no load" conditions (i.e. no external endpoint forces). However, the gains were insufficient in magnitude to maintain within 20-50 microns a desired position against up to 3 Newtons of resistive force (requirements set forth in the preceding chapter). In short, the system behavior of the stimulator changes as forces upon the endpoint change due to increased compression of the fingerpad. Higher forces are thus required to achieve the desired position, but the

damping of the system is increased as well. To compensate, k_p could be increased in proportion to force. This was accomplished in software by first allowing PD control to achieve the desired position, a task easily performed unless endpoint forces increased. Then, until the desired position was achieved within the acceptable error of 20 microns, k_p was "slowly" increased to produce greater motor torque and consequently, greater endpoint force. The drawback to this control strategy is that it too overdamps the system. Velocity is restricted by the rate of "compensation" when the forces are high. This rate was not measured but is reflected by the choices later discussed of velocities and frequencies used in experimental design. Overall, this is basically a form of adaptive control.

Another measure made in the course of defining the gains, k_p and k_v, was of minimum control frequency. It was discovered experimentally that simultaneous control of the links (i.e. updating of motor torque in proportion to position and velocity) needed to be performed at greater than 1 kHz for stable control, with higher frequencies producing more stability and less vibration. However, the control frequency was limited by the number of operations, particularly floating-point, taking place in the software during a control interval, the speed of the A/D board, and the speed of the CPU. Taking all of these factors into account, the optimal control frequency was limited to 2 kHz, and it was at this frequency that the device was run to actually test and to verify the correct control gains mentioned above.

4.7 Inverse Kinematics

Since actual position and velocity were measured in terms of angles and the desired endpoint motions of the stimulator were Cartesian (x-axis translations), a transformation of coordinate frames was required. This was accomplished by using

inverse kinematics equations to transform coordinate frames. If the stimulator is viewed from the side, it can be represented as shown in Figure 4-9, with the two measured joint angles represented as θ and ϕ.
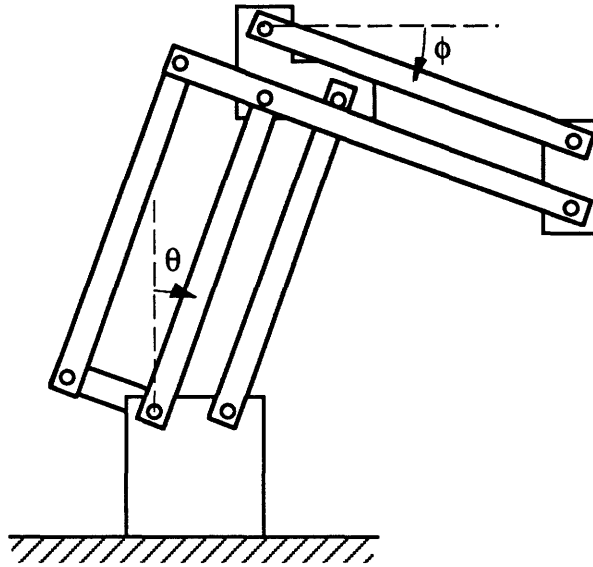
Figure 4-9: 2-D schematic of the tactile stimulator and joint angles.

If the drawing is further simplified, the stimulator can be represented by a two bar linkage with some arbitrary end effector as shown in Figure 4-10.
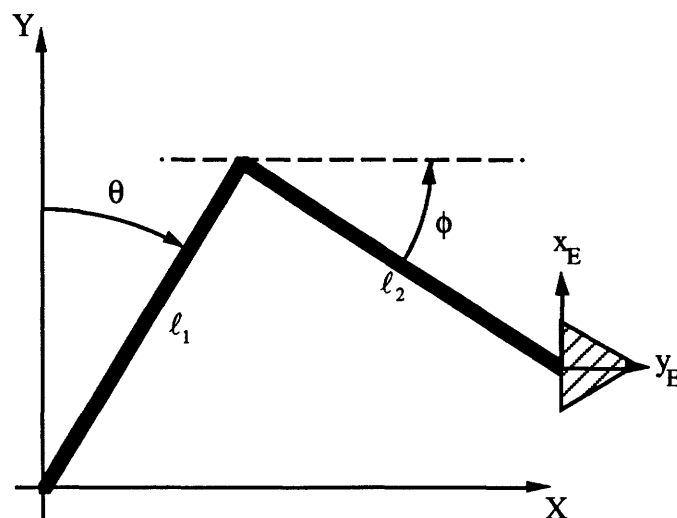
Figure 4-10: Stimulator represented as a two-bar linkage.

A Cartesian coordinate base frame is indicated in the preceding figure, as the base frame in which stimulator motions will be prescribed during experiments. To make use of inverse kinematics for the simple linkage, the following angles are defined, where counterclockwise rotation is positive (refer to Figure 4-11):

$$\theta_1 = 90° + \theta \qquad (4\text{-}2)$$

$$\theta_2 = \phi - \theta_1 \qquad (4\text{-}3)$$

Note again that the signs in (4-2) and (4-3) are based upon the way the angles are defined in Figure 4-10 (i.e. θ is negative; ϕ is positive). Applying these new angles to the simplified, two-link diagram produce the schematic shown in Figure 4-11. Because the stimulator is designed to preserve end effector orientation at all link positions, the end effector coordinates (x_E, y_E) remain fixed.
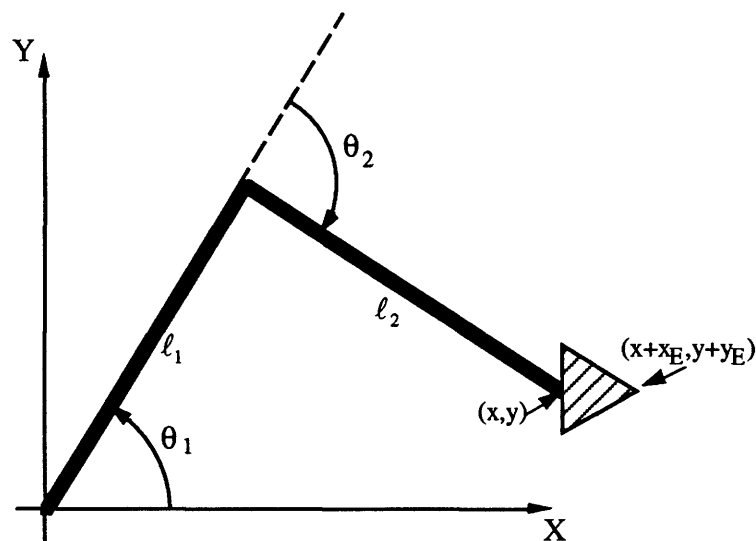
Figure 4-11: Two link mechanism with "kinematics" angles shown.

The forward kinematics equations for this arrangement of links and angles is:

$$\begin{bmatrix} x \\ y \end{bmatrix} = \begin{bmatrix} \ell_1 \cos\theta_1 + \ell_2 \cos(\theta_1 + \theta_2) \\ \ell_1 \sin\theta_1 + \ell_2 \sin(\theta_1 + \theta_2) \end{bmatrix} \qquad (4\text{-}4)$$

$$\begin{bmatrix} \dot{x} \\ \dot{y} \end{bmatrix} = \begin{bmatrix} -\ell_1 \sin\theta_1 - \ell_2 \sin(\theta_1 + \theta_2) & -\ell_2 \sin(\theta_1 + \theta_2) \\ \ell_1 \cos\theta_1 + \ell_2 \cos(\theta_1 + \theta_2) & \ell_2 \cos(\theta_1 + \theta_2) \end{bmatrix} \begin{bmatrix} \dot{\theta}_1 \\ \dot{\theta}_2 \end{bmatrix} \qquad (4\text{-}5)$$

Solving for the angles in terms of Cartesian coordinates and further taking account of the fact that the link lengths are equal (i.e. $\ell_2 = \ell_1 = \ell$) gives:

$$\theta_2 = \cos^{-1}\left(\frac{x^2 + y^2 - 2\ell^2}{2\ell^2} \right) \qquad (4\text{-}6)$$

$$\theta_1 = \tan^{-1}\left(\frac{y}{x} \right) - \tan^{-1}\left(\frac{\ell \sin\theta_2}{\ell + \ell \cos\theta_2} \right) \qquad (4\text{-}7)$$

$$\begin{bmatrix} \dot{\theta}_1 \\ \dot{\theta}_2 \end{bmatrix} = \frac{\ell}{\ell^2 \sin\theta_2} \begin{bmatrix} \ell\cos(\theta_1 + \theta_2) & \ell\sin(\theta_1 + \theta_2) \\ -\ell\cos\theta_1 - \ell\cos(\theta_1 + \theta_2) & -\ell\sin\theta_1 - \ell\sin(\theta_1 + \theta_2) \end{bmatrix} \begin{bmatrix} \dot{x} \\ \dot{y} \end{bmatrix} \qquad (4\text{-}8)$$

The derivation of the inverse kinematics equations is not shown because they are fairly common to texts on robotics control and motion planning. Also, it is important to be aware that (4-7) has two possible solutions based upon the choice of quadrants for θ_2. The angle can be positive or negative, and hence elbow down or elbow up, respectively. In all of the figures of the links, the stimulator is shown in the elbow up position, where θ_2 is negative based upon the definition of counterclockwise being the positive direction.

Given equations (4-6), (4-7), and (4-8), joint angles and velocities could be prescribed to the stimulator based upon the desired Cartesian path. The desired values were entered into the proportional-derivative control law described earlier as desired position and velocity. An intermediate step involved calibrating one position of the stimulator at known angles and Cartesian endpoint coordinates. This was necessary because the potentiometers can measure only change in angle (relative position). Using angles and levels, the stimulator was fixed in a position where $\theta=90$ degrees and $\phi=0$. At this base position, with the links perpendicular, the Cartesian endpoint coordinates are simply the link lengths.

4.8 Two-Axis Force Sensor

The end effector of the stimulator consists of a two-axis force sensor to which various types of indentors/probes can be attached. It was designed to measure the desired range of normal forces as well as a smaller, more accurate range of shear forces. The construction includes a coupling that allows any indentor or probe with the proper fixture and length to be mounted to the sensor and used in experiments. The force sensor, built by Dr. David Brock at the AI labs at MIT, is depicted below in Figure 4-12.
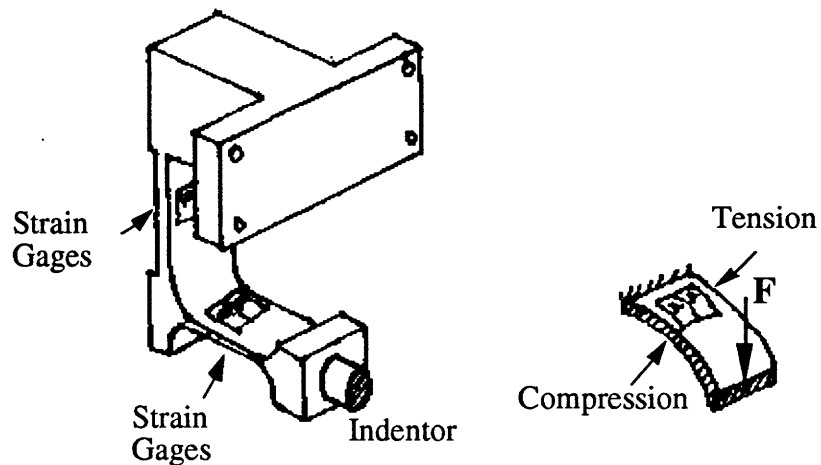
Figure 4-12: Two-axis force sensor.

The design of the sensor is based upon the principle of measuring strains in a cantilever beam subjected to bending by forces and moments. Basic beam theory holds that the strains experienced at a location on the beam are directly proportional to the bending moment at that point, which, in turn, is proportional to the forces and moments applied at the end of the beam. Pairs of 5 kΩ MicroMeasurements™ strain gages were mounted (using M-Bond™ adhesive) on both faces of each of the sensor's two beams. With this arrangement, when forces or moments are applied to the end of a beam, one pair of gages experience tension and the other two are under compression (see right hand side of Figure 4-12). Strain gages experience a change in resistance proportional to micro-changes in their length (strain). In basic applications, such as measurement of forces and moments in the beam, it is general practice to mount two pairs of gages "back to back" in this manner, wiring them together to form a Wheatstone bridge circuit as shown in Figure 4-13.
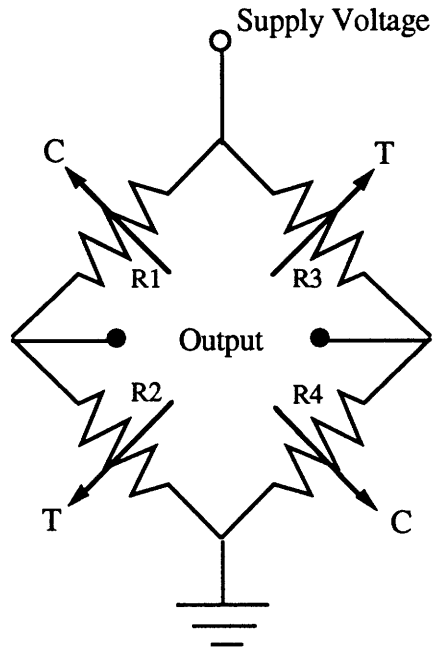
Figure 4-13: Strain gage bridge circuit (T=tension; C=compression)

Each arm of the bridge circuit behaves as a voltage divider, and the output is the measured difference between the two dividers. The Wheatstone bridge is desirable because it compares ratios (the outputs of the two dividers) and is thus insensitive to supply changes (Horowitz and Hill, 1989) and common noise. In addition, the full bridge allows for even temperature distribution and compensation in the set of four gages. Output voltage relates simply to input voltage according to the following equation, which again draws from the fact that V_{out} compares the output voltage of two divider circuits.

$$V_{out} = \left(\frac{R_4}{R_3 + R_4} - \frac{R_2}{R_1 + R_2} \right) V_{in} \qquad (4\text{-}9)$$

Each gage used for this particular application is rated to have a base resistance at zero strain of 5kΩ and experiences a change in resistance such that the ratio of that change to

40

the base resistance is proportional to the strain by its "gage factor"—a MicroMeasurements specification (in this case the gage factor is approximately 2).

Both bridge circuits were powered from an alkaline DC battery supply, and the outputs were separately balanced, filtered and amplified. Early testing of the sensor was performed with a relatively inexpensive AC to DC power supply common to the potentiometer circuits. Unfortunately, power supplies can suffer microvolt changes across reference ground due, for instance, to the capacitive effects of ground loops. This fact became evident in the amplified sensor signal, which was sensitive to these changes in reference ground, despite the bridge circuit configuration. For this reason, bridge supply was provided instead by 9 volt alkaline batteries, configured to provide +9V/Gnd/-9V for instrumentation amplifier supply and with +9V regulated to +5V for constant bridge supply. This configuration produced an isolated common ground for the sensor circuitry. Additionally, bridge balances were added to zero the output difference before amplification. By having zeroed the bridge outputs, only the changes in strain were recorded and amplified. This is important to the design, since the gages are often individually pre-strained after mounting (varying in resistance from one gage to another), and the bridge can conceivably produce a non-zero output under no load conditions. Amplification of the microvolt outputs of the Wheatstone bridges was performed by Burr-Brown™ instrumentation amplifiers, which provided both a gain of 1000 and common mode noise rejection. But, in spite of the latter, it was still necessary to low-pass filter the high frequency noise remaining in the amplified output signals of the sensor. The basic diagram of the circuit components for an individual bridge is shown in Figure 4-14. Based again upon preliminary testing, frequency spectrum analysis and a known range of waveform frequencies that would have to be measured, the cutoff frequency of the RC-filters was set at 150 Hz.
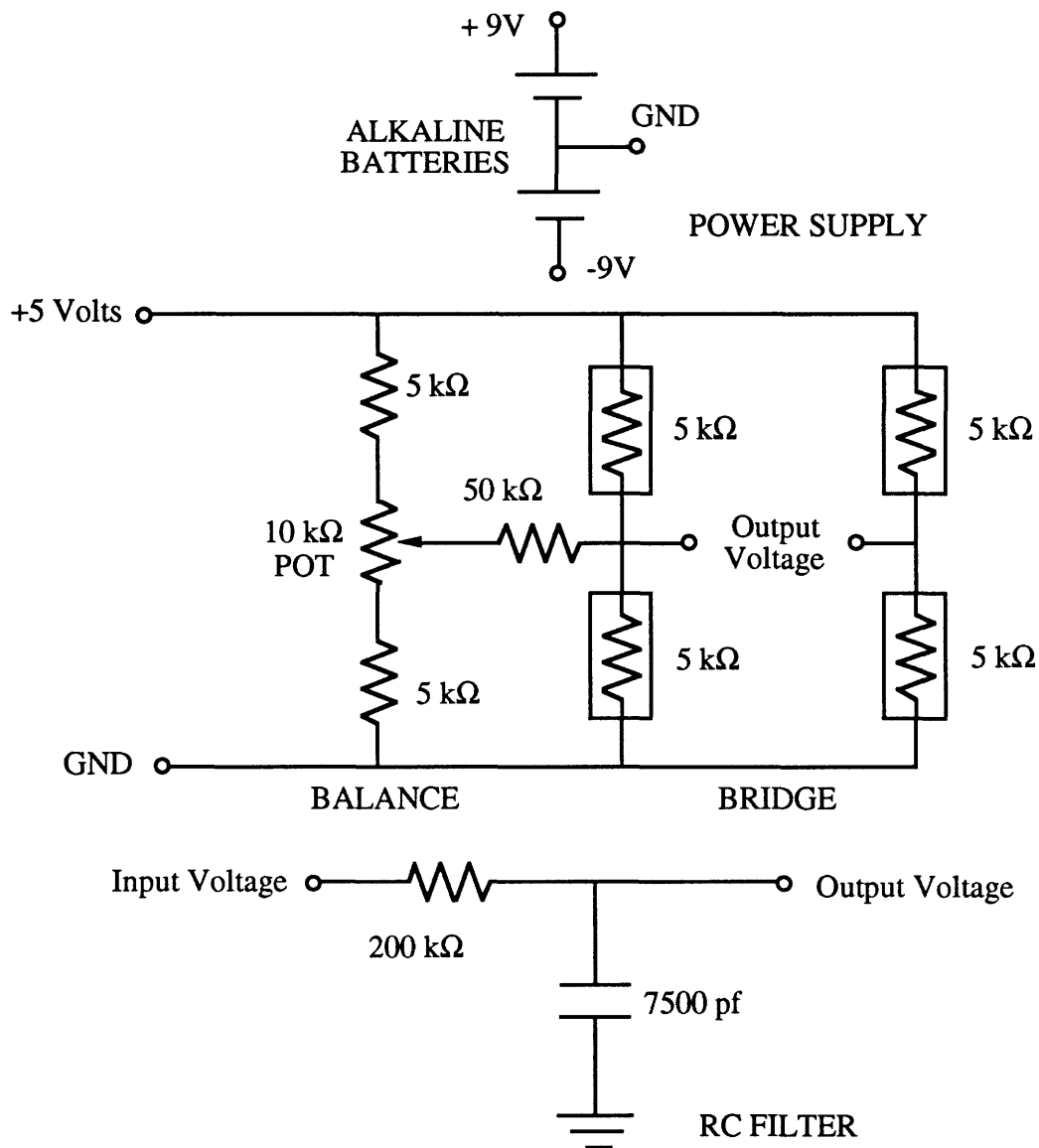
Figure 4-14: (a) Power supply, (b) bridge balance, and (c) RC filter.

The force sensor was calibrated by applying a series of known forces to the endpoint and measuring the corresponding voltage changes in the bridges. The first basic step in this process was to define the endpoint for which to generate calibration constants. The sensor shape was simplified into a structure like the one shown in Figure 4-15. The

measured forces at the endpoint are shown along with the moment created on beam BC

by a shear force at A.
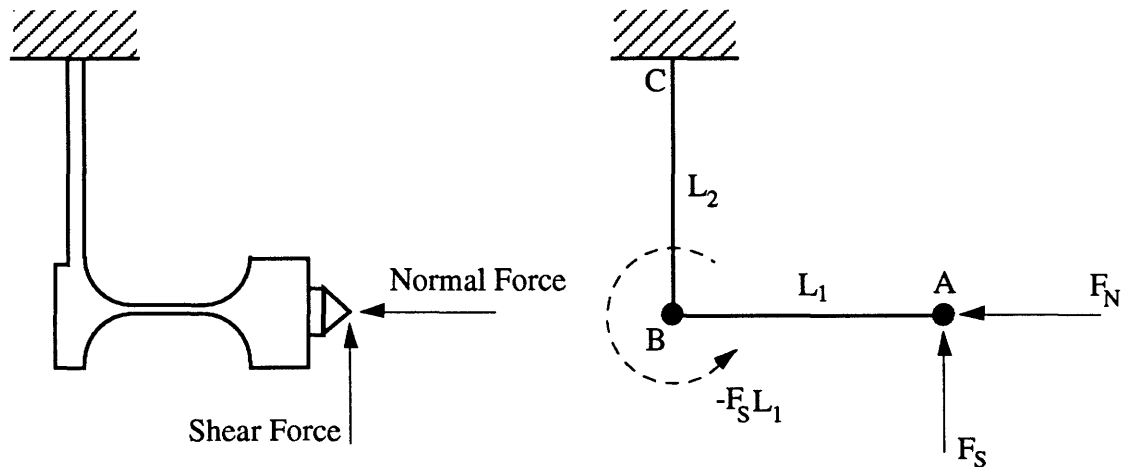
Figure 4-15: Force and moment depiction on the 2-axis force sensor.

Assuming that deflections due to loading are small, and that the joint between the two

beams is a sufficiently rigid connection, a simple force balance can be applied to the

sensor. It is assumed for this calibration that the resultant force produced by the finger

will always be in the center of the indentor, along the axis shown. This condition can be

met in the experimental protocol in the way the indentor and finger are lined up with

respect to each other. Similarly, if the length of the indentors is constrained, L_1 can be

kept constant as well. Under these specifications, a normal force, F_N, (according to the

drawing) will produce bending in Beam 2. A shear force, F_S, will produce bending in

both beams, due to the force at point A and the bending moment it creates at point B.

Strains in a beam experiencing bending are proportional to both forces and moments

according to basic beam theory. In fact, if a section of the beam subjected to bending is

cut away, strain at a particular location can given by:

$$\varepsilon_x = -\frac{M_b y}{EI_{zz}} \qquad (4\text{-}10)$$
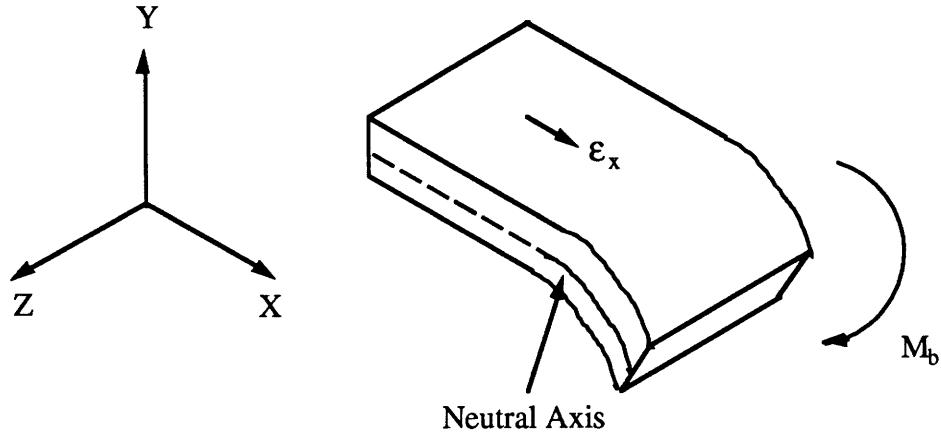
Figure 4-16: Beam under bending conditions (not *pure bending*).

In equation (4-9), ε_x is strain, M_b is moment, y is the distance from the neutral axis, E is Young's Modulus of the material, and I_{zz} is the moment of inertia of the beam. For each beam and its strain gages, all but M_b are constants. The forces applied perpendicular to the neutral axis of the beam produce bending moments at each cross-section in the beam equal to the force multiplied by the distance from point. Therefore, after picking points B and C as calibration points, the bridge output from each beam can be assumed to be functions of the forces applied at the endpoint. A normal force will produce bending in Beam 1, while a shear force will produce bending in both Beam 1 and Beam 2. The preceding relationships come from the facts that (1) strain is proportional to the moments in the beam and (2) voltage output of the bridges is, in turn, proportional to those strains. Because the four gages in a bridge are all equidistant from the neutral axis and are assumed to be well-aligned at the same axial location along the beam, the strains they experience should be equal in magnitude. Only the signs vary between the pair in tension and the pair in compression. Working this relationship of resistance change

corresponding to a given strain experienced by the set of gages in a bridge into equation (4-9) produces

$$V_{out} = \left(\frac{R_2 + \Delta R}{R_1 - \Delta R + R_2 + \Delta R} - \frac{R_4 - \Delta R}{R_3 + \Delta R + R_4 - \Delta R} \right) V_{in} \qquad (4\text{-}10)$$

which, since $R_1 = R_2 = R_3 = R_4 = 5k\Omega$ (base resistance) further reduces to the following

.

$$V_{out} = \left(\frac{\Delta R}{R} \right) V_{in} \qquad (4\text{-}11)$$

As stated previously, the resistance ratio is proportional to strain which is, in turn, proportional to the moments in the beam at the bridge location. Combining all of this information, bridge outputs are related to the endpoint forces according to the following equations.

$$V_1 = k_a \left(F_s L_1 \right) \qquad (4\text{-}12)$$

$$V_2 = k_b (F_N L_2) - k_c \left(F_s L_1 \right) \qquad (4\text{-}13)$$

The constants of proportionality (k_a, k_b, and k_c) are the calibration constants of the sensor for the particular point A where loads are applied.

By applying a variety of forces using the weights, calibration constants were determined and checked, and the true accuracy of the sensor was determined for forces at a point A, defined by $L_1 = 27.45$ mm and $L_2 = 24$ mm. The constants used for force measurement were $k_a = 50.5$ A/D board counts / (mm * Newtons), $k_b = 15$, $k_c = 17.25$. Using this method of calibration, though, the calibration constants are truly accurate only

in predicting loads at the same point. The drawing of the force sensor in Figure 4-16 also indicates that Beam 1 is thinner than Beam 2. With this feature, Beam 1 experiences more strain for the same force (since the moment of inertia of the beam is significantly decreased). Accordingly, measurement of shear force is much finer than that of normal force, in keeping with the design constraints outlined in Section 3.2. The safe range of normal force is on the order of ± 3.5 N and ± 1.0 N for shear force. This "safe range" is limited by the electronics (± 5 volt input limits on the A/D channels) and the yield stress limits of the aluminum beams, where elastic deformation gives way to plastic. Plastic deformation in the beams should be avoided since it affects material properties of the aluminum and seriously degrades the performance and resolution of the sensor. The accuracies of the two axes of force, based upon electrical noise and counts resolution are 0.005 N and 0.001 N, respectively. It is important to state again that the constants and measurements of resolution and accuracy are for loads at the particular point A at which the sensor was actually calibrated. Therefore, it was important to constrain the dimensions of the separate indentors such that both L_1 and L_2, as described in the figure, were held constant.

In addition to calibrating force vs. voltage output of the sensor, it was necessary for position accuracy of indentation stimuli to determine deflections in the beam as a function of normal force. The measurement of the stimulator joint angles and the kinematics transformation to Cartesian coordinates can determine the position of a fixed endpoint on the stimulator with high accuracy (20-50 microns), based upon a few assumptions. The most important to consider is that bending in the stimulator links and play in the bearings is well below the accuracy limits (i.e. that the structure is "rigid" and changes only orientation, not shape). For the forces imposed on the endpoint, bending in the links is negligible. Similarly, play in the bearings is within the proposed accuracy. However, the force sensor design is based upon the principle of measuring strains

produced by bending, and the position of the indentor relative to base of the force sensor can not be accounted for by the joint angles. To compensate, a micrometer was used to determine a calibration constant relating deflection of Beam 2 of the sensor to normal force output. The experimental shear forces and the bending produced in Beam 1 were small enough to be nearly within the desired position accuracy. With the micrometer, fine, incremental deformations were applied to the sensor along the normal axis (x-axis). Simultaneously, normal force output corresponding to beam deflection was calculated using the calibration constants and equations (4-12) and (4-13). A new constant was found that relates 0.1 mm deflections to 70 A/D board counts of equivalent normal force. In determining horizontal (normal) position of the indentor relative to the endpoint of the stimulator, the normal deflection of the beam was taken into account using readings sampled from the force sensor. The stimulator had to therefore compensate in position for endpoint normal force on the sensor to achieve the desired indentor position.

4.9 Final Design Issues and Assembly

All of the components were assembled to form the device shown earlier in block diagram form in Figure 4-1. This included the robot itself (including a coupling to attach the force sensor), the various sensors and A/D board, the motors and amplifiers and the PC and control software. Some general practices that were implemented in final assembly included placing as much shielding between the computer and A/D board and the force sensor as possible. The former produced most of the electromagnetic noise picked up by the sensor. Wire lengths were kept short and shielded and the wires themselves were made up of twisted pairs whenever possible. The motors were shielded in foil and grounded, again to decrease noise that could be picked up in the Wheatstone bridge circuitry. Perhaps one of the more subtle issues was to isolate the PC from

ethernet connections, which contributed a significant (order of magnitude) increase in noise picked up by the A/D board itself.

For reference, a listing of parameters of the stimulator are listed below.

Parameter	Value
AD Board Accuracy	12 bit
AD Board Range (bipolar)	±5 volts
	0 to 4098 counts
Upper link	
link length	76.2 mm
position encoding	618 counts/degree
Lower link	
link length	76.2 mm
position encoding	589 counts/degree
Endpoint Horizontal Travel	1 cm ± 20 microns
Endpoint Vertical Travel	1 cm ± 20 microns
Proportional Derivative Control Constants	
Upper k_p	3 counts/mm
Upper k_v	4 counts*sec/mm
Lower k_p	5 counts/mm
Lower k_v	8 counts*sec/mm
Control Frequency	2,000 hz
Sampling Frequency	500 hz
Motor Low-Pass Filtering Frequency	150 hz
Force Sensor Low-Pass Filtering Frequency	150 hz
Force Sensor Constants	
k_a	50.5 counts/Nmm
k_b	15 counts/Nmm
k_c	17.25 counts/Nmm
L_1	27.45 mm
L_2	24 mm
Force Sensor Range	
Normal Force	±(3.5 ± 0.01 N)
Shear Force	±(1.0 ± 0.001 N)

Chapter 5

Design of Experiments

Once (1) the tactile stimulator was complete, (2) the experimental goals laid out and (3) the basic characteristics of the fingerpad established, the actual experiments were designed. This process involved choosing indentor geometries and depths of indentations, as well as the velocities and periodic waveforms with which to prescribe the stimuli. Additionally, some optimization had to be made of the number of subjects and the number of experiments in order to remain within time constraints of the project and within the limitations in data processing. This chapter outlines each of these issues and presents the procedure used in experiments.

5.1 Indentor Geometries

To meet the requirement that the contact profile be varied reasonably to represent diverse types of fingerpad loading, three different indentors were chosen. A point indentor (rounded to a 0.25 mm radius) and a circular flat plate of 40 mm diameter (larger than the fingerpad area of contact at the highest force) were picked as the two extremes of loading profiles. A 6.35 mm diameter cylindrical rod (flat faced circular indentor) was chosen to represent an intermediate case between the two extremes (e.g. a small button or

switch). These indentors were also consistent with those chosen for *in vivo* compressibility experiments (Srinivasan *et al.*, 1992). Figure 5-1 below shows the indentors in 2D and the basic orientation of indentation with respect to the fingertip.
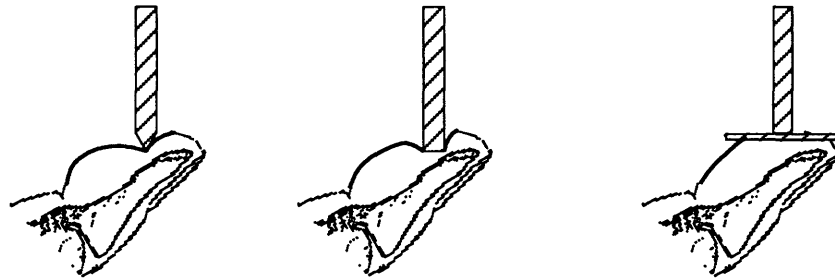
Figure 5-1: Three indentor shapes and corresponding fingertip deformation.

5.2 Indentation Stimuli

The indentation stimuli were chosen based primarily upon the expectations of viscoelasticity and nonlinearity as well as an interest in the impedence of the fingerpad tissues as a function of frequency. First, it seemed clear that the steady state response of the fingerpad to deformations should be recorded at several depths because of the nonlinear mechanical behavior of the pulp. This would allow a general characterization of stiffness or compliance of the fingerpad. Next, to understand the viscous nature of the finger, ramp inputs at several velocities were chosen. The previous two "experiments" were efficiently combined into *ramp and hold* indentations, involving indentation at specified ramp velocities and depth varied from trial to trial. More complex stimuli were needed to gain insight into the frequency response of the pulp and the contribution of inertial elements (i.e. mass). To this end, *sinusoidal* indentations at varied starting depths, frequencies and amplitudes were included in the generic list of stimuli. In all

cases, these stimuli would be made normal to the fingerpad along one axis, as described in Chapter 3.

The next level of experimental design was to specify the depths, velocities and frequencies to be applied to the fingertip. For consistency of results, the index finger of the right hand was chosen as the test area on all subjects. Some limitations were imposed upon the protocol by stimulator itself. Specifically, velocities could only be controlled up to approximately 32 mm/sec against the resistive normal forces produced by the fingerpad during indentation. Under these same conditions, the frequency control was limited to about 16 Hz. Further, the force response of the fingerpad against the flat plate generally exceeded 3 N (the maximum endpoint force that could be generated by the stimulator) at depths over 2 mm. Therefore, the depths chosen ranged from 0 to 3 mm with the point and circular indentors and 0 to 2 mm with the flat plate in increments of 0.5 mm. In the typical fingerpad, 3 mm of indentation is high and close to maximum indentation. In fact, the range of depths chosen is typical of indentations experienced during manual exploration and manipulation. Velocities for ramps were picked logarithmically as 1, 2, 4, 8, 16, and 32 mm/sec. Sinusoidal frequencies were decided upon in a similar manner to be 0.125, 0.25, 0.5, 1, 2, 4, 8, and 16 Hz.

Further refinement was made of the stimuli after preliminary experiments of both stimulator performance and general fingerpad response. For these tests, the fingernail was glued to a rigid aluminum post, with the finger axis perpendicular to the normal and shear axes of the force sensor. The observations made were that steady state force during the ramp/hold experiments did increase nonlinearly. However, steady state force at a particular depth of indentation was independent of ramp velocity, though there were certainly significant differences in dynamic force response to increasing rate of indentation (i.e. during the ramp phase). This was sufficient to describe the first specific criteria for the experiments. At one ramp velocity, ramp/hold stimuli would be given at

the full range of depths for a particular indentor. And, at two depths, the response to the entire spectrum of velocities would be recorded. Sinusoid stimuli were more challenging to refine. The preliminary tests were done by ramping to specified depths and waiting for steady state response to be achieved. Then, sinusoidal inputs of varying amplitudes and frequency were tested. What was seen was that response did indeed change as a function of frequency. Control of these inputs, though, was not very precise at amplitudes of 1 mm and higher. Two starting depths and two amplitudes were chosen for testing at the eight frequencies previously mentioned. The starting depths chosen were 1 and 2 mm, and the amplitudes 0.25 and 0.5 mm. The stimuli are compiled below.

Ramp / Hold	Velocity	Depth
1	1 mm/sec	1, 2 mm
2	2 mm/sec	all depths
3	4 mm/sec	1, 2 mm
4	8 mm/sec	1, 2 mm
5	16 mm/sec	1, 2 mm
6	32 mm/sec	1, 2 mm

Sinusoid	Amplitude	Starting Depth	Frequency
1	0.25, 0.5 mm	1 mm	0.125 to 16 hz
2	0.25, 0.5 mm	2 mm	0.125 to 16 hz

The sinusoids were applied by ramping to the starting depth and waiting up to 5 seconds for steady state indentation response before applying the sinusoid. A generic plot of the two types of stimuli, similar to that given in Figure 3-2 is depicted again in Figure 5-2.
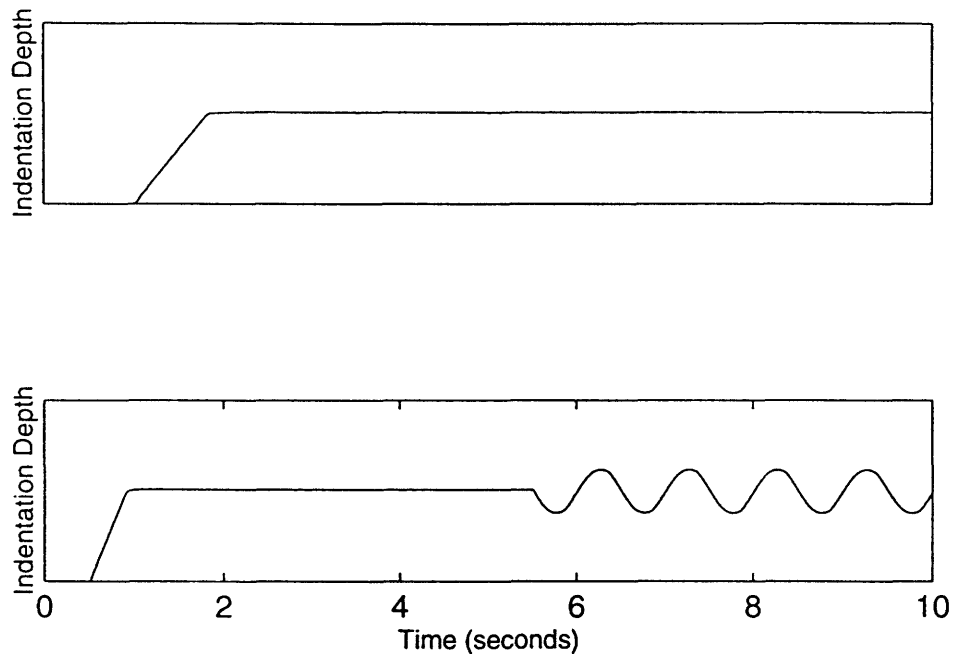
Figure 5-2: (a) Ramp/hold input, (b) ramp/hold/sinusoid input.

5.3 Experimental Setup

To complement the tactile stimulator, a fixture was constructed for the support and restraint of subjects' fingers. One of the constraints involved was that the finger be very rigidly supported so that fingerpad indentation response would never be confounded with motion of the base to which the fingertip was glued. Also, because of the general curvature of the finger and the fact that much tactual exploration of objects occurs with

the fingers angled at about 30 degrees with respect to the surface of the object, the finger was angled for the actual experiments. This actually depicted in Figure 5-1. The fixture was constructed from aluminum and securely fixed to a steel base as shown in Figure 5-3.
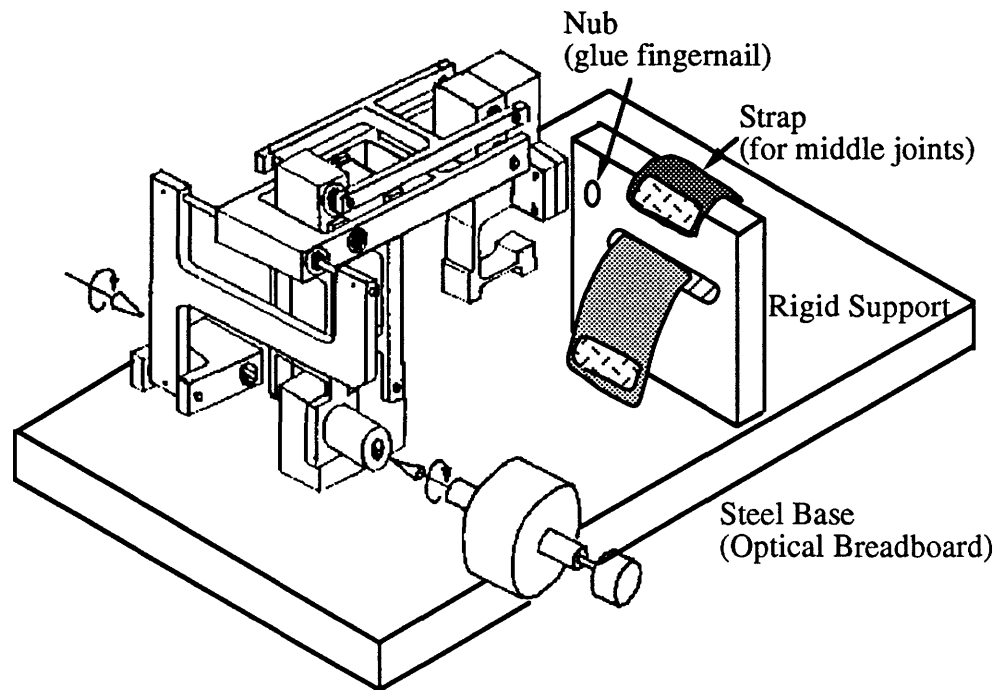
Figure 5-3: Finger support.

The fingernail is glued to the aluminum nub on the support with a drop of fast setting superglue. This provided rigidity and prevents motions of the fingertip. A strap is also shown in the figure, and its purpose is to provide additional support against motions and tremors in the finger during indentation. Care was needed in using the strap so that the blood supply to the finger was not noticeably constricted. The combination of the glue and strap was very effective at restricting any motion of the finger during the trials, as observed by all of the subjects and the experimenter. This was also evidenced by the lack of large shifts in force response data acquired that could be attributed to subject motion.

Subjects were seated at the device with their hands below heart level (to maintain adequate circulation) and with both hand and elbow supported on a stiff foam padding.

5.4 Preliminary Experimental Protocol

With the indentation stimuli chosen and the hardware completely assembled, a basic protocol was generated, tested and then refined into its final form. Time, x- and y-displacements, and normal and shear force were the variables recorded in each of the experiments. For ramp/hold experiments, it was sufficient to record data for 10 seconds (steady state force was reached in less than 5 seconds). For ramp/hold/sinusoid, the hold portion was reduced to 5 seconds and sinusoids were given for 10 seconds or for the length of time required to complete at least two full waves. Data was sampled at 500 Hz to give a small enough period for reliable numerical filtering and discrete time modeling and analysis. The lengths of the experiments were limited by (1) the amount of static data that could be held in arrays (in software; 640K) during one experimental trial (before the data was saved to file and the arrays cleared) and (2) the desire to minimize the experimental time for the comfort of the subjects. Subsequently, sampling frequency was also bounded by the same constraints and several passes were made before optimization the combination of experimental times and sampling period. Acquired data was saved to Matlab™ binary files to optimize hard disk space and speed up read/write time during subsequent analysis. It was under these additional criteria that several series of stimuli were tested on several subjects with each of the three indentors.

Preliminary testing with all of the stimuli on five different subjects' index fingers yielded important modifications in the protocol. First was the definition of 0 indentation or the starting point. Due to the nonlinearity of the fingerpad, differences in starting points (or relative indentation depths) between repetitions of the same stimulus on the

order of 0.25 mm yielded up to 50% deviations in steady state force response. Thus, it was necessary to take a great deal of care in determining initial contact of the probe with the fingerpad surface the first time a stimulus was given and to fix that as the reference starting point for an entire set of stimuli. To achieve a consistent starting position, stimuli sets had to be run in single sittings with the finger glued in one, set position. Also, it was clear that the finger required time to reform its original shape after each indentation. This time was on the order of 30 seconds, and such a waiting period was added to the protocol between stimuli. Additionally, because of the nature of tissues during cyclic loading, it was necessary to precondition the fingerpad to loading (Fung, 1990). Preconditioning refers to a shift to the right in the stress-strain curve for the tissue after repeated cycles of loading. This was seen in the fingerpad, which after several loadings did not reform completely to its original position. Preconditioning occurs because the internal structure of the tissues tends to change with cycling (Fung, 1990). This need was met in the experiments by ramp indenting the finger to maximum depth 10 times and performing full ramp/holds (with reforming time allowed between cycles). Prestressing the tissues in this manner was successful in creating a repeatable response in the fingertip. And the last features of the protocol that were modified were the length of the experiments and the number of trials performed. In testing biological tissues, *in vivo*, it seemed essential to base conclusions on the average response over several repetitions of the same loading and the repeatability of those responses. Therefore, the final protocol was changed to allow three repetitions of each stimulus. A fine point existed, however, over how to implement the repetitions (i.e. consecutively, or from sitting to sitting on separate days). Initial tests involved three sittings of two to three hours each for subjects, where all of the stimuli with all three indentors were given once each time. The results showed a distinct lack of repeatability in the DC level of the responses, though not in form or shape. Further investigation revealed that the discrepancies were, in fact due to small (circa 0.25 mm)

differences in what was perceived as 0 indentation and minor deviations in finger orientation and position after gluing. Quite likely, there were some changes from day to day in the fingers themselves due to climate, circulation, etc. For the time being, it was more important to have reliable and repeatable results that could be well explained and understood. So, after an extensive amount of data on 5 different subjects was acquired and analyzed, the conclusion was made that the experiments should be run in three sittings, one per indentor. At each sitting, three consecutive repetitions of stimuli would be given in order of increasing ramp/hold depth and then velocity and following in order of increasing frequency, amplitude and then starting depth for the sinusoidal stimuli. The sittings were, as mentioned two to three hours long, and the subject finger was glued in the same position the entire time with a fixed starting point for all indentations. This minimized, at least, variations in data based on experimental setup errors, though the biological variations among subjects and time varying properties of the finger were still present and evident in the results.

5.5 Experimental Protocol

After the extensive preliminary testing, the final protocol for experiments was assembled and used to acquire data on 5 subjects varying somewhat in age, size and sex. Sampling frequency was set at 500 Hz, as mentioned, with time, x- and y- displacements of the indentor, and normal and shear forces recorded. Experimental times were also fixed as described at the end of the previous section. The protocol is outlined briefly in bullet form below. It covers the procedure used at each sitting for the particular indentor being used (point, circular or flat plate).

Experimental Protocol

- Glue the nail of subject's index finger to post; finger angled at 60 degrees relative to the indentor path.

- Strap proximal joints of finger to support and allow subject to achieve a comfortable position with elbow and hand supported and below heart level.

- Take an offset reading from force sensor to get 0 N force level.

- Position indentor tip such that center is barely contacting the center of the contact region. Fix that position as preliminary starting point.

- Precondition. Indent at slow ramps (2 mm/sec) up to maximum allowed depth for indentor 10 times. Allow up to 30 seconds for fingertip to reform shape after each indentation.

- Acquire new starting position of indentor tip based on when the subject reports that the indentor is barely contacting. Visual references and force sensor output are used as additional indications. Fix starting point and record as 0 indentation.

- The subject's finger must now remain glued and fixed in the same position for the entire sitting with the indentor. If this condition is not met, the experiments must be repeated from the start.

- Ramp/Hold indentations. All depths at 2 mm/sec. Three repetitions of each depth with up to 30 second inter-stimulus interval. Then, increasing ramp velocities at first to 1 mm and then to 2 mm depths. Again, repeat and reform.

- Sinusoidal indentations. At 1 mm starting depth, 0.25 mm amplitude, indent in increasing frequency. Increase amplitude to 0.5 mm. Increase starting depth to 2 mm and impose stimulus at 0.25 mm amplitude and then 0.5 mm. Three consecutive trials of each. Allow an inter-stimulus interval of 30 seconds for the fingerpad to reform between subsequent trials.

Chapter 6

Experimental Results

Complete sets of the indentation stimuli (Chapter 5) were delivered to the right (dominant) index finger of five different subjects during a one week period. Basic measurements were made of each finger's dimensions as well as the indentor/fingerpad contact area as a function of depth. After verifying the repeatability of the normal force data (i.e. that variations between repetitions of identical indentation stimuli were on the order of 5-10%), the traces were subjected to zero phase shift numerical low pass filtering to smooth out any remaining higher frequency noise components in the output signals. Shear force data was small as expected, verifying the "normal-ness" of the indentation, and therefore, shear displacement of the indentor and force response were given little consideration in the presentation of results and modeling analysis. This chapter focuses upon describing normal force response characteristics from ramp/hold and sinusoid experiments with the three indentors on all five subjects. The entire data set in is presented in Appendix B.

6.1 Subject Data

The five subjects used in the experiments were picked for their availability and willingness to participate as well as for variations in finger size, shape, stiffness, etc. All of the subjects are right-handed and work in an academic environment, which affects characteristics such as softness. In this paper, they will be referred to by subject numbers, as given in the following table:

Subject	Sex	Age
1	female	23 years
2	male	19 years
3	male	23 years
4	male	39 years
5	male	21 years

Table 6-1: Subject designations, sex and ages.

Using Permalastic™ dental cement, molds were made of each of the index fingers used in the experiments. Slow setting epoxy was poured into the molds to create replicas of the fingers that captured fine detail of the epidermal papillary ridges and the nail in addition to macroscopic features such as shape and/or curvature. A scanned image of the finger replicas is shown below as Figure 6-1.

Figure 6-1: Photograph of a penny and the 5 epoxy fingertip replicas.

Measurements of thickness, length, and width were made on the rigid epoxy replicas according to the guidelines in Figure 6-2. Volume of the fingertip (from the distal joint to the tip) was measured separately by submerging the fingertip replica and noting water displacement in a graduated cylinder.
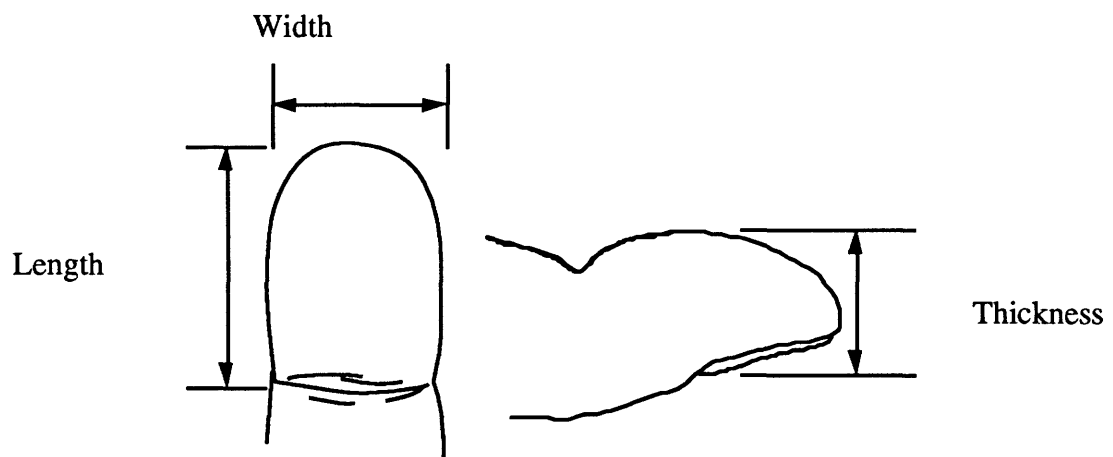
Figure 6-2: Measurement guidelines for fingertip.

The measurements made on each subject's finger are given in the following table. Errors in measurement were estimated to be on the order of 5%.

Subject	Thickness	Length	Width	Volume
1	10.1 mm	24 mm	16 mm	3.7 cm^3
2	11.9 mm	26 mm	17 mm	5.0 cm^3
3	11.7 mm	28 mm	17 mm	4.2 cm^3
4	12.5 mm	28 mm	18 mm	5.1 cm^3
5	13.0 mm	26 mm	19 mm	5.9 cm^3

Table 6-2: Macroscopic fingertip dimensions.

6.2 Processing the Experimental Data

This section describes the force response characteristics to indentation for the set of subjects. First, some general features of the raw data are shown to explain the choices made in filtering and averaging strategies. Figure 6-3 shows the unfiltered input and output data from three repetitions on Subject #4 of a typical 2 mm/sec ramp, 2 mm starting depth, 0.25 mm amplitude, 1.0 Hz frequency ramp/hold/sinusoid indentation with the circular indentor.
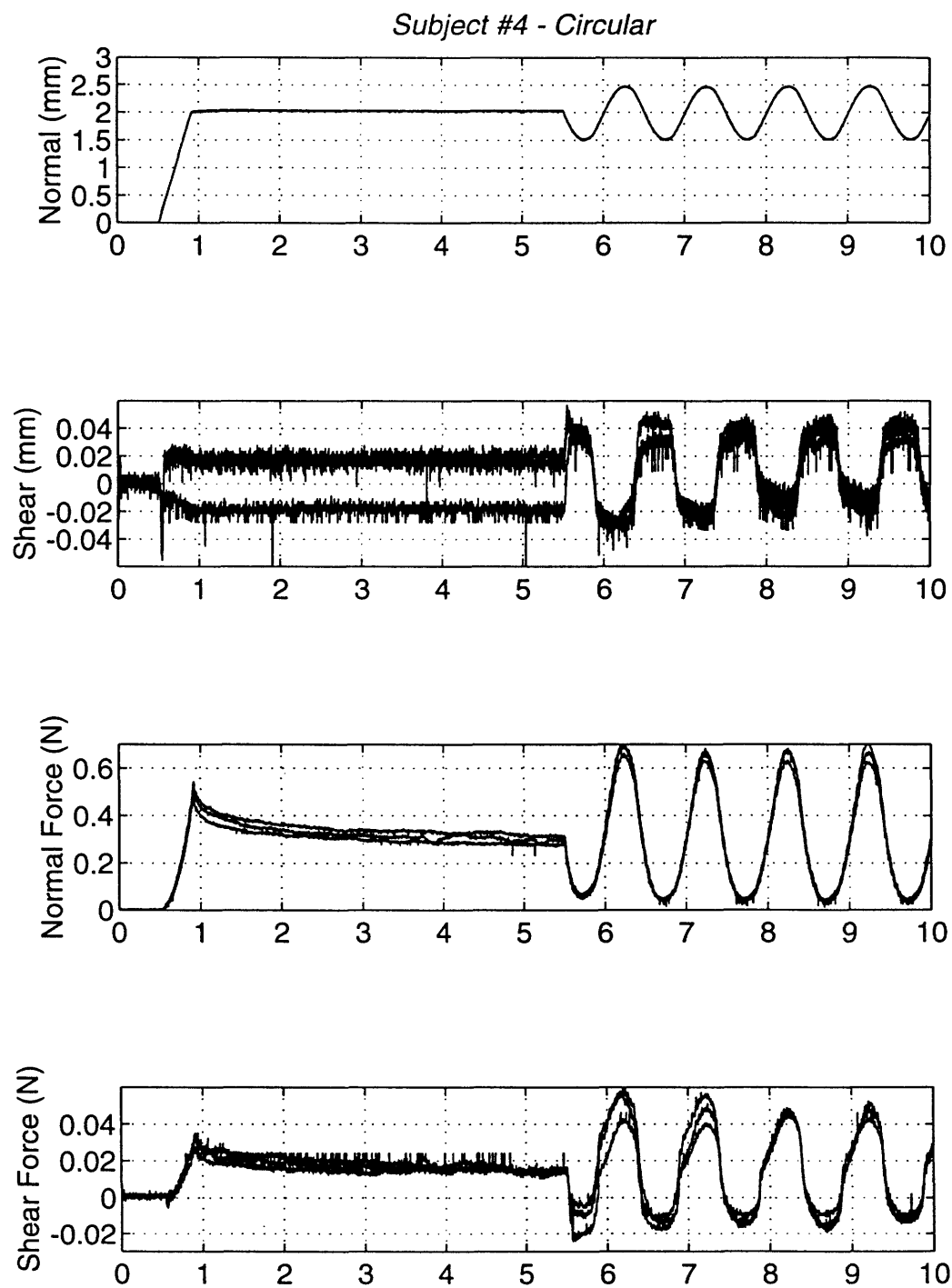
Figure 6-3: Raw ramp/hold/sinusoid data for Subject #4 w/ circular indentor.

In the figure, it should be noted for one that shear force is less than 10% of the corresponding normal force for that indentation. At least some portion of the resultant shear force can be attributed to limited sensor resolution (on the order of a few grams weight). Additionally, there exists some shear displacement that was not prescribed but is within the endpoint resolution of the potentiometers (20-40 microns). And lastly, according to the argument presented in Section 3.2 and Figure 3-3, minor rotations in the finger about its axis and/or asymmetry of the tissue will produce a component of force in the shear direction. Based upon the relative magnitudes of shear force, though, it was logical to conclude that the finger was well-oriented and that the input indentation stimulus was well-prescribed. The shear force and displacement data is of relatively the same magnitude for all subjects with all stimuli and is not dealt with further in this thesis. Another obvious feature of the raw data were the presence of high frequency components, originating at various stages in the electronics despite filtering. A unity gain, zero-phase, low-pass, numerical Butterworth filter was used in Matlab™ to remove noise in the data. The cutoff frequency was chosen by analyzing the frequency spectrum of the data with the highest frequency components (i.e., the 32 mm/sec ramp/hold and the 16 Hz sinusoids). Based upon this analysis for ramp/hold experiments, cutoff frequency was set at 10 Hz and for ramp/hold/sinusoids, 50 Hz. As is evident in Figure 6-4, the signal processing removed a significant portion of the noise components without distorting real data. And lastly, the data from the three repetitions of each indentation stimulus was repeatable on the order of 5-10%. Each set or trio of normal indentation and force response was subsequently averaged to form single, mean traces of input and output. In Figure 6-4, the normal force data from Figure 6-3 is shown filtered and averaged. The remaining responses portrayed in the thesis have been processed in the same manner.
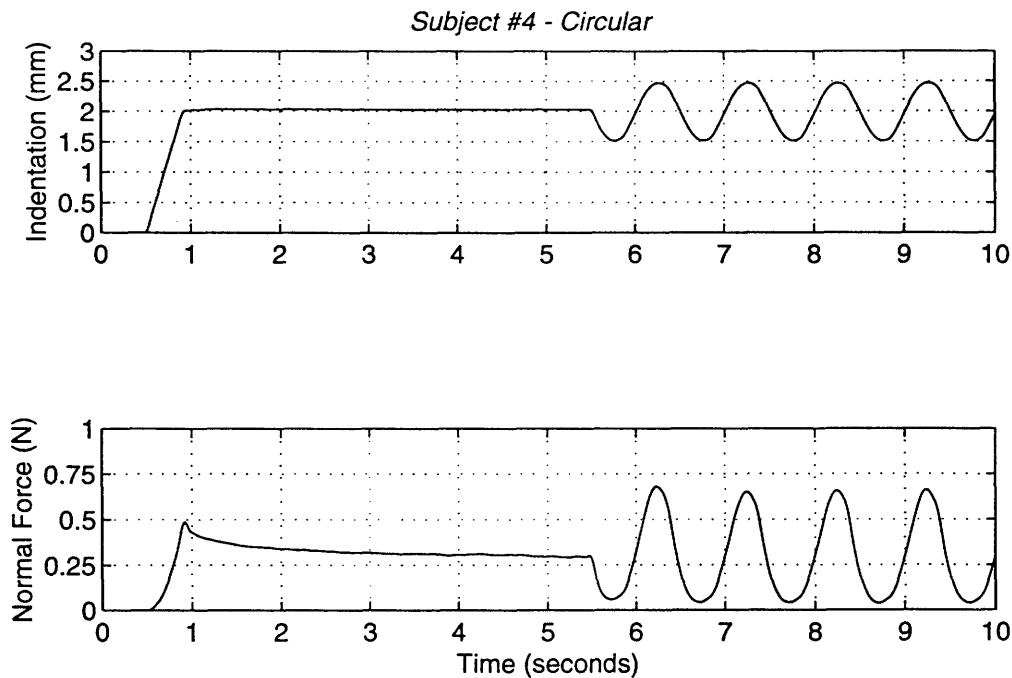
Figure 6-4: Averaged and filtered normal force data from Figure 6-3.

6.3 Ramp/Hold Experimental Results

This section presents ramp/hold data from all the subjects and, to avoid miring this chapter in graphs, ramp/hold/sinusoid data from *only* Subject #4, whose force response best fits the mean of the data from all subjects. There was a significant amount of subject to subject variability in response magnitude, as will be shown in plots of steady state force data from ramp/hold experiments. However, the forms of the responses themselves did not vary noticeably. Attempts to normalize this data with respect to finger dimensions, such as those given in Table 6-2, have so far met with little success, and this too will be shown graphically. Figure 6-5 contains the normal force response to ramps at 2 mm/sec and holds at all depths for each indentor, (a) point, (b) circular and (c) flat

plate. Figure 6-6 contains plots of the response to all velocities of ramps at both 1 mm and 2 mm depths for all indentors. The surface areas of the indentors and approximate relative contact areas are given in the following table.

Indentor	Surface Area	Contact Area
Point	0.2 mm^2	0.2 mm^2
Circular	32 mm^2	increases from 0 to 32 mm^2 as indentation depth reaches 0.5 mm; 32 mm^2 for subsequent depths
Flat Plate	larger than fingerpad	increased w/ depth

Table 6-3: Indentor surface and contact areas.

Contact area directly affects the total volume of material compressed during indentation and therefore the measured resultant force response. Also, the profile or projected area of material deformed increases as a function of depth even with the point indentor. All of this accounts in part for the nonlinearity that will become evident in the characteristic responses to be shown in the following pages. Additional discussion of the causes and effects of nonlinearity on modeling will be made later in this and the next chapter.
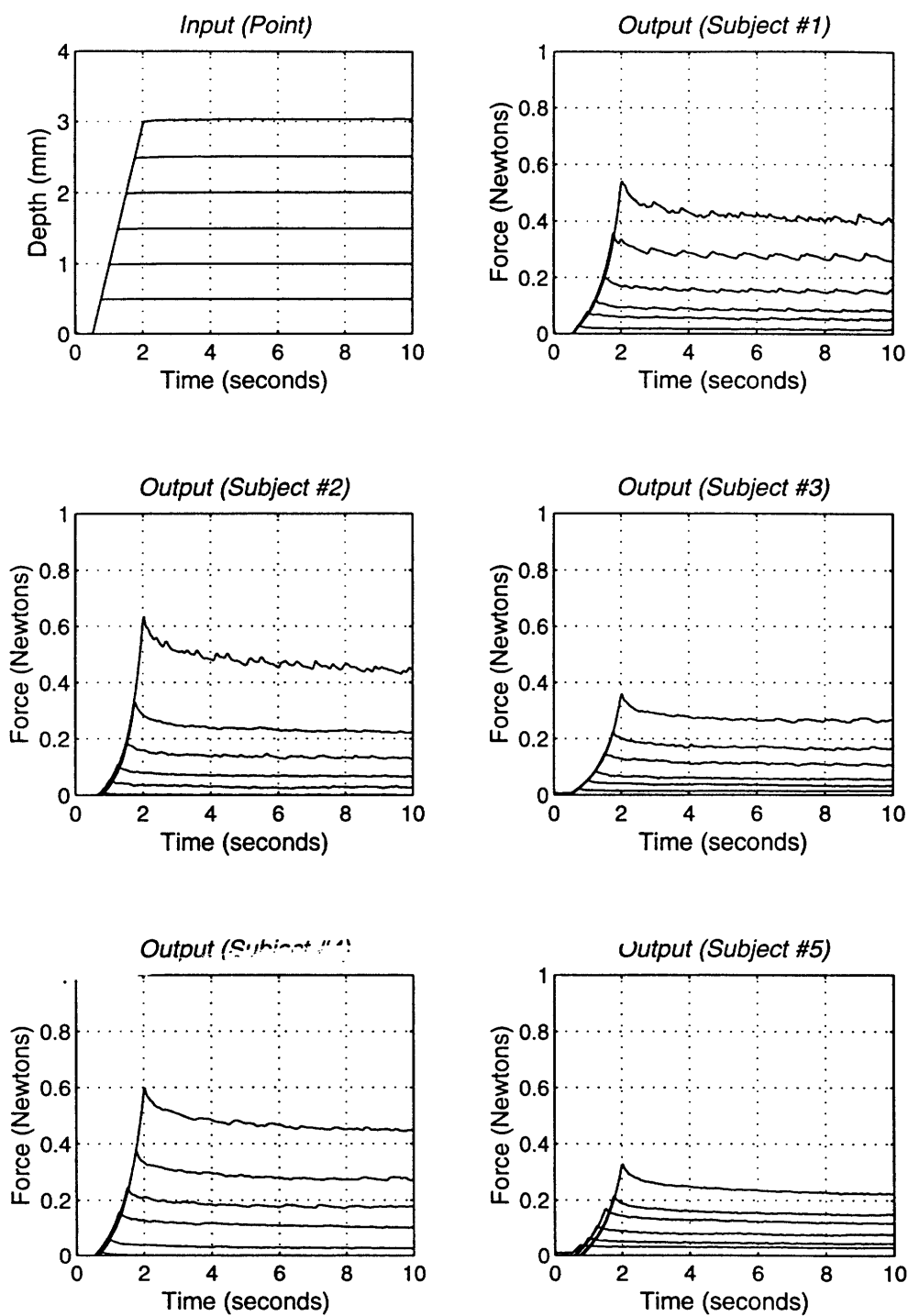
Figure 6-5 (a): Ramp/hold results with point indentor for all depths and ramp velocity of 2 mm/sec.
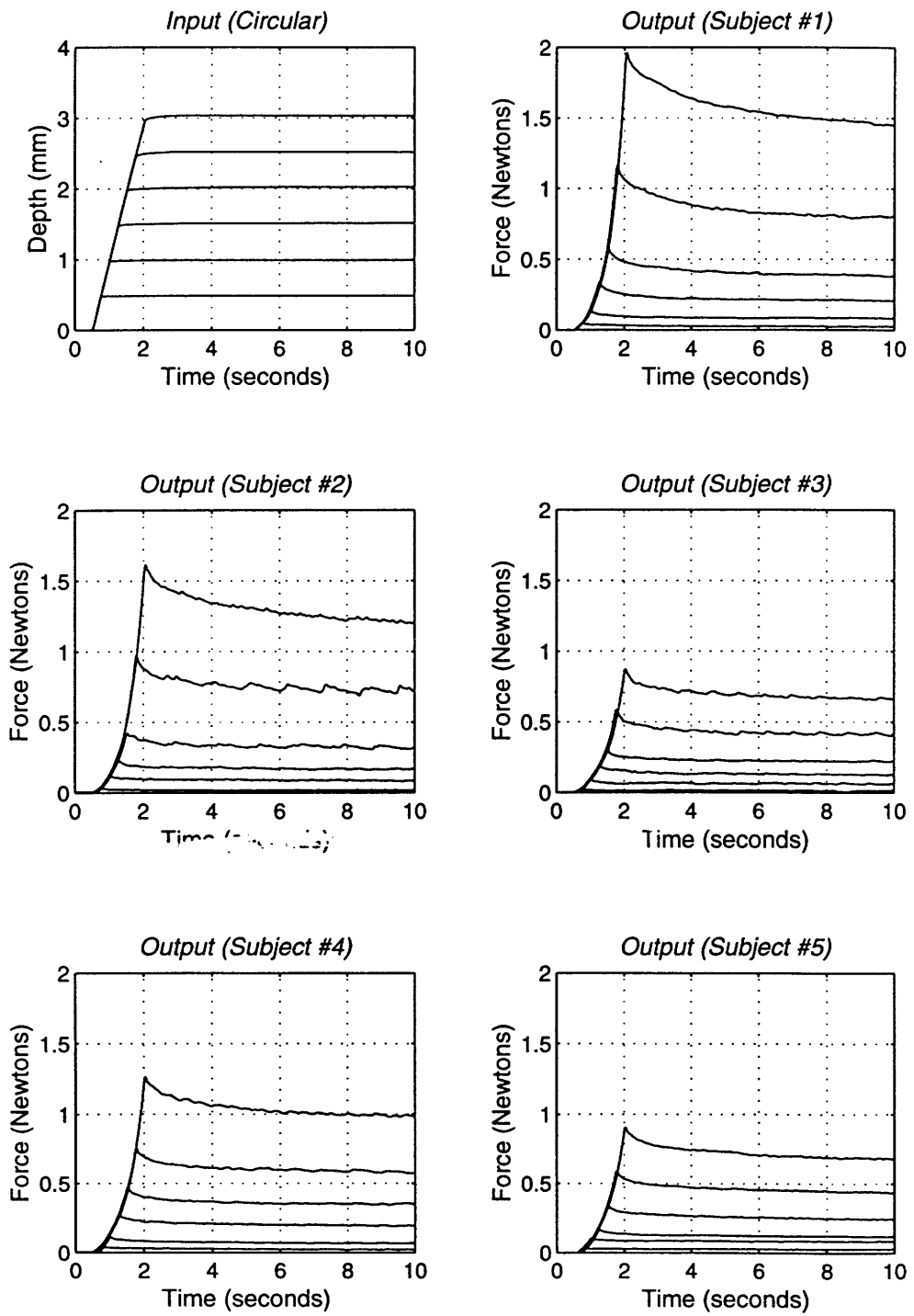
Figure 6-5 (b): Ramp/hold results with circular indentor for all depths and ramp velocity of 2 mm/sec.
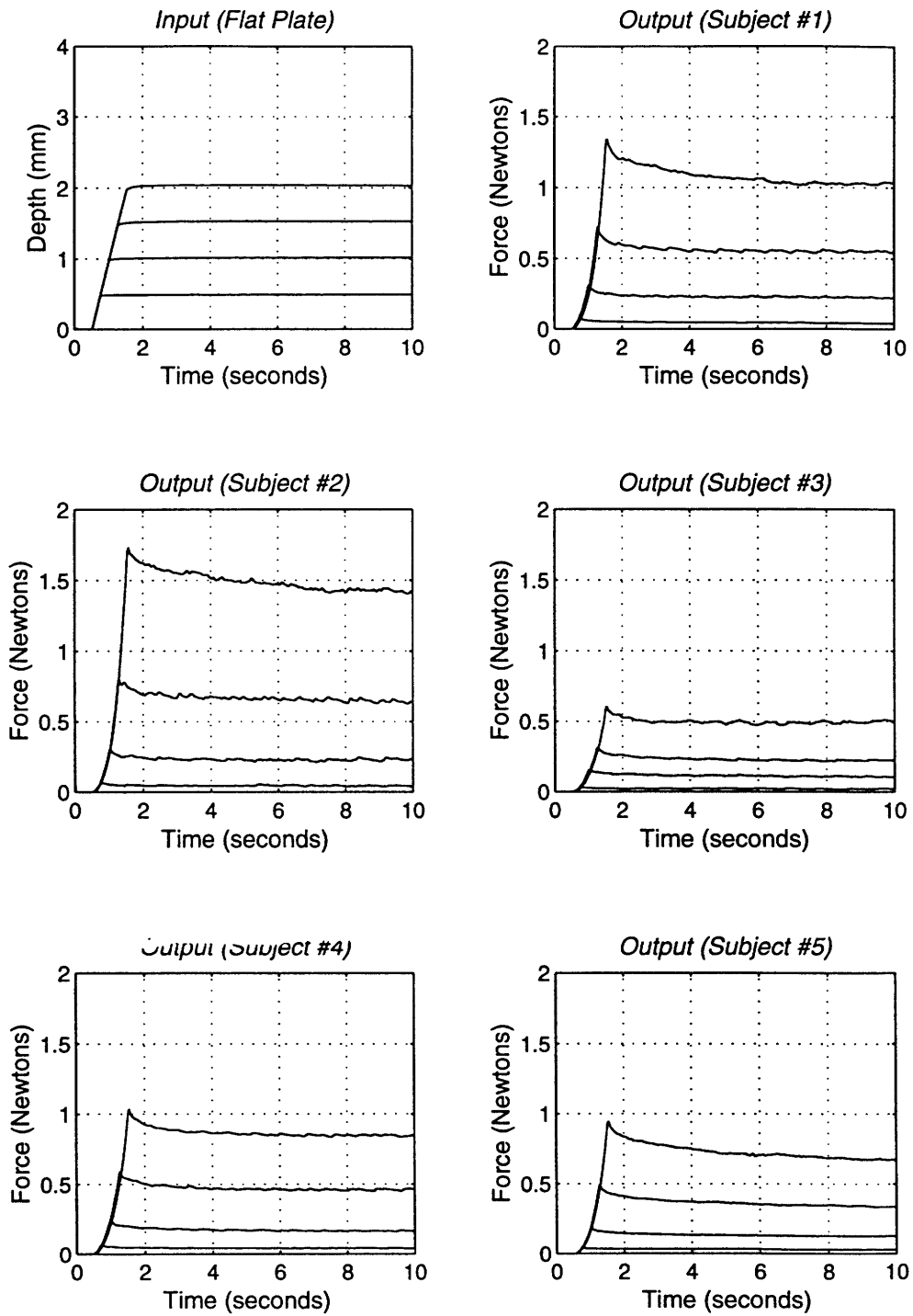
Figure 6-5 (c): Ramp/hold results with flat plate indentor for all depths and ramp velocity of 2 mm/sec.
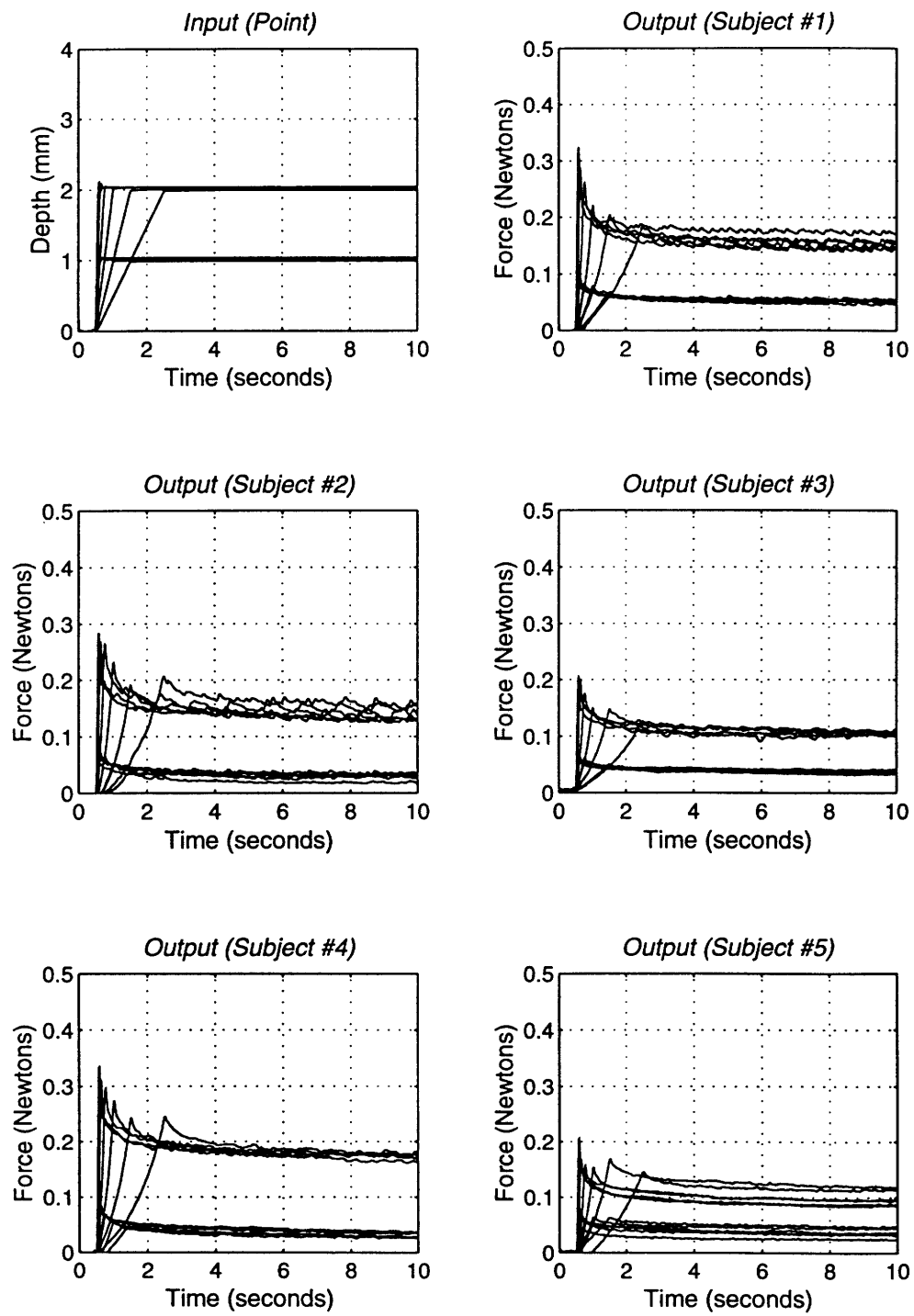
Figure 6-6 (a): Ramp/hold results for point indentor at 2 mm depth, all ramp velocities.
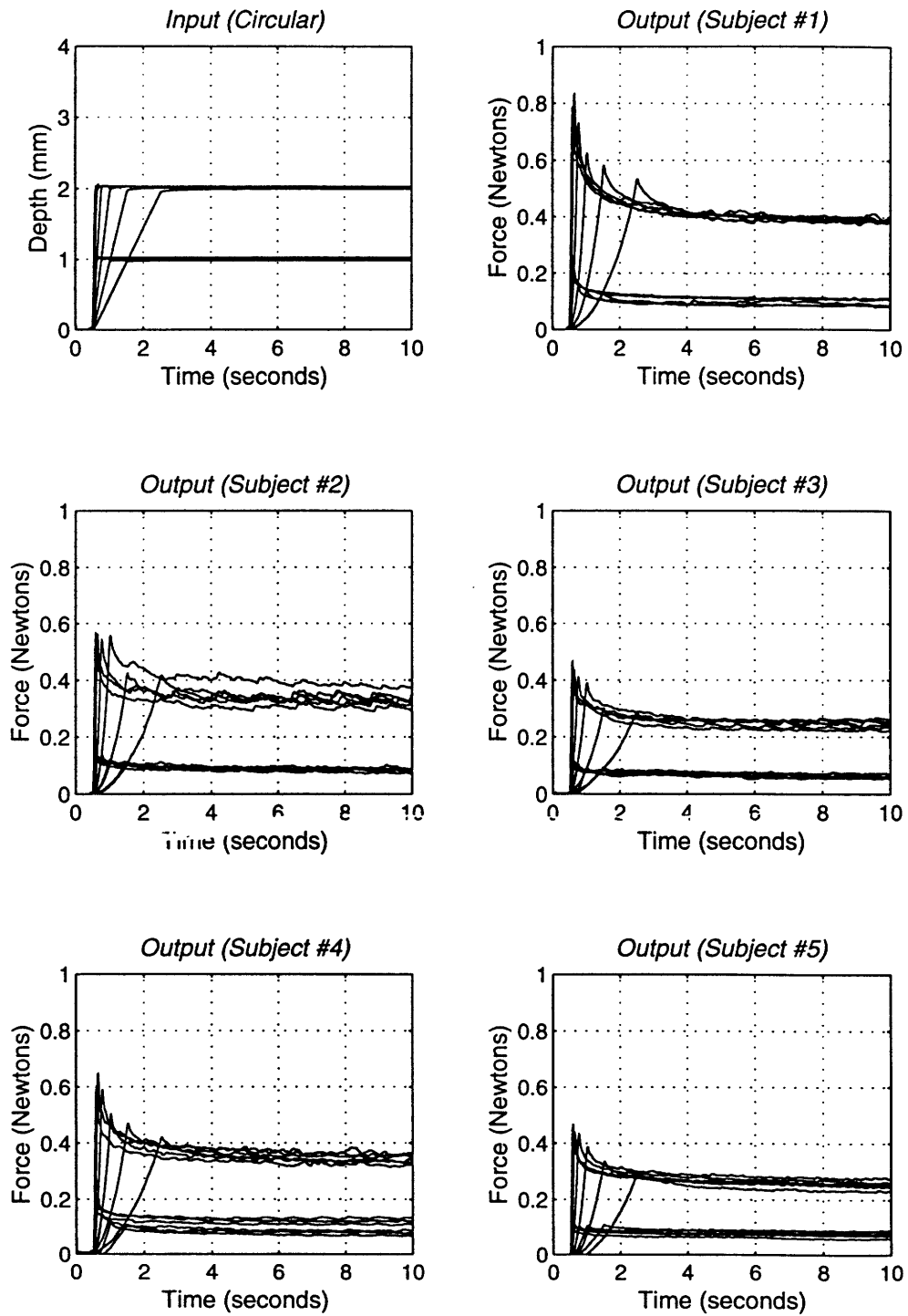
Figure 6-6 (b): Ramp/hold with circular indentor for 2 mm depth, all ramp velocities.
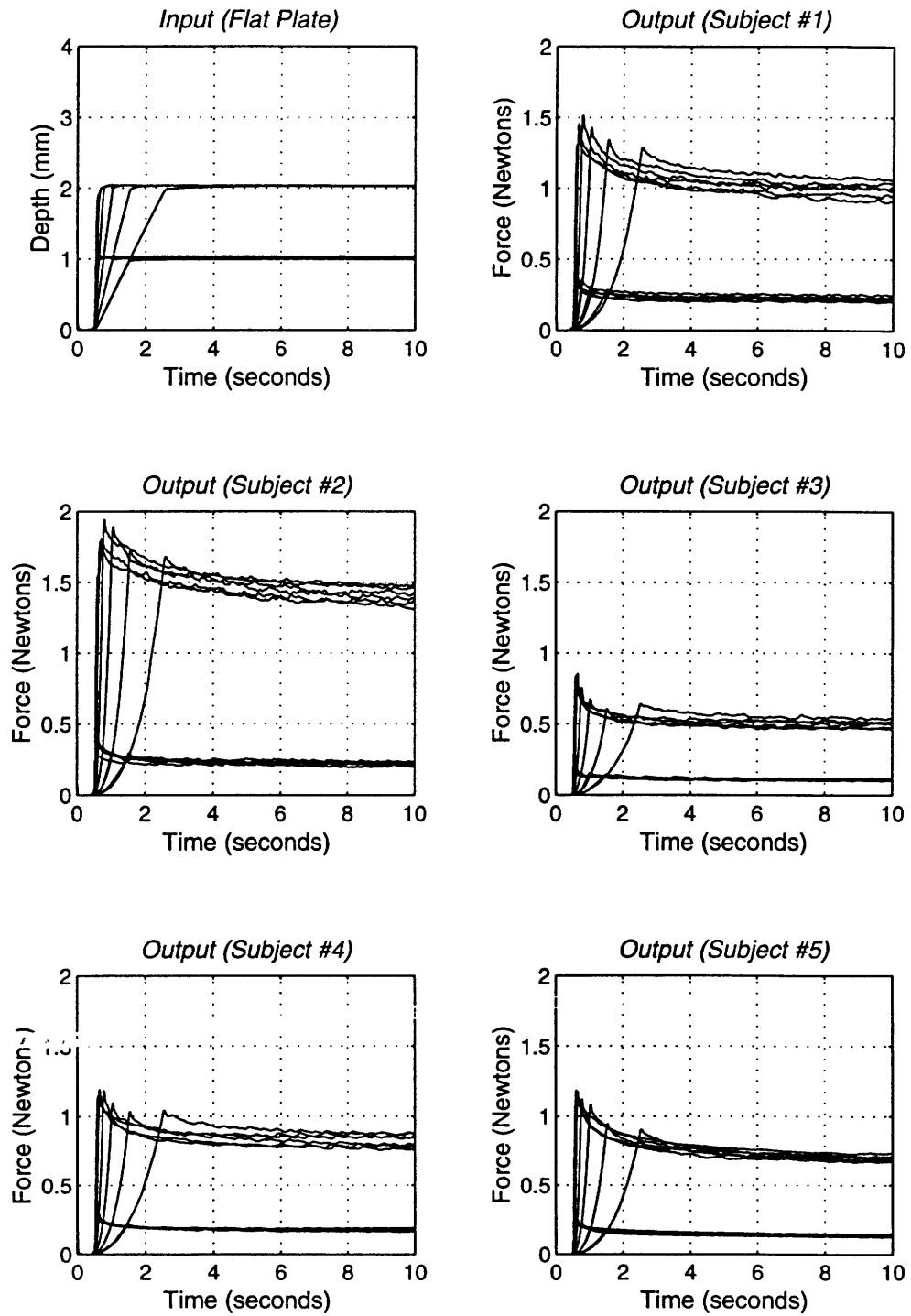
Figure 6-6 (c): Ramp/hold with flat plate indentor for 2 mm depth, all ramp velocities.

The force axes in the preceding graphs were changed with respect to indentor type because, as expected, relative force magnitude increased with indentor contact area. Figure 6-5 shows a clear variation in the mechanical response characteristics of the fingerpads of the subjects. Also noteworthy among the features of the output response are that (1) force magnitude for Subject #5, who has the largest finger, is significantly smaller than magnitude for Subject #1, who has the smallest finger, (2) magnitude of the responses for Subject #2 and Subject #3, who have fingers with similar dimensions are very different, and (3) at the point where the indentor stops indenting and holds a steady position, there is initially a peak force which decays to a steady state force, both of which are, in turn, nonlinearly dependent on indentation depth. The force during steady indentation (hold) is nearly constant within about 5 seconds, and therefore, only 10 seconds worth of data was taken and shown here. Figure 6-6 makes clear the fact that the steady state force reached after the response decays from the peak force is not dependent upon the velocity of indentation. Peak force itself is clearly a function of ramp velocity and appears nonlinear, which shows the dependence of force response to indentation rates. A discussion of results will touch more upon these and other issues related to the nature of the data.

To view the basic nonlinearity of the fingertip in simplest form, steady state forces as functions of indentation depth and indentor were plotted separately, and attempts were made at normalization with respect to thickness and volume of the fingertip to form an even more concise picture. Figure 6-7a consists of three graphs, each containing plots of steady state force (the average force value between 9 and 10 seconds after the initiation of the ramp) vs. indentation depth for all 5 subjects with a particular indentor. Figure 6-7b normalizes these plots with respect to measured fingertip thickness, and Figure 6-7c with respect to fingertip volume, as given in Table 6-2. Figure

6-7d plots the average steady state force vs. indentation depth for the non-normalized data corresponding to Figure 6-7a on all subjects with standard deviations shown as I-bars.
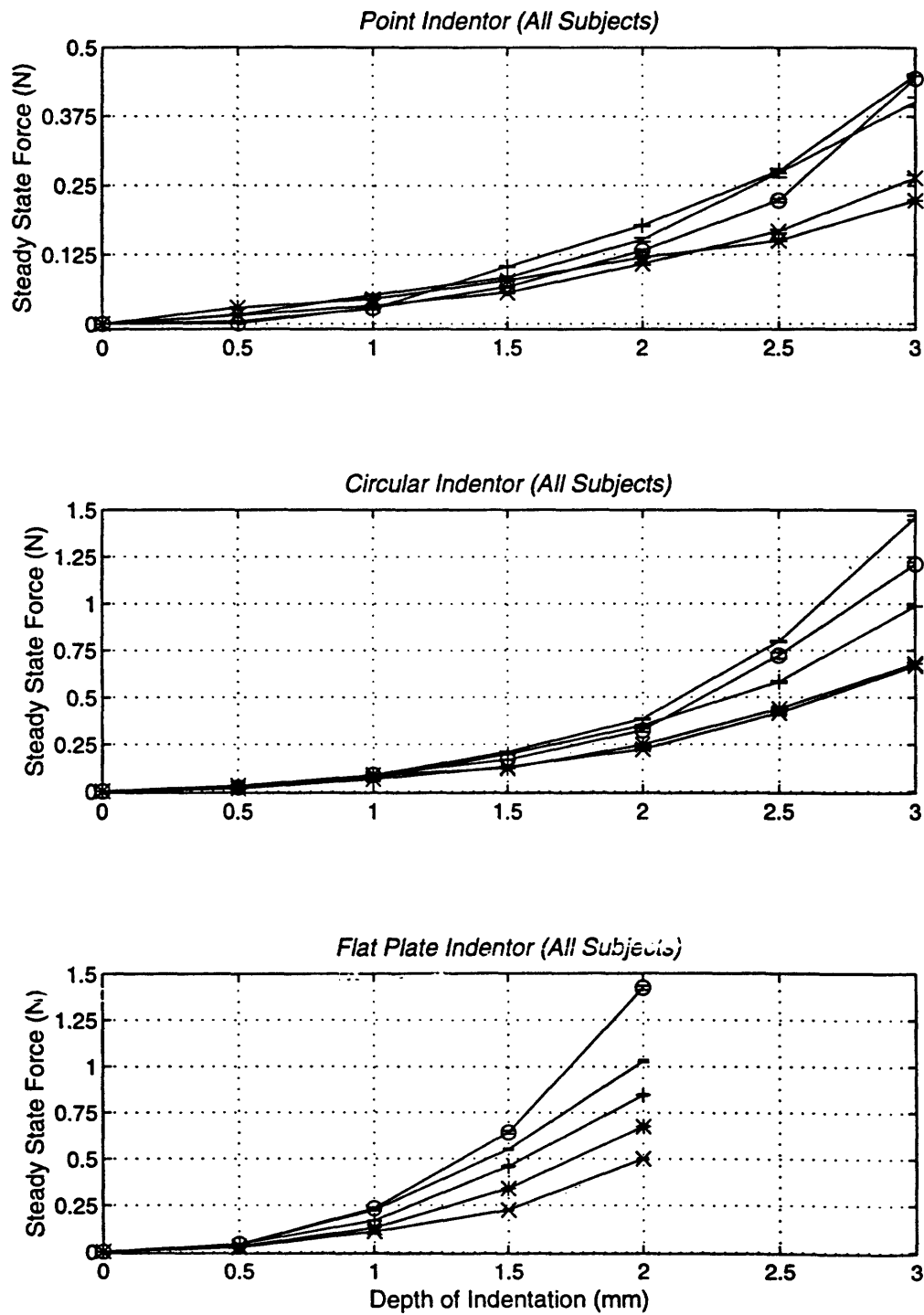
Figure 6-7 (a): Steady state force vs. depth for all subjects.
(1 = -; 2 = o; 3 = x; 4 = +; 5 = *)
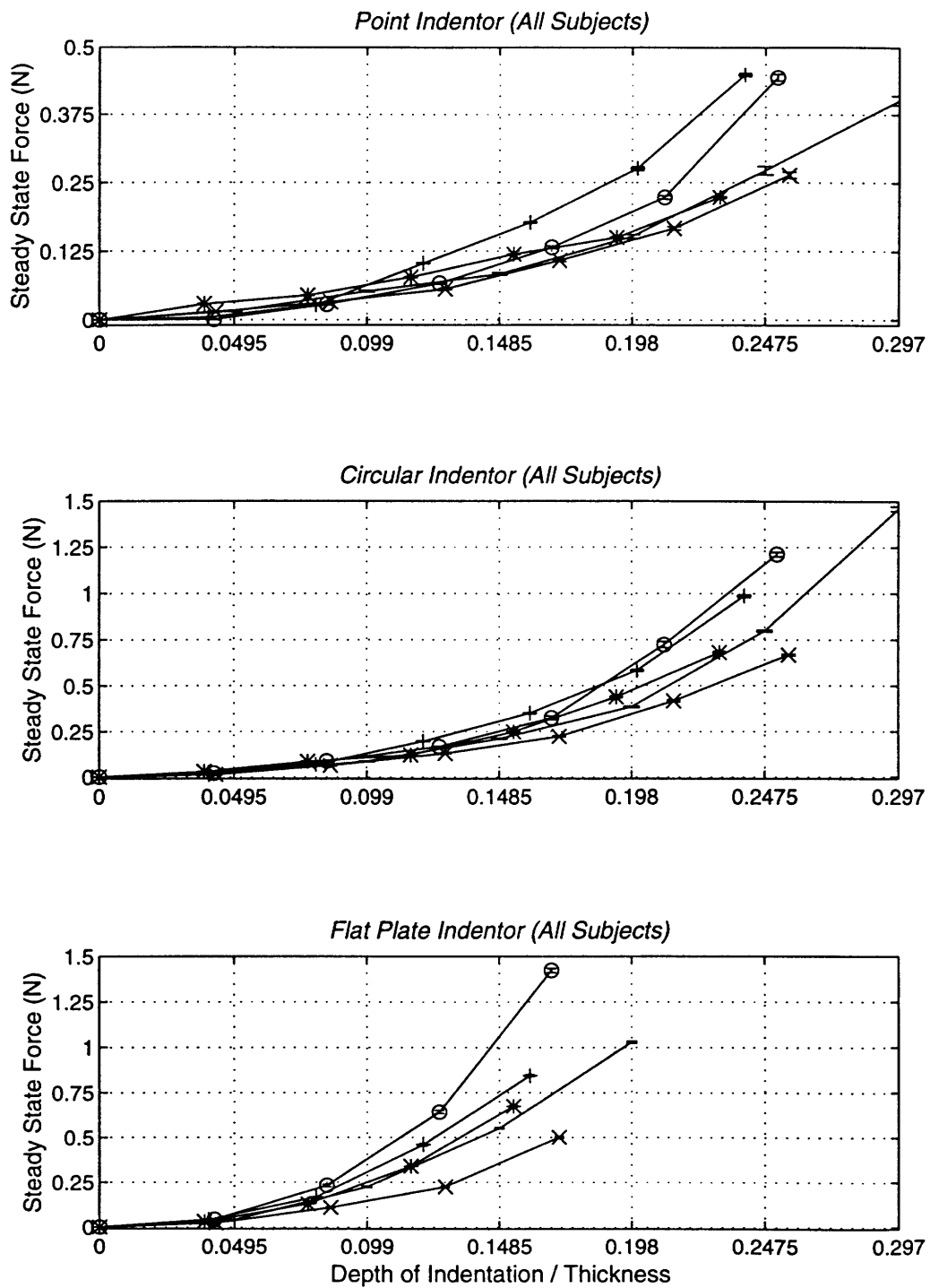
Figure 6-7 (b): Steady state force vs. depth for all subjects, normalized wrt thickness.
(1 = -; 2 = o; 3 = x; 4 = +; 5 = *)
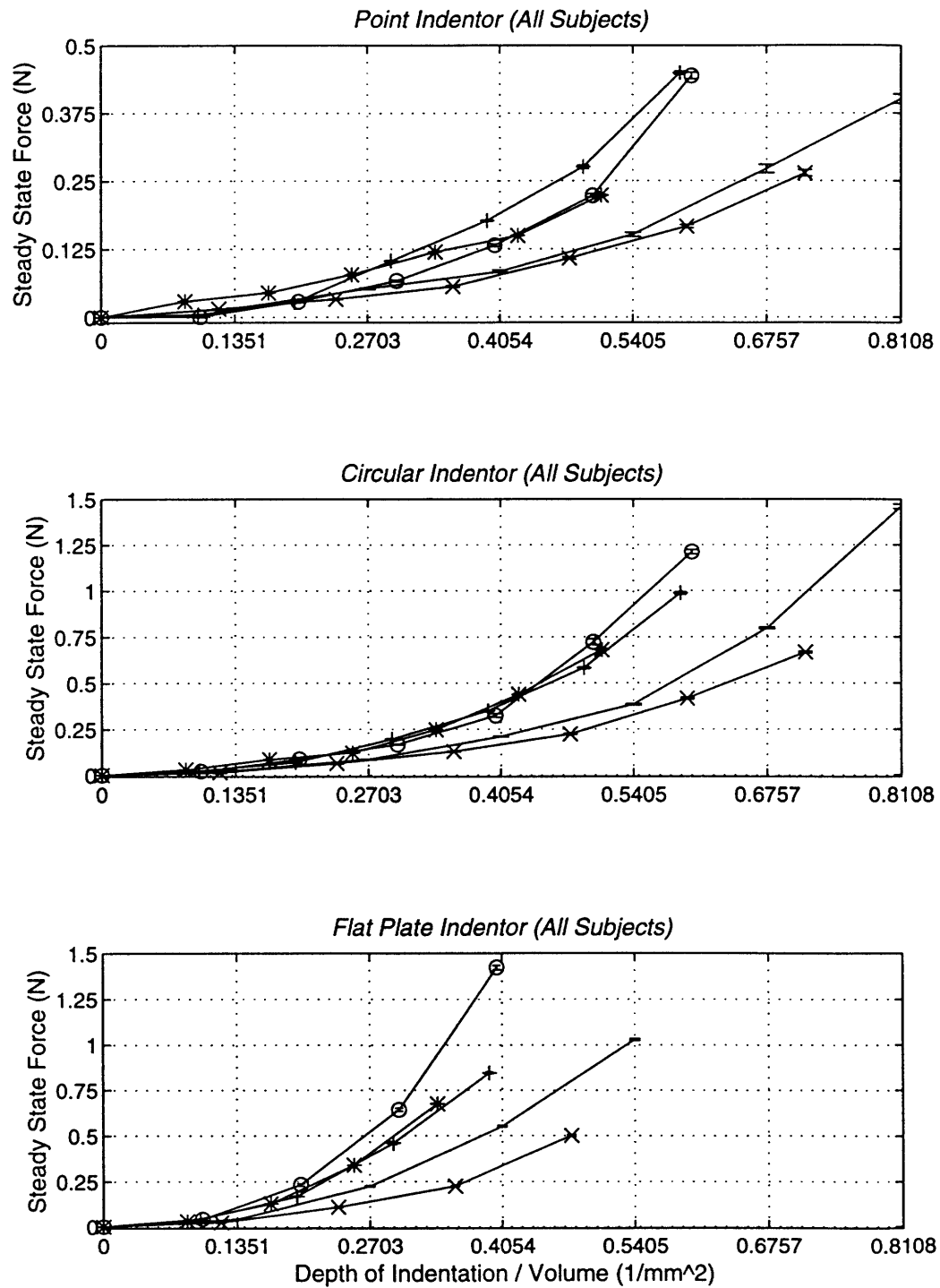
Figure 6-7 (c): Steady state force vs. depth for all subjects, normalized wrt volume.
(1 = -; 2 = o; 3 = x; 4 = +; 5 = *)
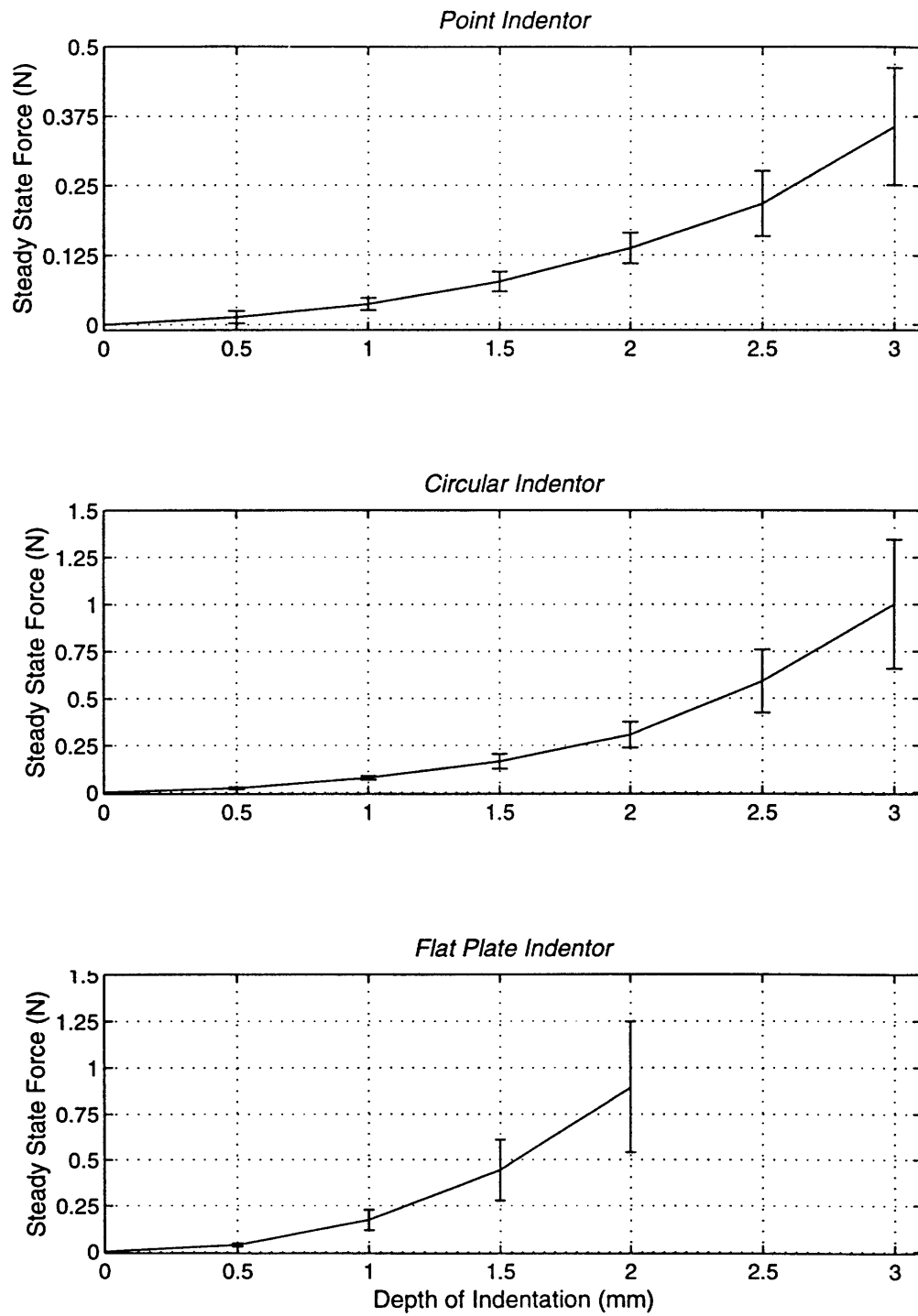
Figure 6-7 (d): Average steady state non-normalized force vs. depth with std.

Figure 6-7a again demonstrates the nonlinear stiffness of the fingertip and the relationship between magnitude and contact area/indentor shape. Clearly, at lower indentation depths, the force values were similar among subjects, while at maximum depth, the variations became more significant (variation relative to magnitude). Nonlinearity of the force response was much more pronounced for indentations with the flat plate as compared to the point indentor. Based upon the profile of indentation and area of contact argument made preceding the graphs, this phenomenon met with expectations. And, the variation in the material properties of biological tissues among subjects is most evident in flat plate steady-state data, where the two most similar subjects in both finger size and age are the most divergent in force response as depth increases (i.e. Subjects #2 and #3).

Normalization with respect to thickness and volume seemed to be a unsuccessful attempt to obtain a general, consistent force response between all 5 subjects. In fact, the mean of the data, shown in Figure 6-7d, despite the large standard deviations, was, of these, the best measure of steady state force response. Additional attempts at normalizing the data with respect to dimensions were not made in the course of this study, based on the presumption that more measurements (e.g. bone diameter) would be required to conduct a more thorough investigation of this kind. However, it was possible to normalize the data with respect to the steady state force value at the highest measured depth of indentation. This is shown following in Figure 6-7e, and for this study, it was the best solution found to normalizing subject force data. It will be utilized later during modeling efforts in Chapter 7.
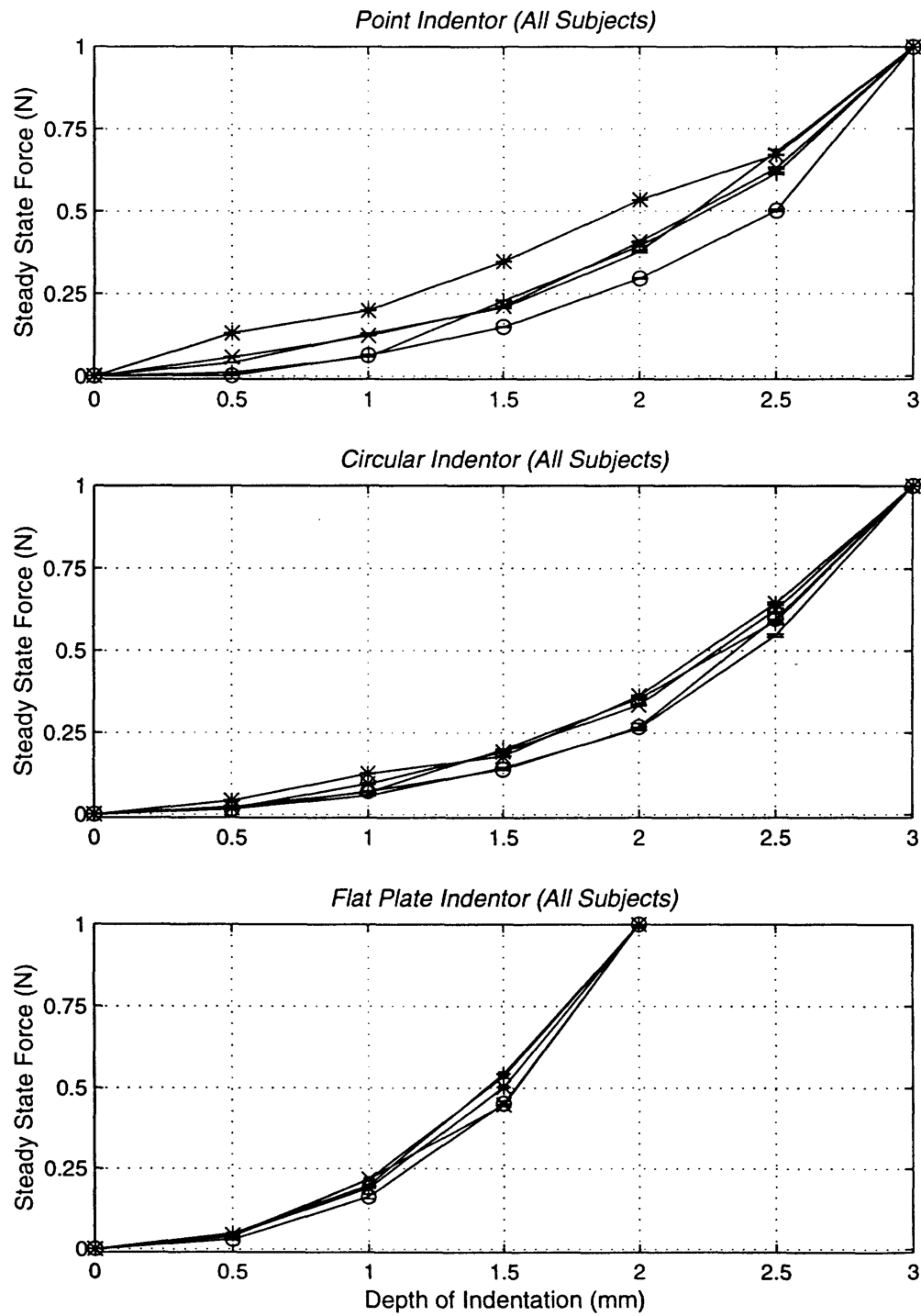
Figure 6-7(e): Steady state force vs. depth normalized with respect to steady state force at 3 mm for point and circular indentors and 2 mm for flat plate.

Normalization with respect to steady state force is clearly better at normalizing subject force with respect to depth. Unfortunately, because forces with the flat plate at 3 mm were beyond the measurable range of the stimulator force sensor, a steady state force value at 2 mm had to be used. Here, its use is shown merely to demonstrate the usefulness of this approach to normalization, which will also be used in the following chapter on modeling.

6.4 Sinusoidal Experimental Results

Substantially more dynamic data was collected, as prescribed in the protocol, but only a portion of it is shown in this chapter. It has already been evidenced that the shape or form of the force response is consistent from subject to subject. What varies is the magnitude of the response, based upon the particular mechanical and physiological properties of the individual fingers. Among the subjects, #4 seemed to fall closest to the mean, with respect to magnitude, as seen in Figure 6-5 of steady state response. Therefore, some of his sinusoidal results are presented here. In Figure 6-8, the inputs and outputs are shown in order of first increasing frequency and then increasing starting depth at an amplitude of 0.5 mm with the circular indentor on Subject #4. All of the 0.5 mm amplitude data is given in Appendix B for all indentors and all subjects. Because the 0.25 mm data was not significantly more linear or different, except in magnitude, it will not be presented in this thesis.
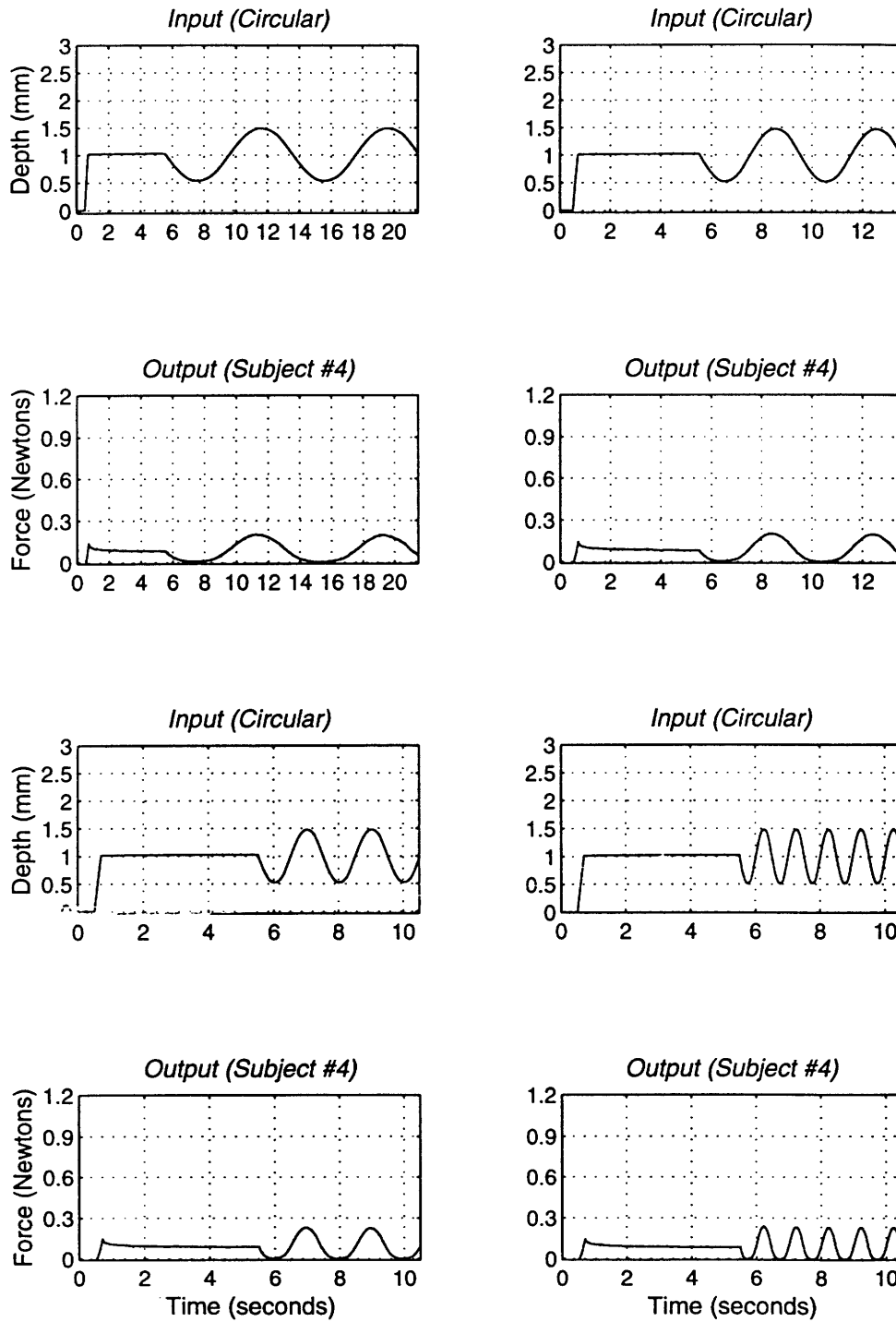
Figure 6-8 (a): Ramp/hold sinusoid results with circular indentor at 0.125 hz, 0.25 hz, 0.5 hz, 1.0 hz at 0.5 mm amplitude and 1.0 mm starting depth on Subject #4.
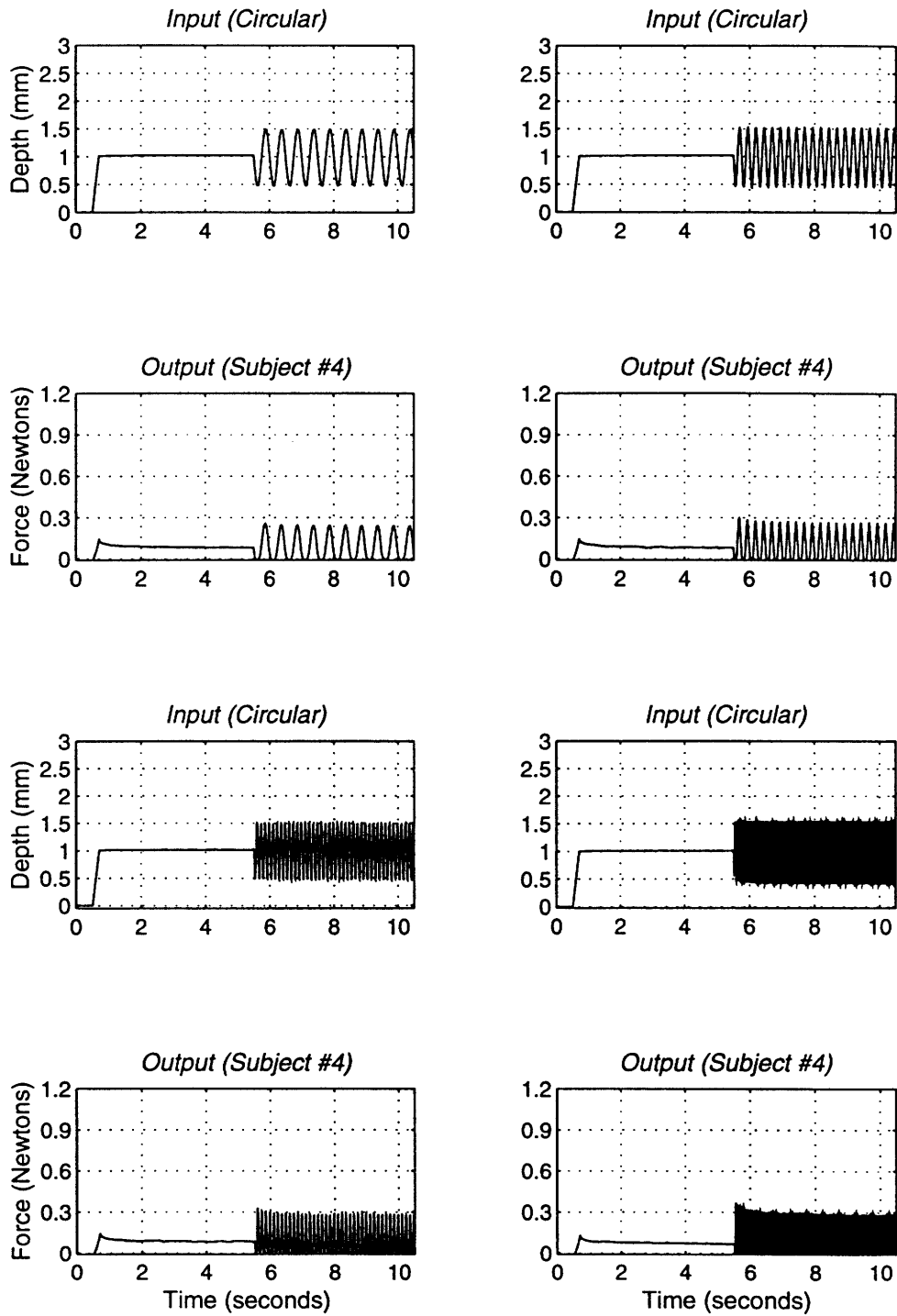
Figure 6-8 (b): Ramp/hold sinusoid results with circular indentor at 2.0 hz, 4.0 hz, 8.0 hz, 16.0 hz at 0.5 mm amplitude and 1.0 mm starting depth on Subject #4.
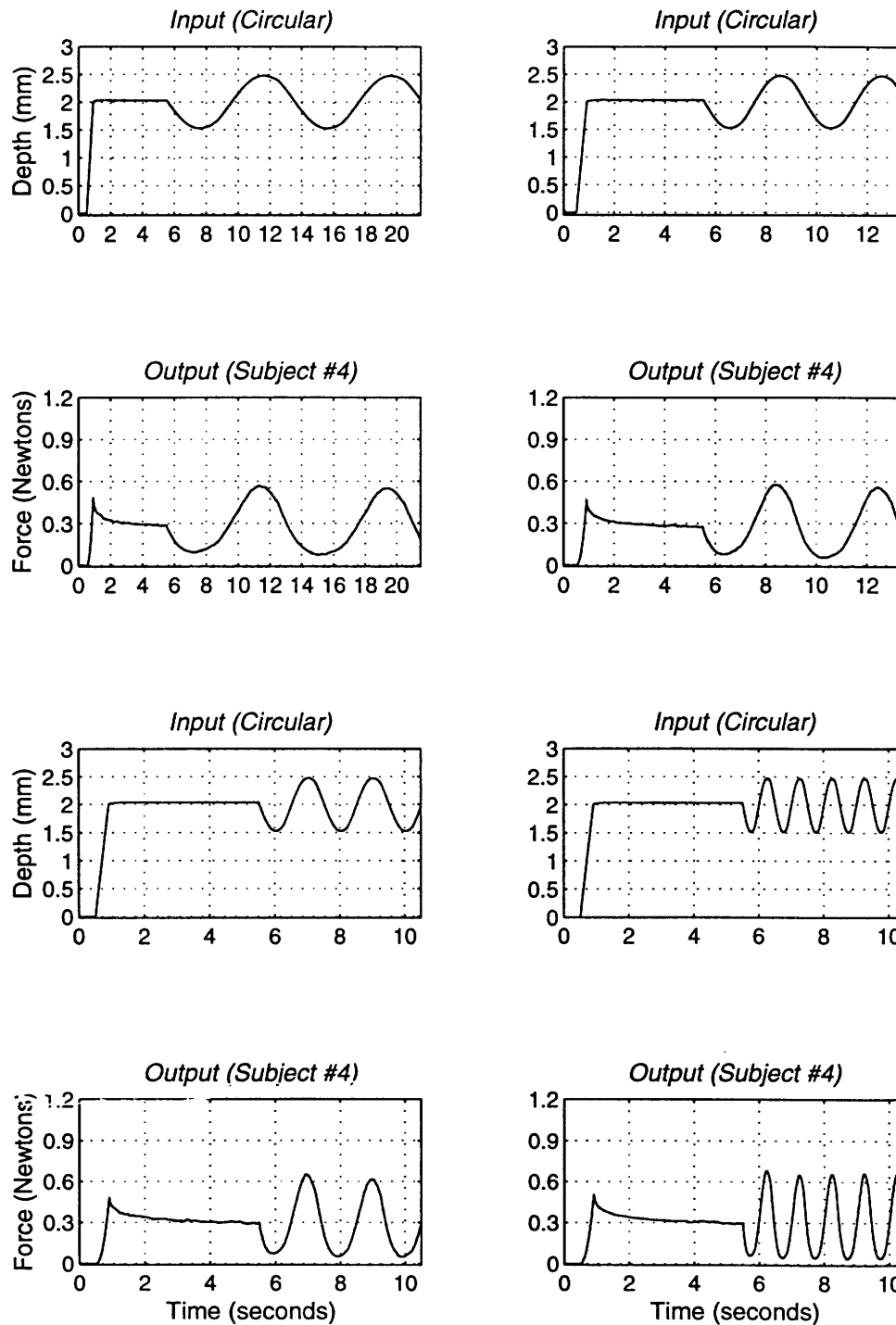
Figure 6-8 (c): Ramp/hold sinusoid results with circular indentor at 0.125 hz, 0.25 hz, 0.5 hz, 1.0 hz at 0.5 mm amplitude and 2.0 mm starting depth on Subject #4.
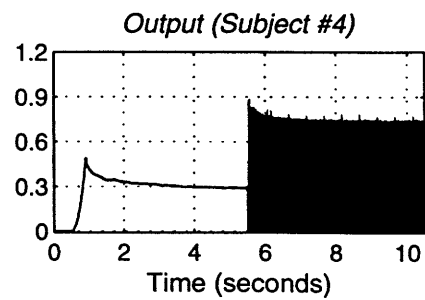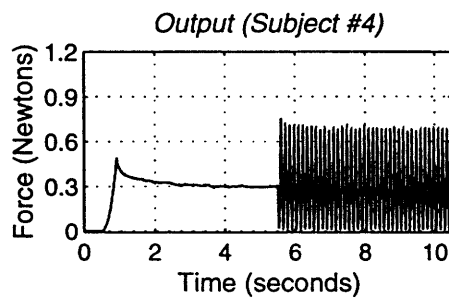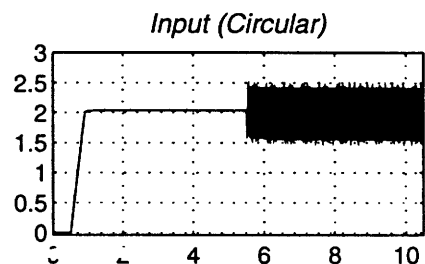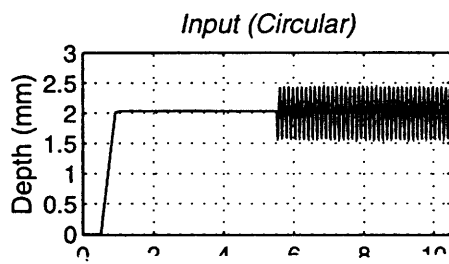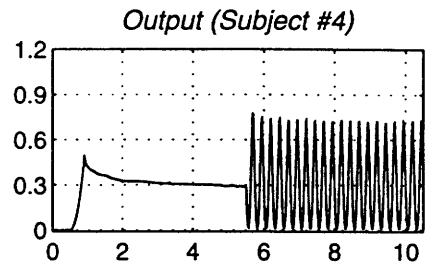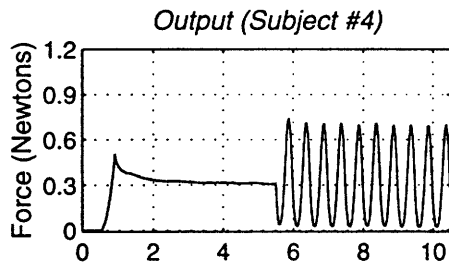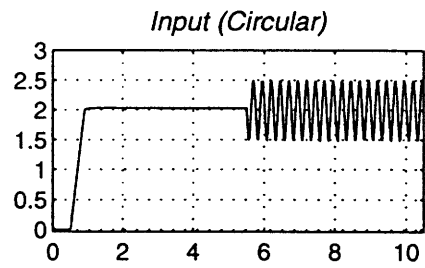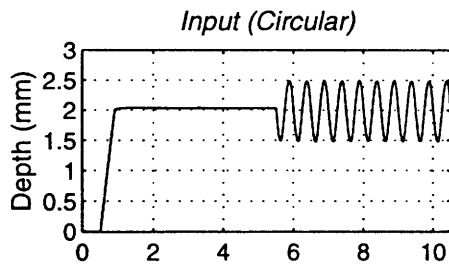
Figure 6-8 (d): Ramp/hold sinusoid results with circular indentor at 2.0 hz, 4.0 hz, 8.0 hz, 16.0 hz at 0.5 mm amplitude and 2.0 mm starting depth on Subject #4.

Again, the response data reflects the nonlinearity of the fingerpad force response to indentation. In plots of force output response, the waveforms are markedly nonlinear (i.e. the top half is not symmetric compared to the bottom half, owing partly to the nonlinear relationship between indentation depth and force). If the fundamental frequency of sinusoidal input indentation and output response are compared for phase difference, a shift of less than 10 degrees was found, in general, for all subjects and indentors. This phase analysis was performed separately in Matlab™, verifying the small order of magnitude of the shift between input and output for all indentations.

In all cases of ramp/hold/sinusoid, the fingerpad was allowed to settle almost completely to steady state force response during the hold before the sinusoids were initiated at least two full waves worth of data were recorded. Point and flat plate data look similar, though the obvious differences in magnitudes exist, and, as expected, there is more nonlinearity in the periodic output waveform with the flat plate (because of changing contact area with indentation depth). In all of the data, it is also evident that the peak to peak magnitude of the cyclic response increases monotonically with input frequency. The presence of nonlinearity in the input-output relationship implies that the standard representation in terms of plots for magnitude and phase with respect to frequency used for linear systems is not strictly applicable.

6.5 Hysteresis Representation of Dynamic Results

A feature of sinusoidal response of tissues that is often observed is the hysteresis, that is, the difference in force vs. displacement (depth) during loading and unloading. Fung (1990) states, "if the [tissue] is subjected to a cyclic loading, the stress-strain relationship in the loading process is usually somewhat different from that in the unloading process, and the phenomenon is called hysteresis." Plotting the cyclic data as

force vs. indentation depth produces a curve graphically used to describe this phenomenon. In Figure 6-9 are plots of 4 frequencies (0.125, 0.5, 2.0, 4.0 hz) at both amplitudes and starting depths for Subject #4 with each indentor, (a) point, (b) circular and (c) flat plate. The graphs contain only the response to the sinusoid (and not the response to the ramp/hold portion of these experiments). The curve of steady state force vs. indentation depth is plotted on the same axes as the zero frequency reference. All of the hysteresis curves are given in Appendix C.
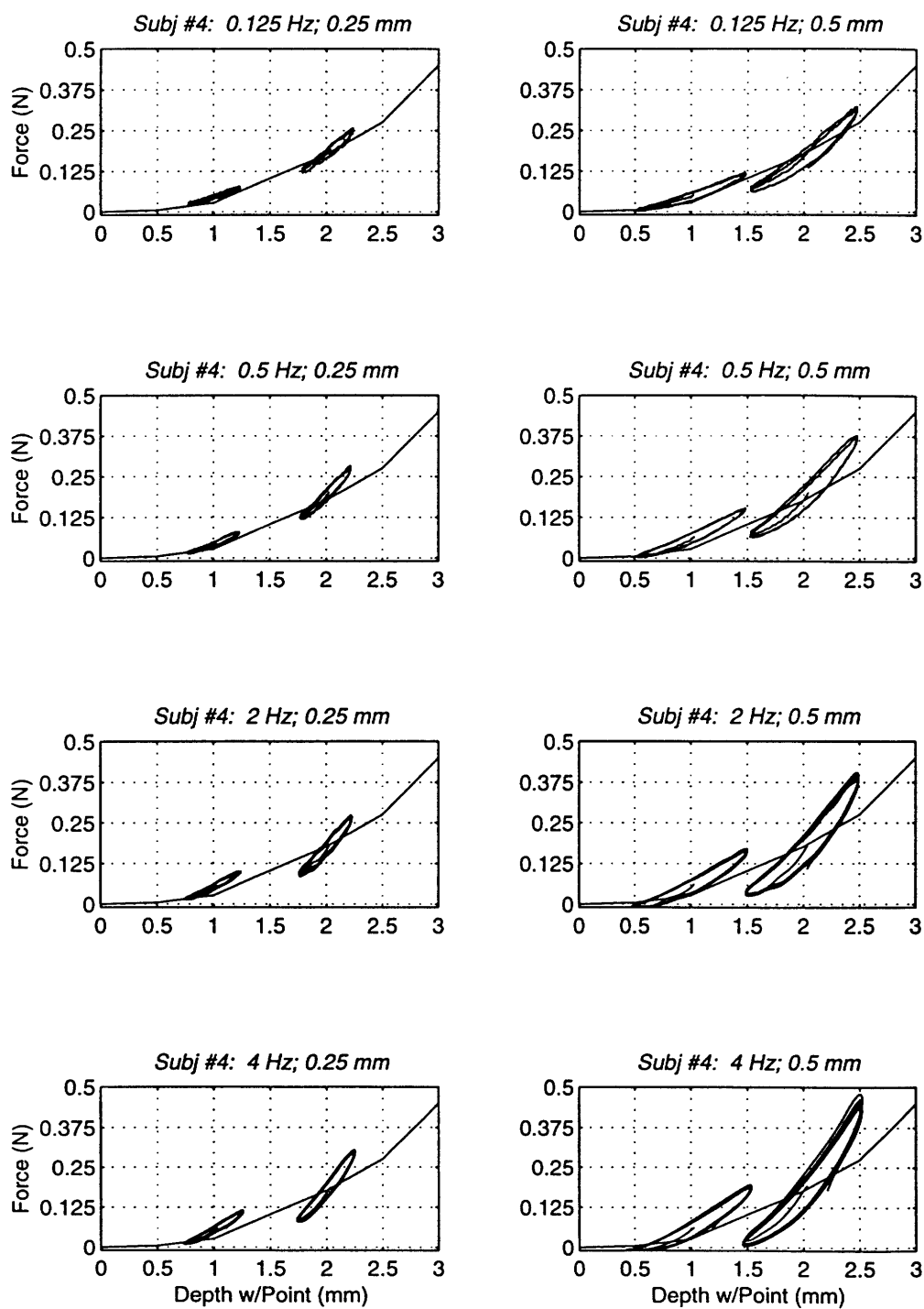
Figure 6-9(a): Hysteresis curves for 4 frequencies on Subject #4 with point indentor.
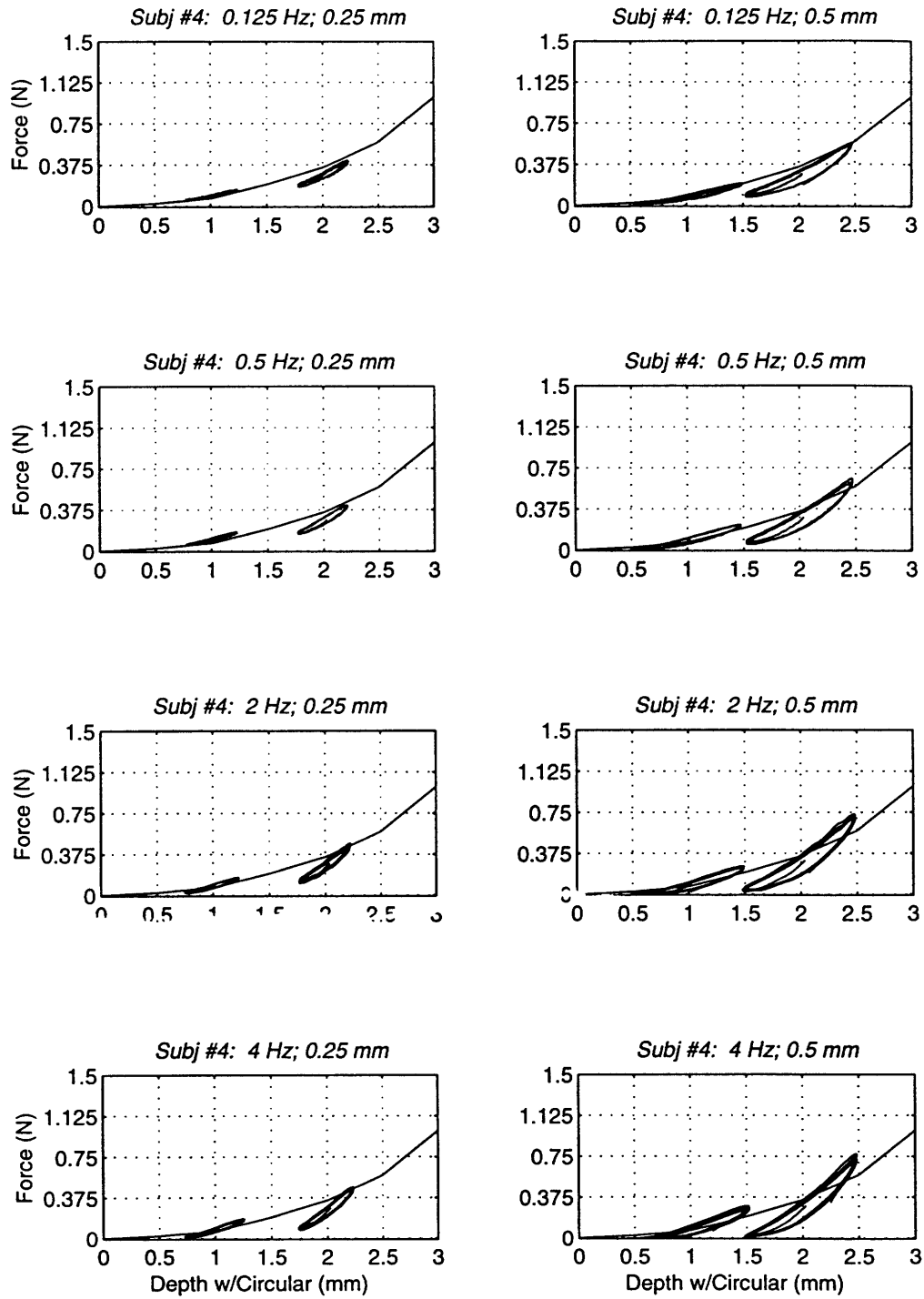
Figure 6-9 (b): Hysteresis curves for 4 frequencies on Subject #4 with circular indentor.
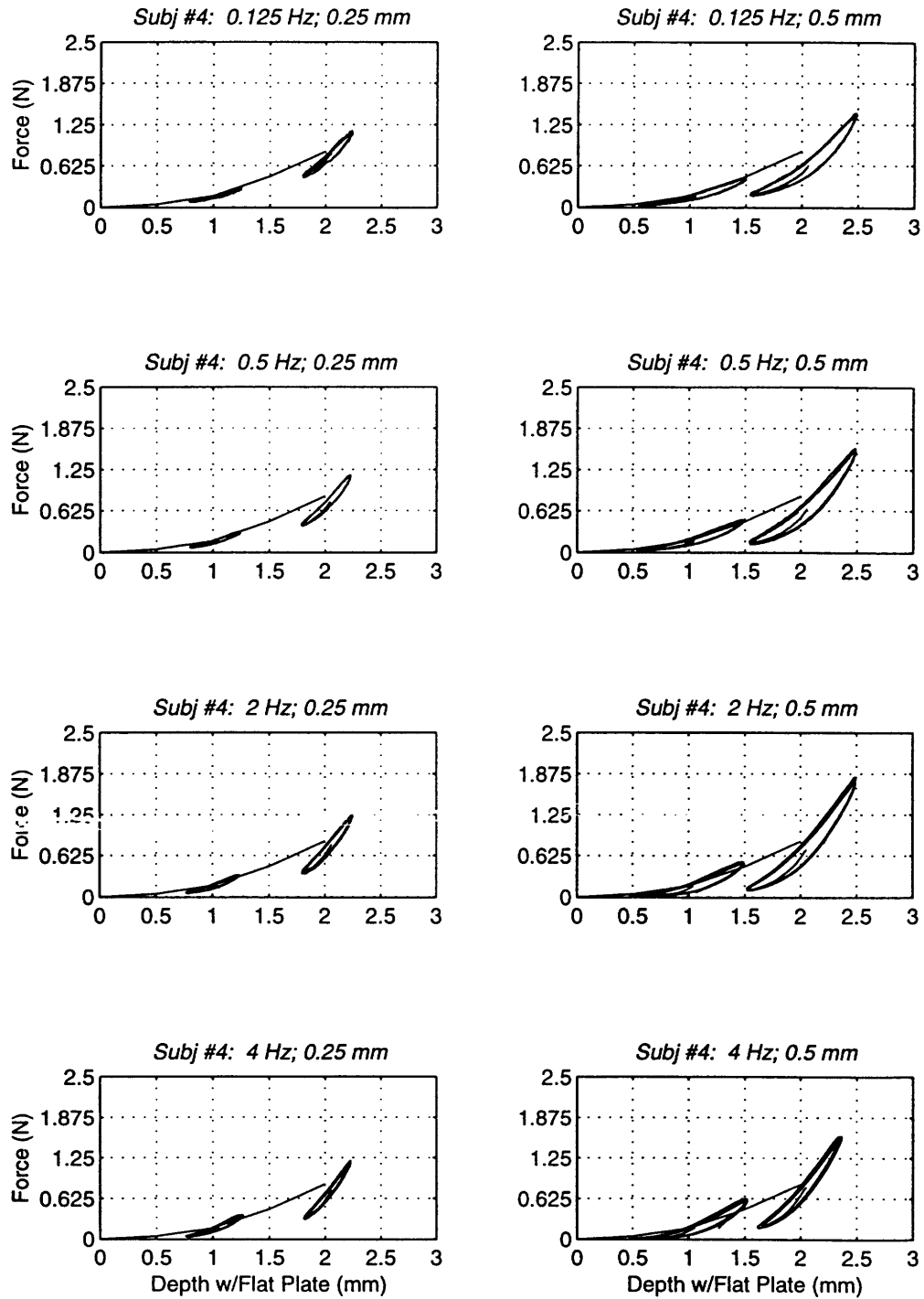
Figure 6-9 (c): Hysteresis curves for 4 frequencies on Subject #4 with flat plate.

What is evident from these curves is the increase in magnitude and slope of the response with respect to indentation as a function of frequency. Matlab™ was used to obtain (1) the ratio (percentage) of the area within the hysteresis curve to the area under the mean of the loading and unloading portions of the hysteresis, and (2) the average slope of loading and unloading portion as functions of frequency and amplitude. Slope was chosen as a measure of stiffness, while "percentage hysteresis" was a measure of magnitude of energy lost. In linear system analysis, this percentage can be used to calculate a "hysteresic damping coefficient." Slopes were determined with a simple line-fitting routine that obtained the best fit using local minima to both the loading and unloading portions of the hysteresis curve. The average of the loading and unloading slopes were then recorded at each frequency in units of N/mm (which translates to stiffness). Area was found discretely by summing the trapezoidal areas under discrete steps of the loading and unloading curves. Area of the hysteresis was then derived as the difference between the area under the loading and unloading curve with units of N*mm. Average area logically followed as the mean of the areas under the loading and unloading curves. In the following figure, the "percentage hystereses" and the slopes of the hystereses are plotted at all frequencies for three indentors and both amplitudes (solid = 0.5 mm; dashed = 0.25 mm) for Subject #4 at each of the two starting depths (1mm and 2mm).
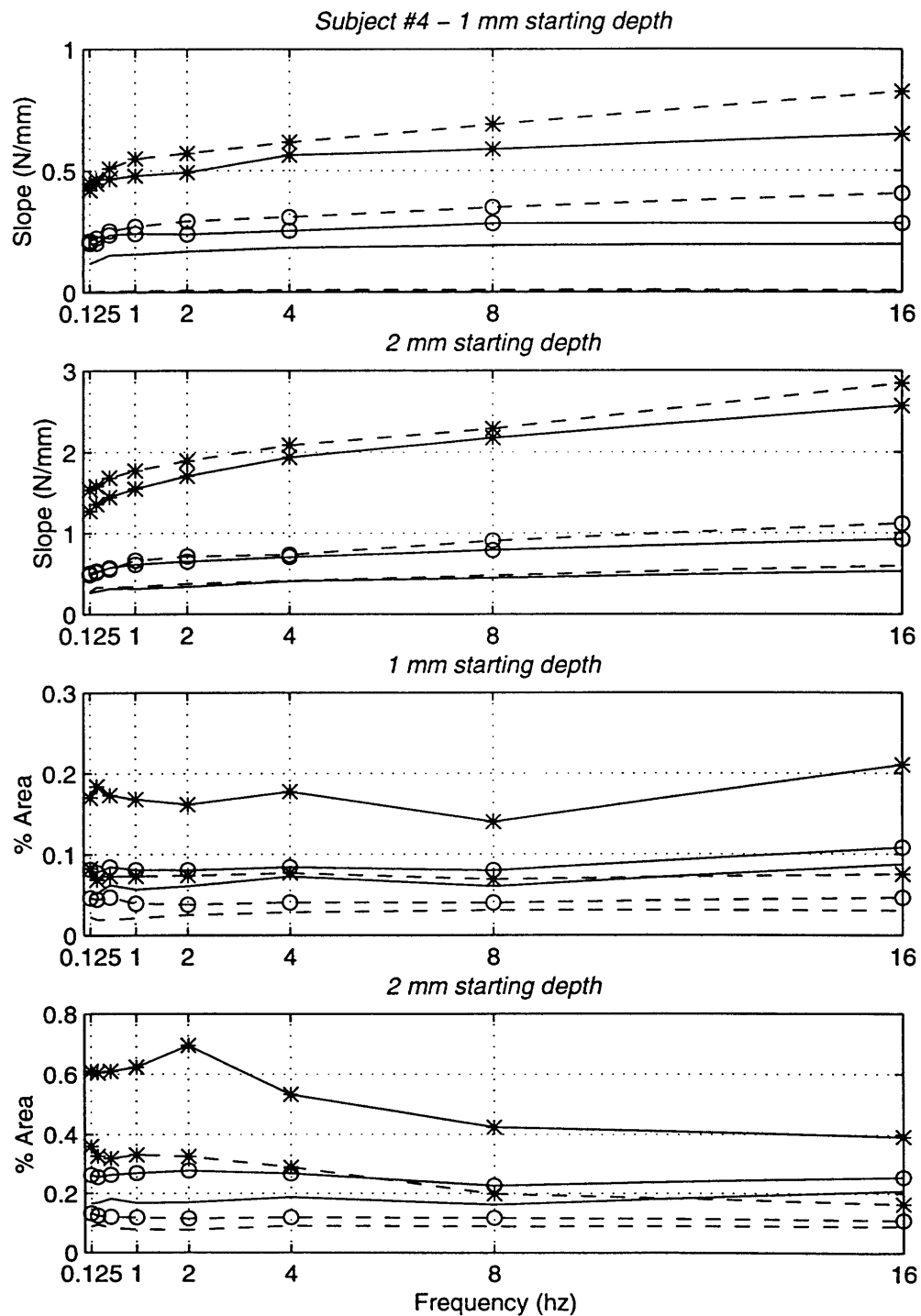
Figure 6-10: Slope and percentage area of hysteresis (versus steady state area) from Subject #4 at 1mm and 2mm starting depths. Solid lines represent 0.5 mm amplitude data; dashed are 0.25 mm amp. Point markers signify point indentor; circles are circular; stars are flat plate data.

6.6 Discussion of Results and Conclusions Drawn

The combination of data from the ramp/hold and sinusoid experiments yielded a great deal of information about some basic properties and mechanical characteristics of the human fingerpad. In addition, the first order processing of the data served to isolate trends and provide insight into future strategies of modeling and normalization. This section discusses some of the conclusions drawn about the nonlinearity and viscoelasticity of the pulp, which will lead into approaches for system analysis and modeling.

The "hold" data immediately direct attention to the nonlinearity of force response with respect to linear indentation stimuli given with any of the three indentors. It is hypothesized that this nonlinearity is due to the anatomical structure of the fingerpad as a multilayered, curved surface that can be approximated to a first-order as a water-filled sac or waterbed (Srinivasan, 1989). The first observation is that the area of fingerpad tissue compressed during indentation is not always solely a function of the contact area at the skin/indentor interface. Proof of this is evident in that the point and circular indentors form a noticeable "crater" during indentation. The projected total area of the "crater" increases with depth. Similarly, though the flat plate forms no crater, contact area between the plate and skin increases relative to indentation depth. If the fingertip is further modeled as a bed of springs, increasing the area of tissue compressed increases the numbers of springs compressed and therefore increases total force. What follows is that force is, in some part, a function of "area compressed," which in turn is nonlinearly related to indentation depth. Additionally, based upon knowledge of the *multilayered, nonhomogeneous* composition of the pulp, there exists an inherent characteristic nonlinearity. This combined nonlinearity appears to be more pronounced with the flat

plate as opposed to the point indentor. This is again at least partially explained by the steeper increase in area of material compressed as a function of depth. There is also much more variation among subjects with the flat plate than with either the circular or point. Differences in curvature among fingers can likely help to explain this, since shape clearly affects total contact area. To demonstrate, the two fingers that are most varied in force response with the flat plate are the two most similar in size (Subjects 2 and 3 in Figure 6-7). Such variation in material properties will be a significant obstacle in forming any type of universal fingertip model.

The force response during ramp indentation (constant velocity) reveals the viscoelastic behavior of the fingerpad. It was noted that velocity of indentation appears to play no direct observable role in steady state force during steady indentation after the ramp. The fingertip does, however, respond directly to the rate of indentation. The force response to the indentation ramp, in all cases, rose nonlinearly to some peak that was sometimes more than twice as great as the corresponding steady state force at the particular depth. During "hold," the force decayed to steady state force at some rate of decay that seemed to be nearly exponential. All of this indicates some rate dependence of fingertip force response in addition to its inherent elasticity, which implies that the pulp needs to be considered a viscoelastic material.

The collected dynamic data both validates the claim that the fingerpad behaves viscoelastically and is nonlinear and provides new insights into the effects of increasing frequency of stimulus. The sinusoid data itself was distinctly asymmetric and hence, nonlinear. That is to say, the response to the sinusoid waveform input was an asymmetric waveform resembling a sine wave but with a larger top "half." More importantly, though, magnitude of the response waveform increased according to frequency. The phase shift between input and output was declared from the analysis described earlier in this chapter to be small (<10°). Hysteresis data revealed increasing slope, and therefore

increasing stiffness, with frequency. At this time, no conclusions were drawn from plots of percentage area aside from the what seems to be a convergence of loading and unloading paths as frequency increases.

These trends of nonlinearity, viscoelasticity and change in output magnitude and finger stiffness with increasing frequency are discussed further in the following chapter as part of the modeling process. Subject to subject variability poses some problem in forming a general model to fit *any* finger, and this topic will be dealt with as best as possible in the next chapter using normalization with respect to steady state force. Nonlinearity of the fingerpad force response to indentation makes sense based upon the multilayeredness of the material and differences in tissue layer properties as well as the increase in the area of material compressed with the given indentor. The physical origin of frequency dependent response is somewhat less clear. But, all of the features noted will be well captured by the model constructed based on this characteristic response.

Chapter 7

Models of the Mechanical Response

Using conclusions drawn from the experimental results and additional analysis and parameter estimation, the characteristic force response of the human fingerpad to indentation was fit with an "approximated" nonlinear viscoelastic mechanical model. The fingerpad clearly exhibits viscoelasticity in that the tissues respond to both deformation and rate of deformation. This chapter draws upon three traditional viscoelastic spring and dashpot models (Figure 3-1) and compares each to the basic form of the indentation force response. The Kelvin model matched the data best only after a series of refinements to account for system nonlinearities and a check of the contribution of inertial elements (masses). At the culmination of this system analysis, a nonlinear Kelvin model is proposed, though due to the complexity of nonlinear modeling, it was further approximated with a series of piecewise linear blocks. Model parameters are estimated for the set of subjects and indentors, and the predictions of force response are compared to the experimental data.

7.1 Viscoelastic Linear Models

The first stage in the modeling process was to compare the ramp/hold response of several linear viscoelastic models to the form of the data presented in Chapter 6. Three mechanical models, mentioned earlier, are common to the discussion of viscoelastic behavior (Fung, 1990). They are shown again in Figure 7-1 for reference.
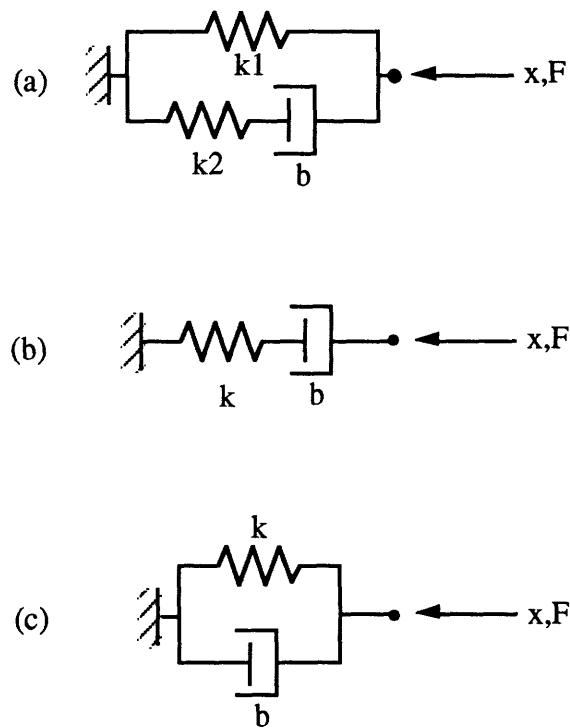
Figure 7-1: (a) Kelvin body; (b) Maxwell body; (c) Voigt body.

The three models are composed of two types of elements--a spring and a dashpot. The linear spring produces instantly a force proportional to the deformation. The dashpot produces a load proportional to the velocity imposed. Without derivation, the constitutive equations for the respective models are:

$$F = kx + b\dot{x} \quad \text{(Voigt Model)} \tag{7-1}$$

$$\frac{\dot{F}}{k} + \frac{F}{b} = \dot{x} \quad \text{(Maxwell Model)} \tag{7-2}$$

$$\frac{b}{k_2}\dot{F} + F = k_1 x + b\left(1 + \frac{k_1}{k_2}\right)\dot{x} \quad \text{(Kelvin Model)} \tag{7-3}$$

Of interest in this study are the relaxation functions of these models, that is, the force response to a step change in deformation. These will give insight into how well each model approximates the phenomena occurring in the fingertip during ramp/hold indentation. Figure 7-2 depicts the relaxation functions of the three models.
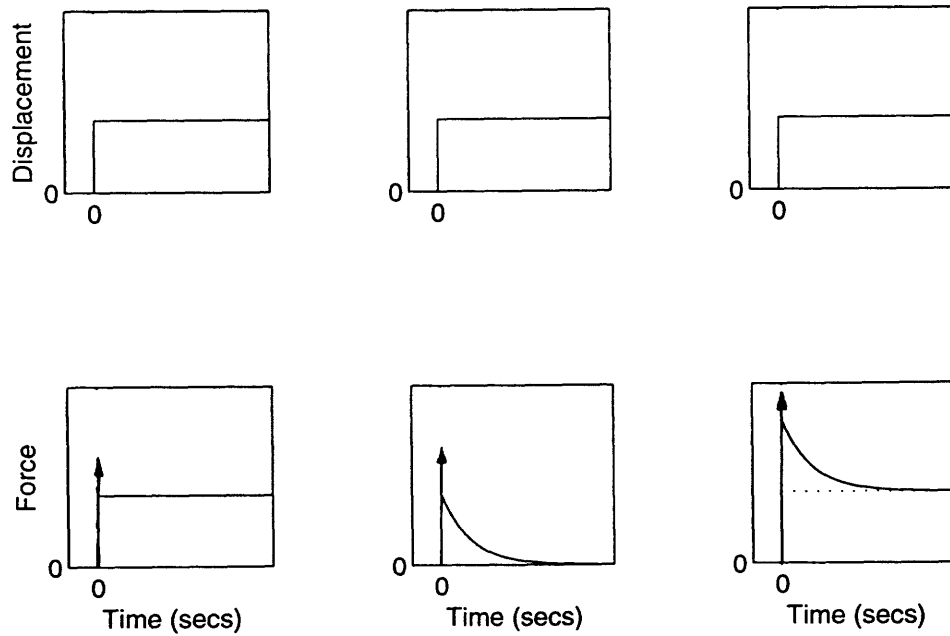
Figure 7-2: Relaxation functions for Voigt, Maxwell and Kelvin models.

Referring back to Figure 6-6 of the results of fingertip indentation to ramp/holds, there is clearly a peak force at the end of the ramp and then a decay to some non-zero force. A

step, which is an instantaneous ramp up, produces a similar response only in the Kelvin model, which is also sometimes referred to as the Standard Linear Model in the context of the biomechanics of tissues (Fung, 1990). Because the relaxation function of the Kelvin block matches the general form of relaxation in soft tissues, it is more commonly utilized in their modeling. However, a simple, linear Kelvin block is typically not able to predict well the dynamic (sinusoid) response of tissue. Fung proposes instead a model composed of a spring in series with an infinite number of Voigt blocks. However, because of the extent of parameter estimation that would be involved in such a model, it did not seem to be a realistic first approach. The logical next step was instead to modify the Kelvin model to better match the static and dynamic experimental data.

7.2 Refining the Kelvin Model

Nonlinearities in fingerpad force response to indentation were described in the previous chapter, and to account for these characteristic features, they required revision of the linear Kelvin Model. This process began by analyzing steady state data. In the Kelvin model, the steady state force response to static indentation reduces to a function of only the parallel single spring element, k_1. Static response data plotted in Figure 6-7 demonstrated obvious nonlinearity, which could be fit with a third order polynomial of the form:

$$F = k_3 x^3 + k_2 x^2 + k_1 x + k_0 \tag{7-4}$$

In representing the mechanical behavior of the fingerpad where there is no initial force before indentation, k_0 is 0. Similarly, all remaining constants are positive, because any indentation produces an opposing force. A polynomial curve fitting function was written

and implemented in Matlab™ to estimate the parameters for equation (7-4) that fit the steady state curves from Figure 6-7 (a). The parameters of nonlinear springs which match the static force response to indentation for Subject #4 are listed below.

	k_3	k_2	k_1	k_0
Point	0.0111 N/mm^3	0.0078 N/mm^2	0.0245 N/mm	0
Circular	0.0020	0.0974	0.0020	0
Flat Plate	0.0314	0.1488	0.0020	0

Table 7-1: Nonlinear spring parameters for Subject #4.

A refined Kelvin model was formed with a nonlinear spring identified for each indentor geometry. This model is reconstructed and labeled in Figure 7-3.
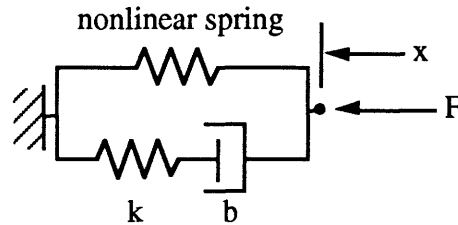
Figure 7-3: The new model, replacing the parallel linear spring with a nonlinear one.

The experimental data was analyzed further to determine whether a model of the form shown in Figure 7-3 could match dynamic response characteristics reasonably well. The force response of the Kelvin block to indentation is the sum of the responses of (1) the parallel spring or, in this case, the nonlinear element and (2) the series spring and dashpot. The parallel spring fully accounts for the non-zero steady state force value. The spring and dashpot account for the peak rise above steady state force during ramp indentation and the subsequent decay during "hold" (see Figure 6-6). The response of the

100

series spring and dashpot must therefore fit the difference between the experimental data and the predicted response of the nonlinear spring element. This difference, when plotted, however, was clearly seen to be nonlinear. Systematic observation of components of the data further indicated that this portion of the response was nonlinear with respect to both depth of indentation and velocity of indentation. In other words, observing again the difference between experimental response and that of the modeled nonlinear spring element, what could also be seen to vary nonlinear with respect to depth and velocity or frequency of indentation. Thus, a *nonlinear* spring and dashpot combination in parallel with a nonlinear spring as modeled above was required to predict the fingerpad's mechanical response. Because a spring and dashpot combination in series produces at least a first order differential equation (see Maxwell model), it was far more complicated to "nonlinearize" the second link.

Some time was invested in exploring the complexity of a nonlinear series spring and dashpot. To start, the spring of the Maxwell link was modeled with several nonlinear forms, including a polynomial relation such as that given in equation 7-4. Similarly, the dashpot was modeled with forms such as $F = bx\dot{x}$. The difficulty lay in that the characteristic equation relating force and displacement of any nonlinear series spring-dashpot link would require solving at best a first order nonlinear system. The task of simulating nonlinear systems and performing the corresponding parameter estimations of the models was viewed as being much more computation and time intensive that was desirable for a first run of modeling. Other approaches were therefore required in order to model the nonlinear system with linear elements.

Another aspect of the model that was briefly investigated was the possible contribution of the mass of the finger and the subsequent necessity of its presence in the model. Mass was added first to the linear Kelvin block to analyze the type of effect it would have on phase and magnitude of the response. Two forms of the models tested are

shown below in Figure 7-4 with corresponding magnitude and phase shift of the mass combined with the series spring and dashpot (bold-faced lines).

$$|H(j\omega)| = \frac{\sqrt{(\omega k - \omega^3 m)^2 + \left(\dfrac{-\omega^2 mk}{b}\right)^2}}{\sqrt{\omega^2 + \left(\dfrac{k}{b}\right)^2}}$$

$$\angle H(j\omega) = 180° + \tan^{-1}\left(\frac{\omega k - \omega^3 m}{-\omega^2 mk / b}\right) - \tan^{-1}\left(\frac{\omega b}{k}\right)$$

$$|H(j\omega)| = \frac{\omega^3}{\sqrt{\left(\dfrac{\omega}{m} - \dfrac{\omega^3}{m}\right)^2 + \left(\dfrac{\omega^2}{b}\right)^2}}$$

$$\angle H(j\omega) = -90° - \left[180° + \tan^{-1}\left(\frac{\dfrac{\omega}{m} - \dfrac{\omega^3}{k}}{-\dfrac{\omega^2}{b}}\right)\right]$$
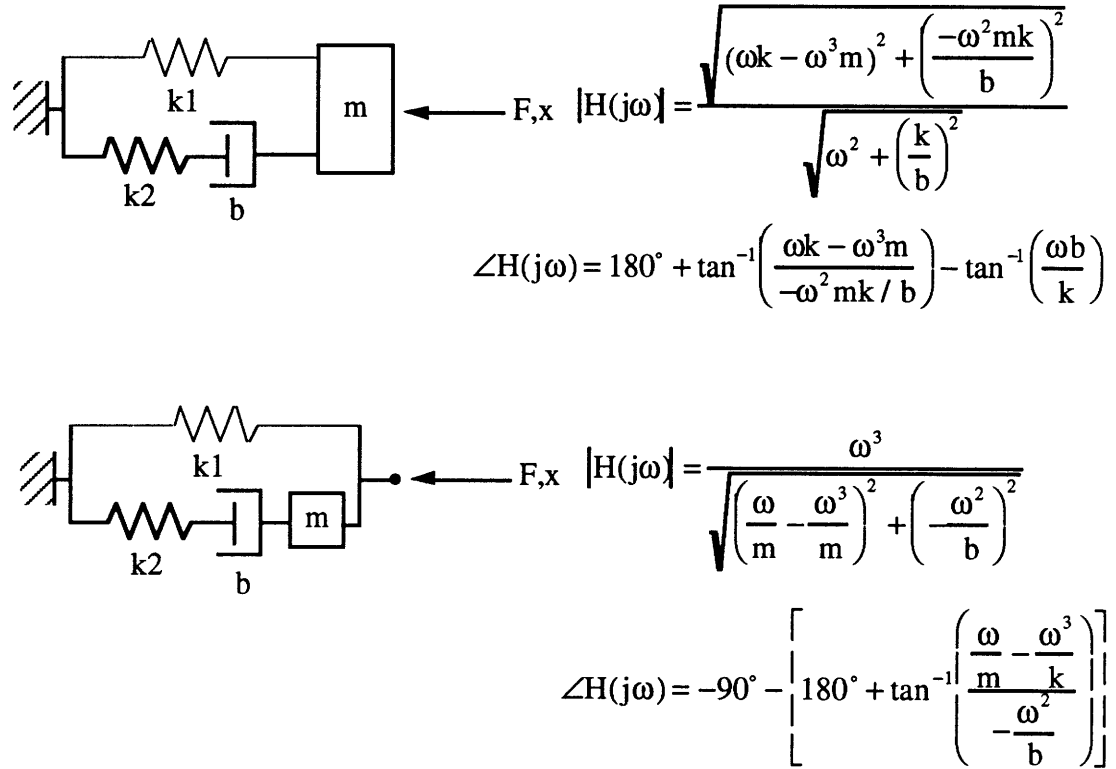
Figure 7-4: Proposed linear Kelvin models with mass added at different locations.

Based upon estimates of fingertip mass (using the density of water and the measured volumes as a crude first approximation) and some estimates of k and based upon ramp/hold data, it was evident that for mass to contribute to magnitude of the model response it would also have to add a significant phase shift of between 90° and 180°. Clearly, this would not match experimental data which show a much smaller phase shift on the order of 10° or less (see previous chapter).

7.3 The Piecewise Linear Kelvin Model

The modeling technique that proved successful was the attempt to approximate a Kelvin model composed entirely of nonlinear elements with a series of piecewise linear blocks. A piecewise linear approach to modeling a nonlinear system seeks to separate the response curve into linear portions that can be more easily handled computationally. The proposed nonlinear model (simplified) is depicted below in Figure 7-5.

nonlinear spring

$\longleftarrow$ x

$\longleftarrow$ F

nonlinear spring + dashpot
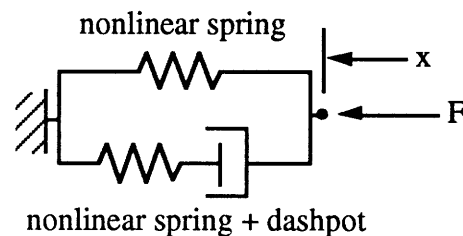
Figure 7-5: Proposed nonlinear model to predict fingerpad force response.

In theory, a model of the general form shown above can predict the observed force responses. Such a model would need to be composed of elements with spring and dashpot coefficients matched to the type of indentor being used. What this model does not possess is the ability to account internally for differences in indentor geometry. In other words, even if we were able to compose an easily solvable function for the nonlinear Maxwell link in the Kelvin model and estimate parameters such that the model response fit with experimental data, a new set of parameters must be defined for each indentor type used as well as for each finger tested. An immediate goal is to generalize the model across subjects, a process dependent upon biological variations and how well experimental data can be normalized (see previous chapter). However, it is not as readily apparent how to create parameters or coefficients for the model that will be valid for all indentors. For that to work with this modeling approach, it will be necessary to further

refine the model into a "bed" of parallel nonlinear blocks. Such a multiple degree of freedom model is essentially a lumped parameter approximation to the continuum mechanics of the fingerpad. For the time being though, a one degree of freedom model (Figure 7-5) is used as a basis for representing fingerpad mechanics, but specific sets of parameters will be given for each indentor type. Part of the reason for limiting the analysis in this way is based upon the fact that experimental data yields only net displacement and force response in the fingerpad as opposed to a distributed loading profile.

The next logical step in the modeling process was to determine a method of simulating a nonlinear Kelvin block as a series of linear Kelvin blocks. The model proposed is shown in Figure 7-6 below.
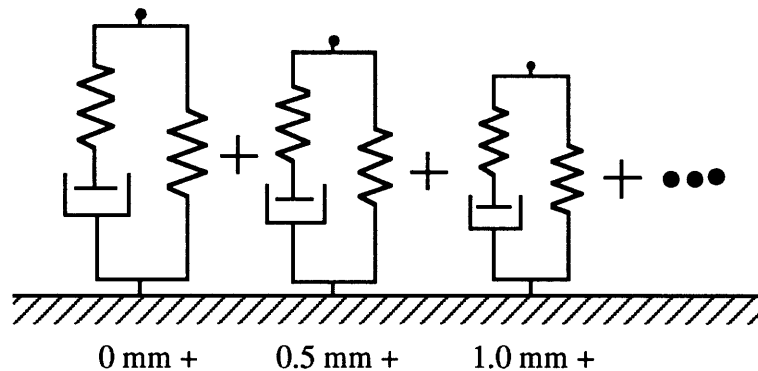
Figure 7-6: Piecewise series of linear Kelvin blocks.

As indentation commences, one linear Kelvin block is compressed. When depth reaches 0.5 mm, a second block begins to deform, its response summing with the first and so on in 0.5 mm increments. This method attempts to approximate a nonlinear response, and can do so with increasing accuracy as step size (in this case 0.5 mm) is decreased and corresponding number of blocks increased. Because static response data was acquired only in half millimeter increments, 0.5 mm was chosen as the step size for the piecewise

model as well. In this approach, the elements within each block of the model are linear, allowing for greater ease in simulations and parameter estimation.

Matlab™ was utilized to perform curve-fitting and parameter estimations in order to identify the coefficients of a piecewise linear Kelvin model of fingerpad force response. Because the depth of indentation during sinusoidal stimuli never exceeded 2.5 mm during the experiments, only five blocks were used in the final model, each successively activated at 0.5 mm increments of indentation depth (i.e. 0 mm, 0.5 mm, 1.0 mm, 1.5 mm, 2.0 mm). This created a set of 15 unknown parameters for the model. Preliminary estimations were performed on the single parallel spring elements of each block by matching the summed piecewise response of the 5 springs to the static indentation data (Figure 6-7) with the same curve fitting and local minimization of model parameters used for the polynomial fitting approximations. Then, referring to the characteristic equations relating force to displacement for the Kelvin model (see equation 7-3) and its derived transfer function (LaPlace Transform), Matlab™ could be used to perform a discrete time simulation of the piecewise Kelvin block system given some arbitrary set of starting parameters. In the simulation, the leftmost block according the previous figure would experience the full indentation. The second would begin to experience indentation after displacement of the first reached 0.5 mm, and so on. Because indentation was measured only at the contact surface in the experiments, it was assumed that all blocks follow the sinusoidal path, though none of the blocks can extend beyond their initial points to experience tension. The measured force response indicated that the indentor never left the contact surface significantly even at the highest frequencies. Therefore, the model is assumed to have followed the indentation time profiles, which must have lower slopes than the model's relaxation rate.

The precise protocol used for simulating the model and estimating parameters consisted of several important steps designed to create a generalized model of fingerpad

mechanical response for each indentor used in the experiments. For each subject and indentor combination, ramp/hold/sinusoid data was loaded at both starting depths (1 mm and 2 mm), 0.5 mm amplitude and all frequencies. Because it was desirable to generalize a model across subjects, response data was normalized with respect to maximum recorded steady state force (see Figure 6-7 (e) and following explanation). The model response for some initial set of parameters was computed using the discrete time simulation of the piecewise linear Kelvin blocks. In this case, preliminary values of the parallel spring element were those calculated from the static data. The remaining values were set to some arbitrary value on the same order of magnitude as the parallel spring coefficients. Then, Matlab™ performed a curve fitting routine that iterated the model parameters until the error between the experimental set and model set was locally minimized. For each indentor, the five sets of three parameters for the five subjects was averaged. The entire procedure was then repeated with this mean set of parameters as the starting values of the local minimization procedure. This was designed to produce parameters for a model that predicts the "normalized" force response of each subject's fingerpad to a given indentation. The final set of parameters for the circular indentor is shown below in a table for each of the five subjects. Note again that the force predicted by the model must be multiplied by the steady state value of force at 3 mm for the circular and point indentors and at 2 mm for the flat plate to determine the normal force response.

	Subject 1	Subject 2	Subject 3	Subject 4	Subject 5
k_{p1}	0.0523	0.0325	0.1232	0.0411	0.0566
k_{s1}	0.0198	0.0218	0.0041	0.0002	0.0176
b_{s1}	0.1410	0.0198	0.1594	0.1033	0.0447
k_{p2}	0.0000	0.0826	0.0087	0.0840	0.0825
k_{s2}	0.0933	0.0420	0.0970	0.0838	0.0688
b_{s2}	0.0657	0.0001	0.0514	0.0461	0.0294
k_{p3}	0.0652	0.0844	0.0359	0.0294	0.1078
k_{s3}	.02386	0.2396	0.2523	0.2252	0.1732
b_{s3}	0.0112	0.0107	0.0053	0.0075	0.0649
k_{p4}	0.0495	0.1260	0.0610	0.0491	0.0493
k_{s4}	0.0000	0.1503	0.0893	0.1105	0.0533
b_{s4}	0.2553	0.0981	0.1991	0.4857	0.1794
k_{p5}	0.2747	0.3896	0.3320	0.2214	0.1588
k_{s5}	0.3932	0.3330	0.2276	0.2751	0.3742
b_{s5}	0.5230	0.7652	0.0306	0.1114	0.7826

Table 7-2: Piecewise Kelvin block model parameters for circular indentor by subject.

Despite attempts to normalize the response data and acquire a set of constant parameters across subjects, there is still noticeable variation down the table. A significant amount of the error can be attributed to whatever method Matlab™ used to minimize error locally between model and real response. Additionally, despite normalization, there still exists variation in subject data (see Figure 6-7 (e)). Following are plots of data predicted by the model (solid line) vs. experimental data (dotted lines) for Subject #1 with the point indentor, Subject #4 with circular and Subject #5 with the flat plate at one depth and amplitude. Predicted data is computed from the parameter set for the particular subject. And for higher frequencies, only the first few waves of indentation are shown for clarity.
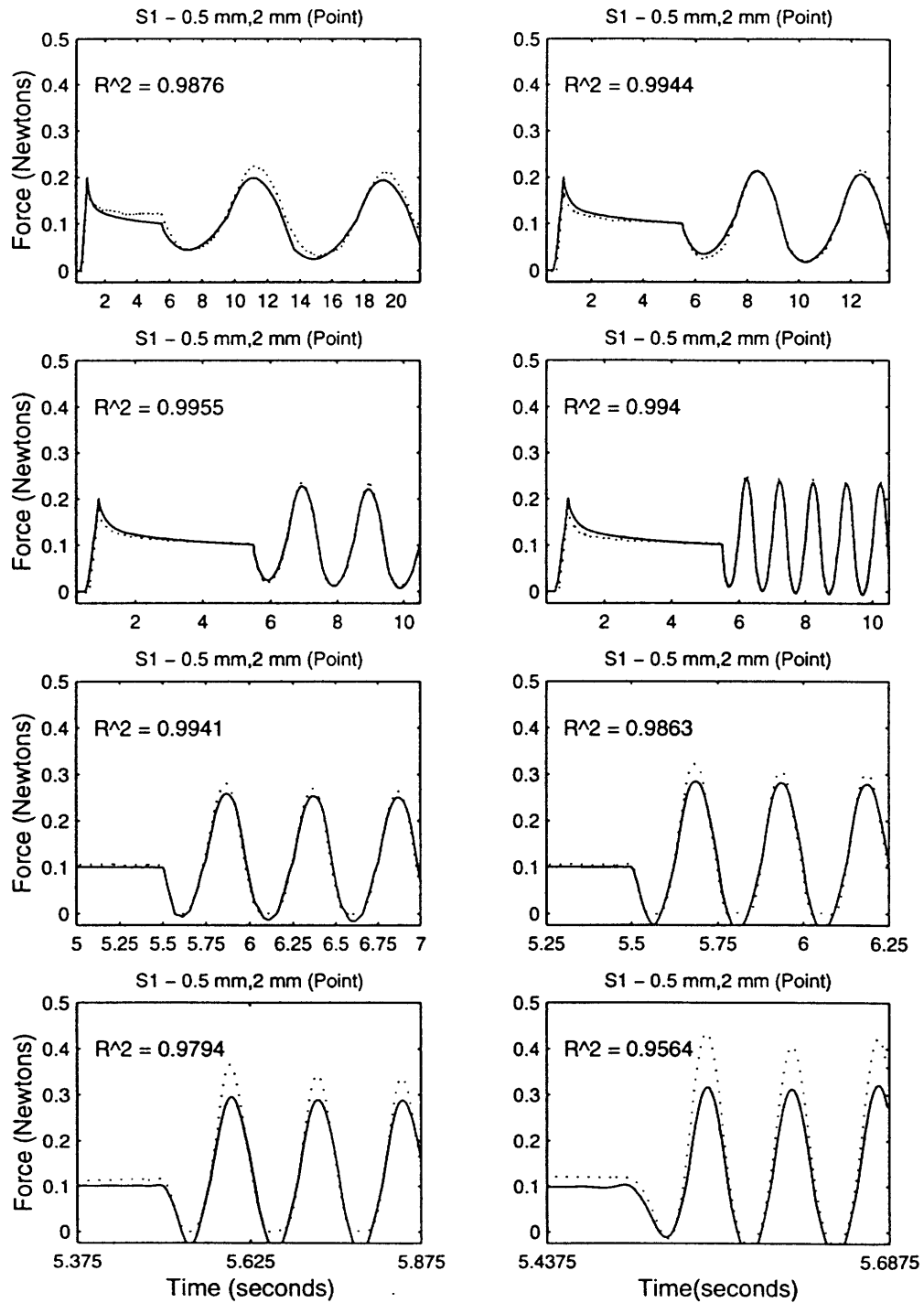
Figure 7-7 (a): Subject #1 model (solid) vs. experimental (dotted) data for ramp/hold/sinusoid given at 2.0 mm starting depth, 0.5 mm amplitude and increasing frequency (0.125 -> 16 hz).
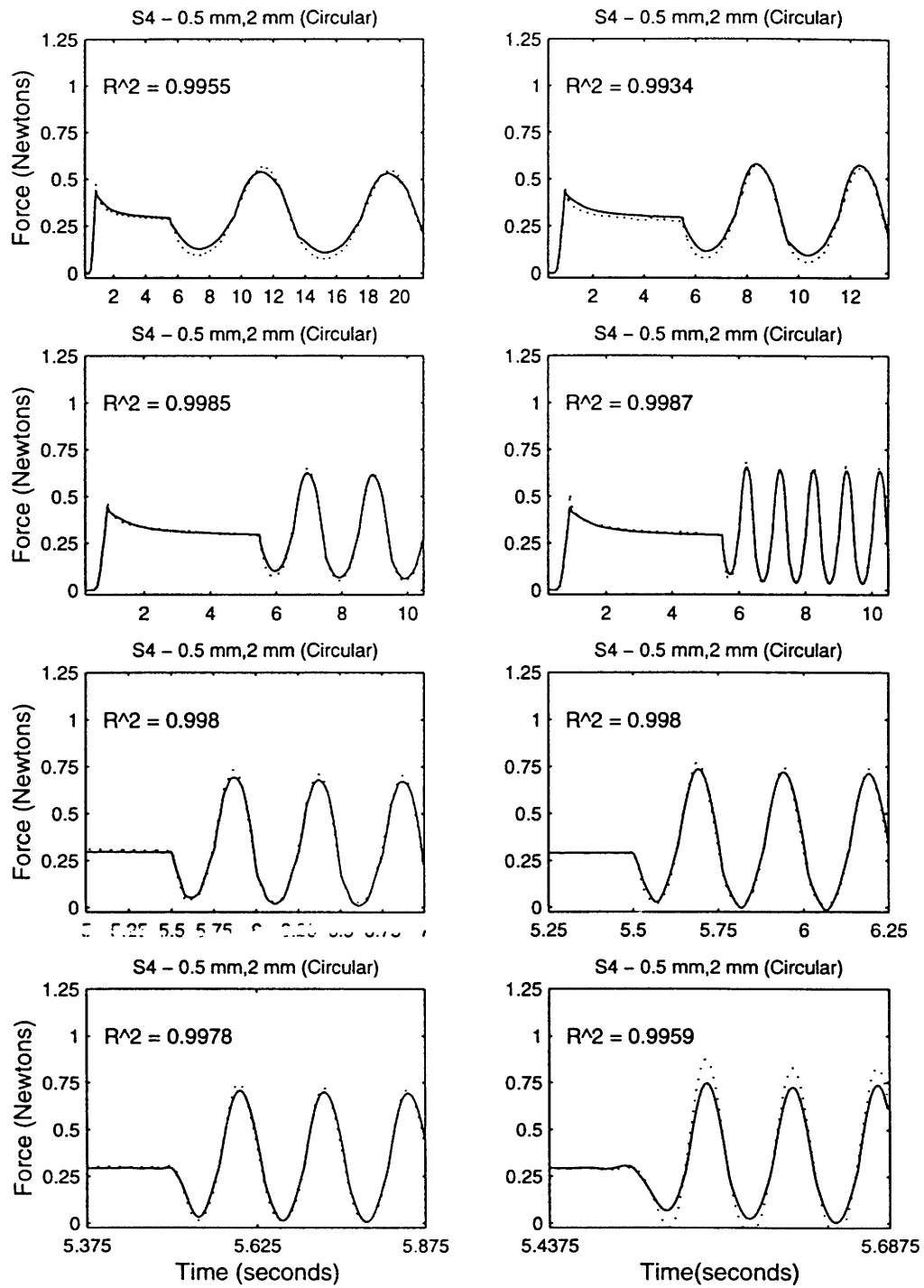
Figure 7-7 (b):   Subject #4 model (solid) vs. experimental (dotted) data for ramp/hold/sinusoid given at 2.0 mm starting depth, 0.5 mm amplitude and increasing frequency (0.125 -> 16 hz).
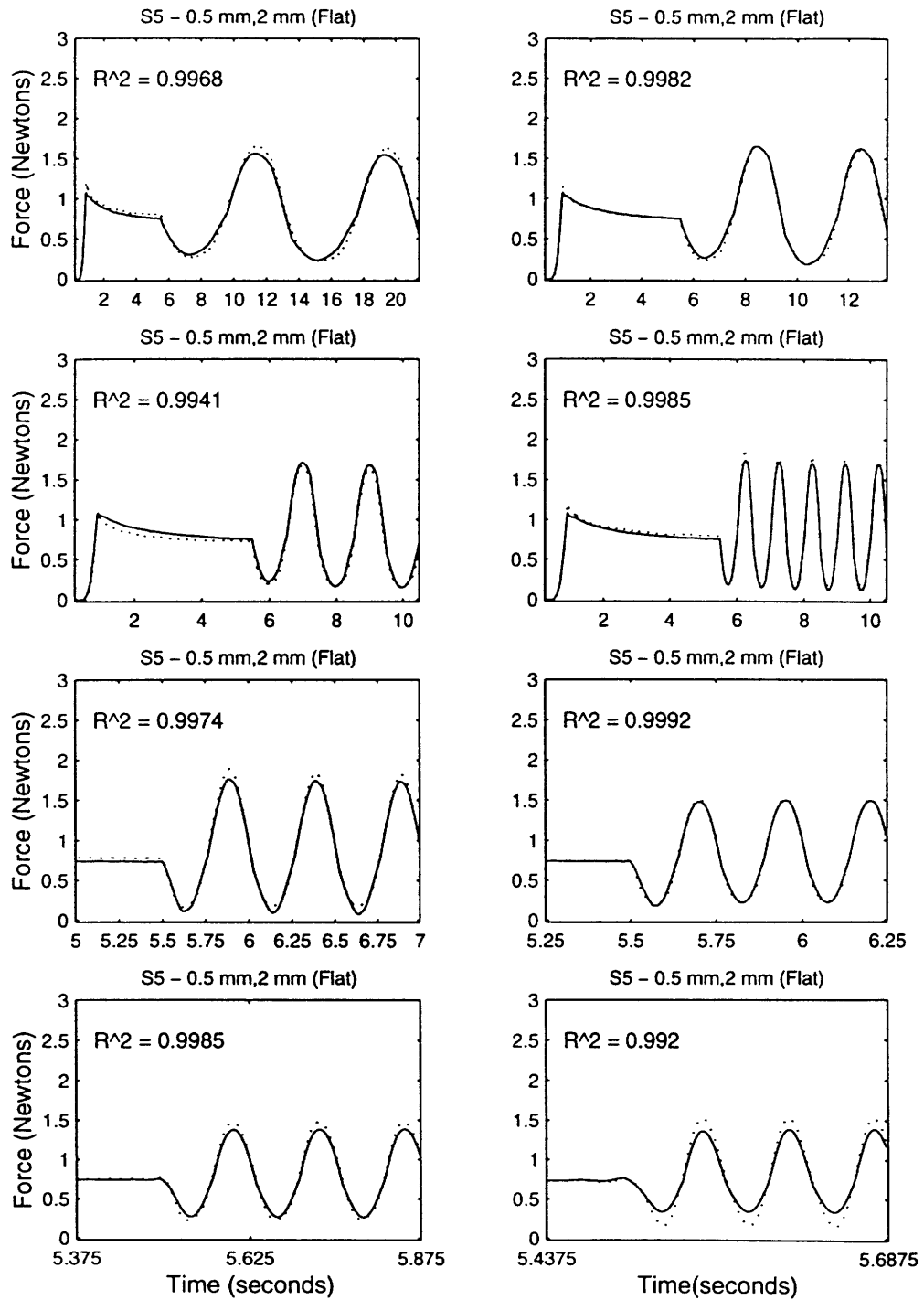
Figure 7-7 (c): Subject #5 model (solid) vs. experimental (dotted) data for ramp/hold/sinusoid given at 2.0 mm starting depth, 0.5 mm amplitude and increasing frequency (0.125 -> 16 hz).

The graphs displayed in Figure 7-8 represent the strength of the model in predicting data for each subject. Additional plots are given in Appendix F. A measure of goodness of fit was computed for these plots using the R^2 statistic which can be defined as:

$$R^2 = 1 - \frac{\Sigma(y_{actual} - y_{estimated})^2}{\Sigma(y_{actual})^2}$$ (7-4)

where y is the vector of force data sampled. A value of 1 would indicate a perfect fit. The R^2 statistics for the subject specific models was typically on the order of 0.95, which indicates a very good fit.

In the application of the final model to haptic device design and further research, it would be advantageous to obtain a more general model to predict the data for several subjects. This was attempted in this study by combining the average values for all subjects as gathered for each indentor. This general model consists of the following parameters, given for each indentor.

	Point	Circular	Flat Plate
k_{p1}	0.0721	0.0612	0.0809
k_{s1}	0.0221	0.0127	0.0710
b_{s1}	0.2889	0.0936	0.0279
k_{p2}	0.0592	0.0516	0.1874
k_{s2}	0.1605	0.0770	0.0600
b_{s2}	0.0643	0.0332	0.8032
k_{p3}	0.0376	0.0645	0.3289
k_{s3}	0.2557	0.2258	0.6000
b_{s3}	0.0198	0.0199	0.0290
k_{p4}	0.0150	0.0670	0.1995
k_{s4}	0.0915	0.0807	0.4798
b_{s4}	0.2428	0.2435	0.5541
k_{p5}	0.2696	0.2753	1.1561
k_{s5}	0.2297	0.3206	0.4677
b_{s5}	0.3230	0.4426	0.7485

Table 7-3: Parameters for a general model composed of averaged subject parameters.

Because the basic model predicts normalized data, the piecewise Kelvin blocks described by the mean set of parameters given in Table 7-3 predict mechanical fingerpad response very well. Again, the model response is multiplied by the factor of steady state, static force for the subject at 3 mm for the circular and point indentors and 2 mm for the flat plate. These values are given for the subjects and indentors in the table below.

	Point (3 mm)	Circular (3 mm)	Flat Plate (2 mm)
Subject 1	0.4016 N	1.461 N	1.03 N
Subject 2	0.4445	1.212	1.422
Subject 3	0.2642	0.667	0.5003
Subject 4	0.4497	0.9872	0.845
Subject 5	0.2234	0.681	0.6753

Table 7-4: Steady state force values used for normalization of data.

In Figure 7-9, the general model prediction versus the real data is shown for all subjects with the circular indentor at 2 mm starting depth and 0.5 mm amplitude at all frequencies. The R^2 statistic is only slightly worse for the general model.
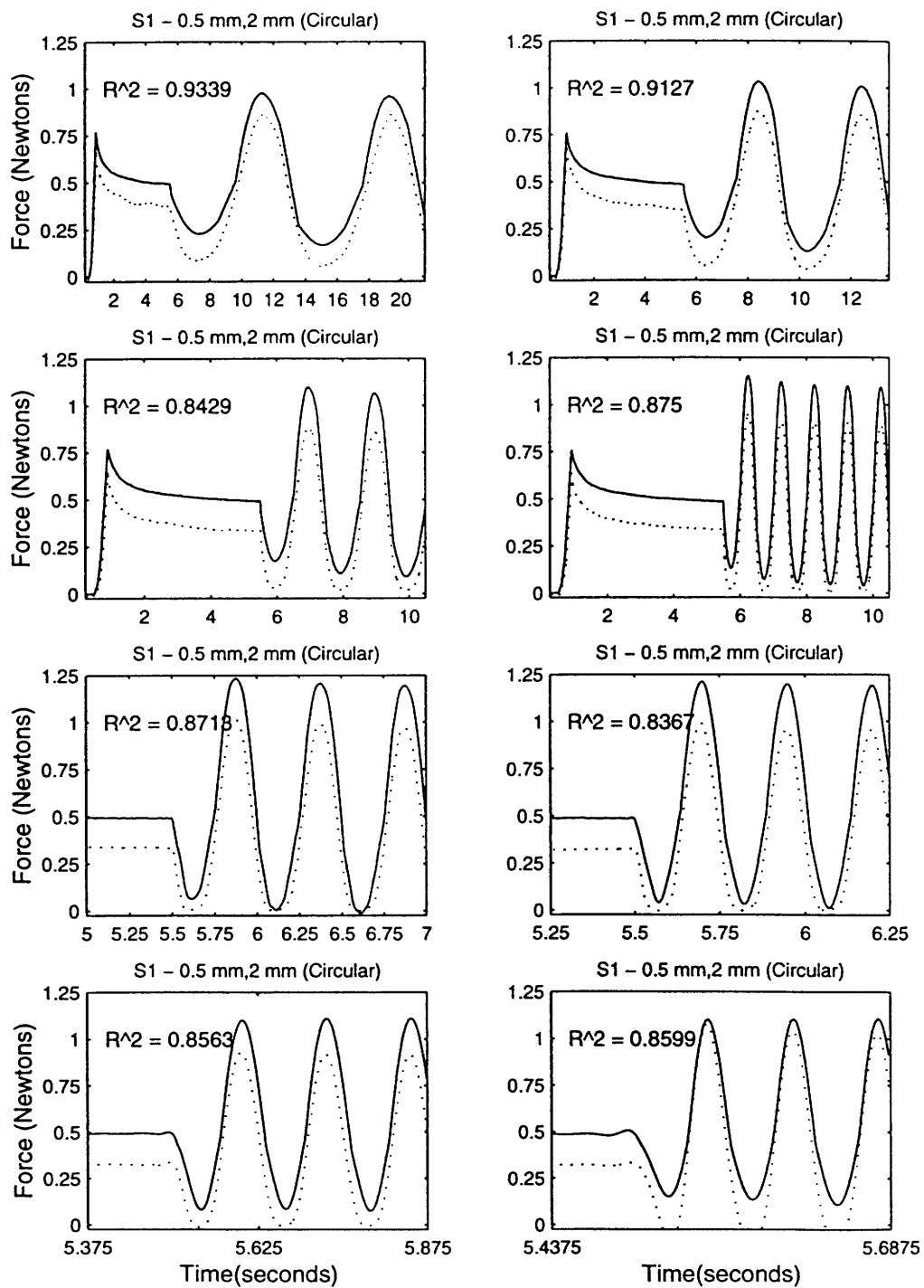
Figure 7-9 (a): General model prediction (solid) vs. experimental data (dotted) at 2 mm start depth, 0.5 mm amplitude for Subject #1 with circular indentor.
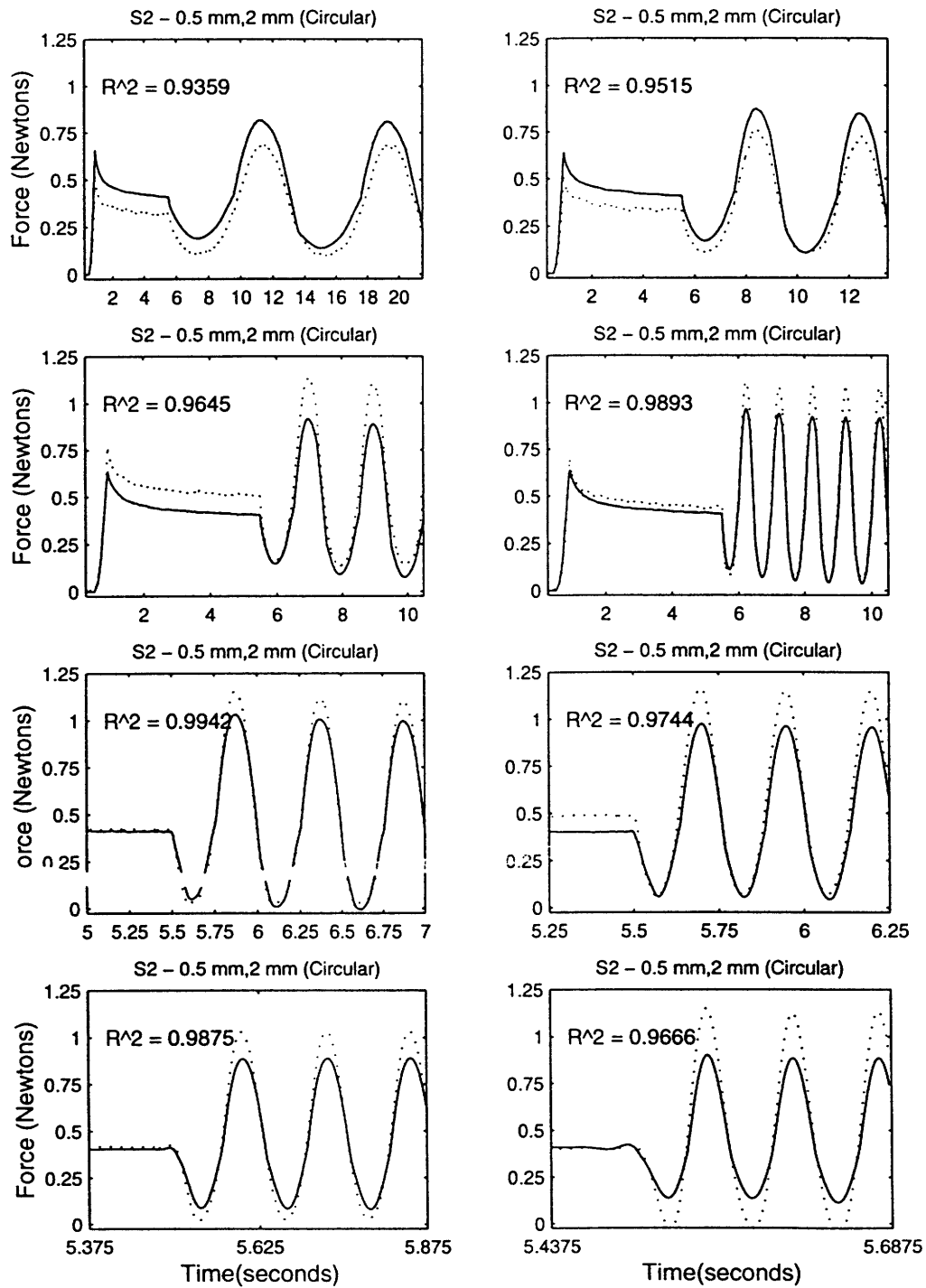
Figure 7-9 (b): General model prediction (solid) vs. experimental data (dotted) at 2 mm start depth, 0.5 mm amplitude for Subject #2 with circular indentor.

115
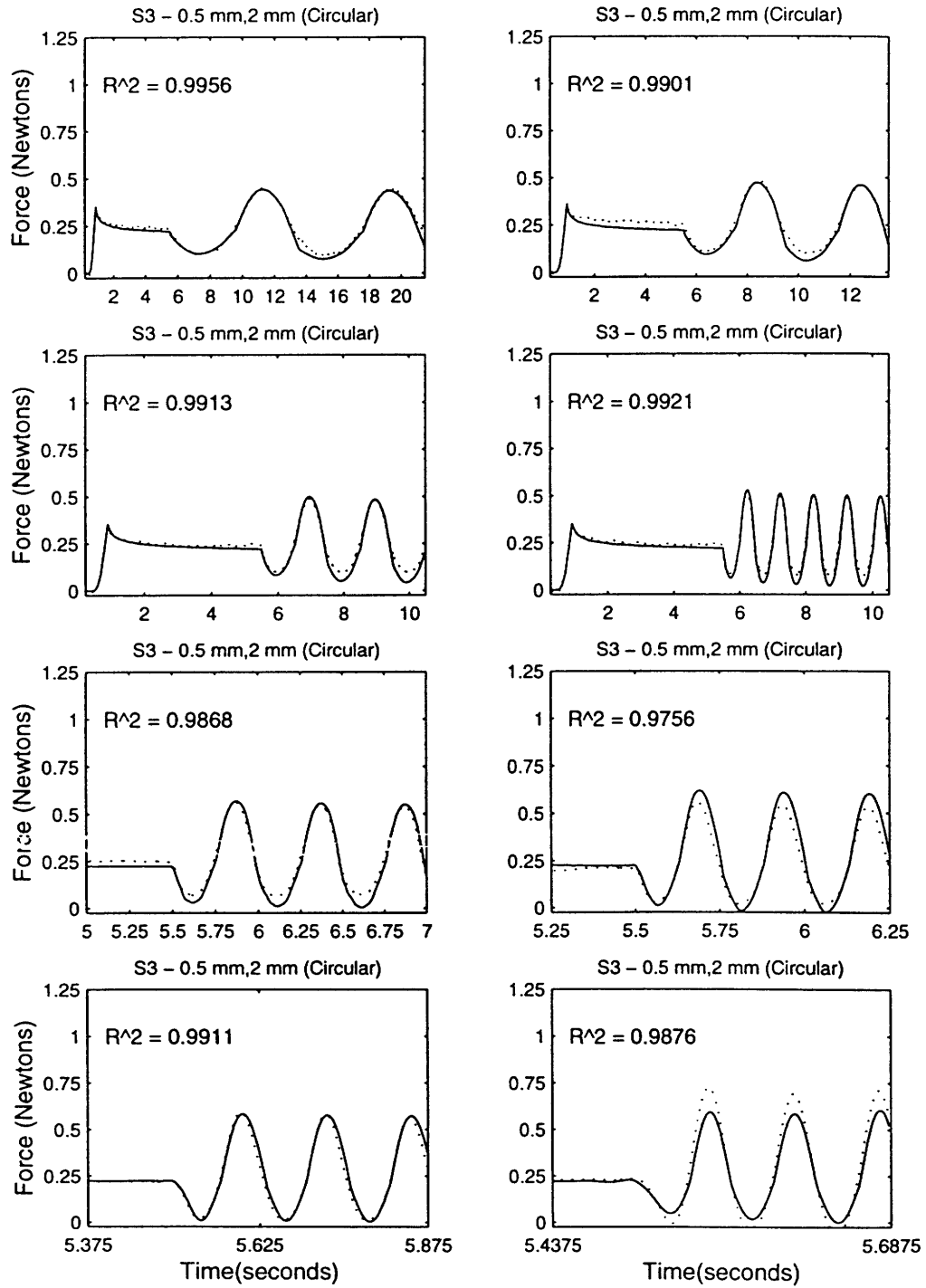
Figure 7-9 (c): General model prediction (solid) vs. experimental data (dotted) at 2 mm start depth, 0.5 mm amplitude for Subject #3 with circular indentor.
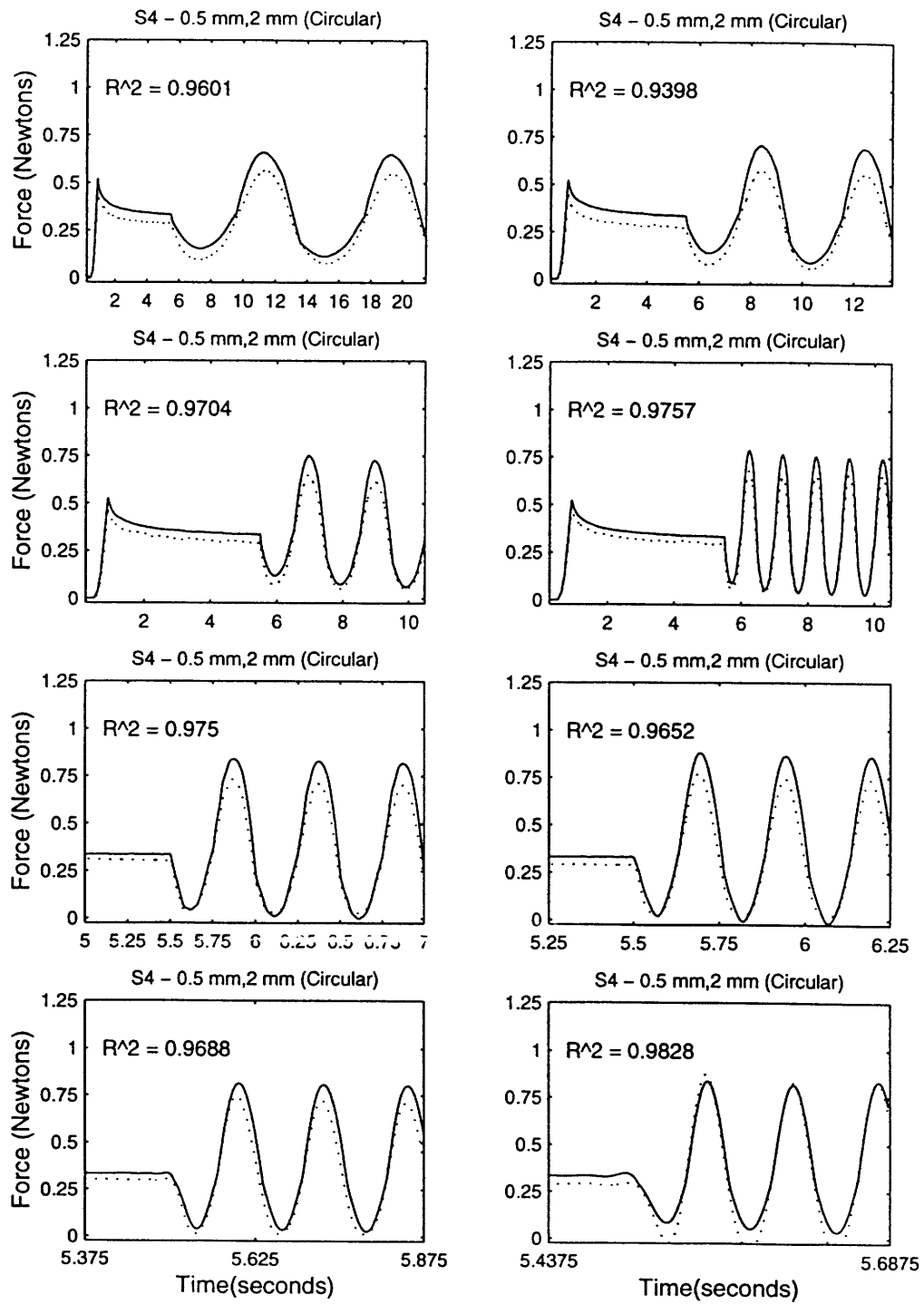
Figure 7-9 (d): General model prediction (solid) vs. experimental data (dotted) at 2 mm start depth, 0.5 mm amplitude for Subject #4 with circular indentor.
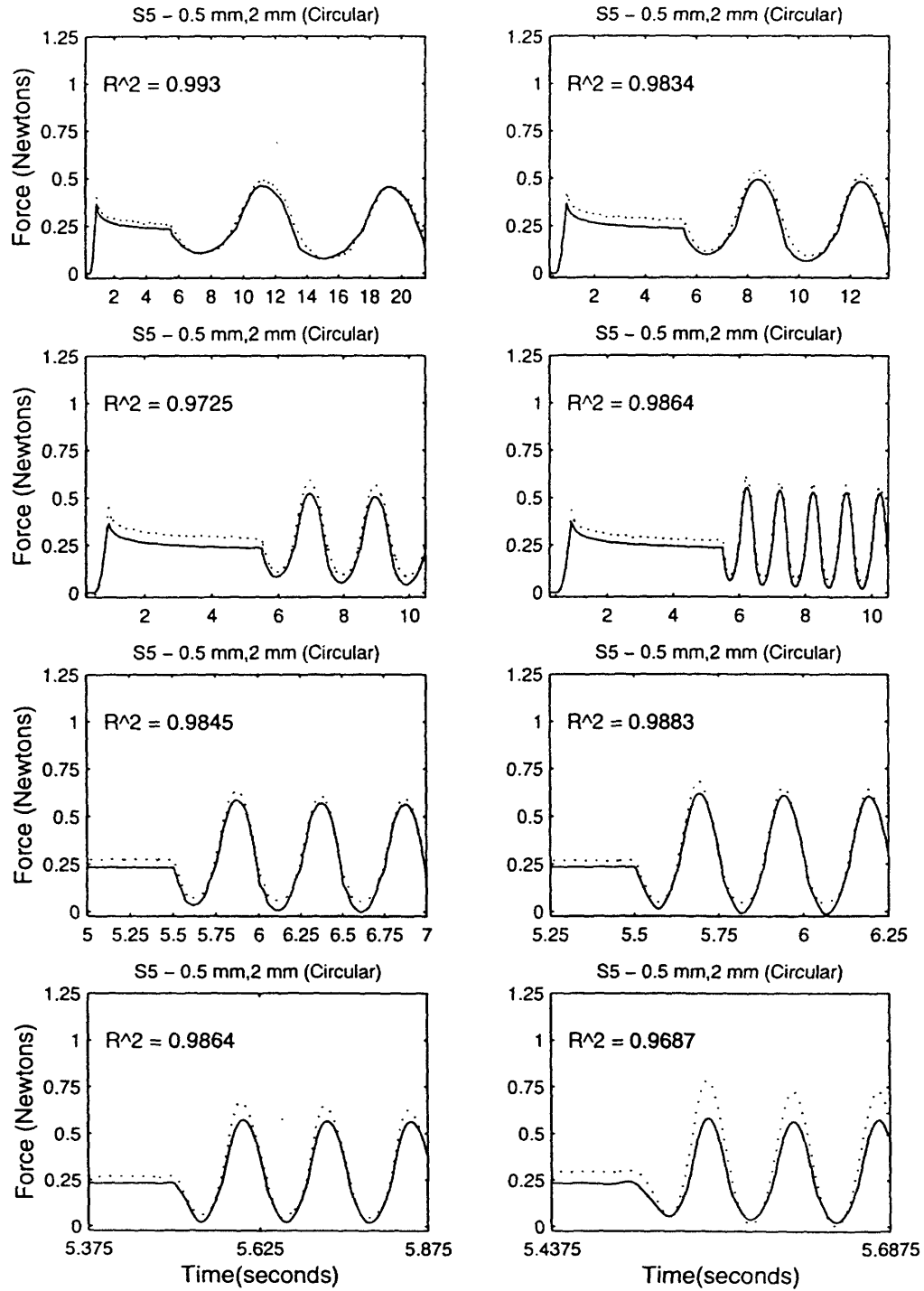
Figure 7-9 (e): General model prediction (solid) vs. experimental data (dotted) at 2 mm start depth, 0.5 mm amplitude for Subject #5 with circular indentor.

Additional plots for the other two indentors are also within Appendix G. There is clearly more work to be performed in generally modeling mechanical properties of the human fingerpad, but the final model presented in this chapter seems to be a good foundation for future iterations. In future efforts, it would be better to view the fingerpad as a "bed" of springs and dashpots, so that the parameter values are independent of the indentors used. This concept is depicted below in Figure 7-9.
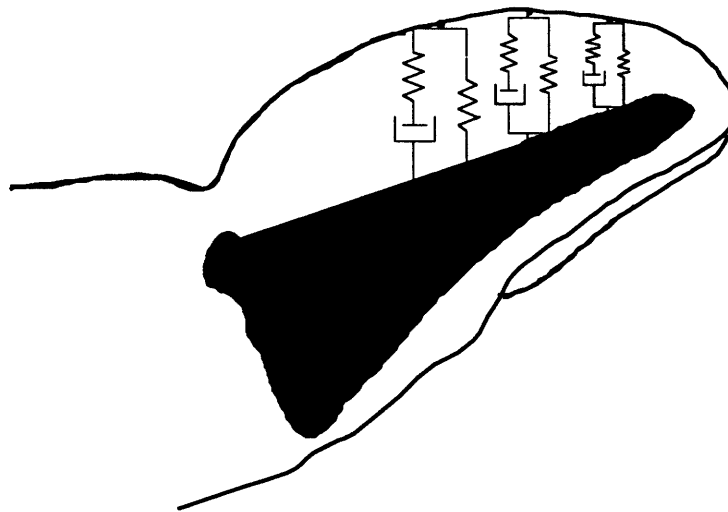
Figure 7-9: Fingerpad depicted as a series of parallel nonlinear Kelvin blocks.

Following previously discussed arguments, each Kelvin block in the model would need to be nonlinear. Solving a model of this form would require much more experimental data and significantly more parameter estimation and system analysis.

Chapter 8

Concluding Remarks

In the course of a project directed at characterizing the force response of the human fingerpad indented *in vivo*, (1) a useful device was constructed for continued use in biomechanical experiments, (2) indentation experiments were designed and carried out on a group of five subjects, (3) an extensive amount of static and dynamic data was collected and (4) a lumped-parameter nonlinear model was developed. Given below is a project summary and concluding remarks that hint at the future of this research, drawing upon what was produced here.

The performance characteristics of the tactile stimulator have been discussed extensively in Chapter 4. It is capable of producing up to 3 Newtons of endpoint force in the defined normal direction with respect to the fingerpad, though less along the shear direction opposing gravity (mounting the stimulator in a different position is likely to improve upon these force characteristics). Position can be controlled to within 20 microns. Velocities up to 32 mm/sec can be controlled with non-zero applied fingerpad forces. The stimulator will be further used to perform a study of frictional properties of fingerprint skin, *in vivo*, and later, psychophysical experiments, requiring even finer precision and control that will be achieved in part by a 16-bit A/D board. As stated earlier, the control code is shown in Appendix A.

In the course of designing and conducting experiments, several insights into fingerpad properties were gained. First, a nonlinear force response is clearly observed with respect to indentation depth. This feature is best demonstrated by the asymmetric shape of the sinusoid response and the nonlinear static steady state force response with respect to depth. Speculations have been made that this nonlinearity is due in part to the multilayered, nonhomogeneous composition of the fingerpad. Additionally, there is a clear increase in the area of material compressed during an indentation, even with the point indentor, which produces a "crater" of increasing projected area. This increase in compressed volume as a nonlinear function of depth is another significant factor in creating the nonlinear characteristic response. And a degree of viscoelasticity is also present, as shown by a decaying force during the "hold" of a ramp/hold indentation. Lastly, the force response of the fingertip is noticeably frequency dependent. That is to say, force magnitude and finger stiffness increase as a function of increasing frequency of stimulation. In short, the fingertip exhibits all of the properties that researchers have found common to biological tissues with significant nonlinearity (Fung, 1990).

Modeling efforts involved several methical steps that yielded a piecewise linear approximation to a nonlinear Kelvin lumped-parameter model. It was clear that the model had to contain elements that would account for both the viscoelasticity and nonlinearity of the fingerpad. Springs and dashpots are the basic mechanical components of common viscoelastic models (Fung, 1990). The phase of the output response indicated that the mass of the finger was unlikely to be significant in magnitude of the force response to indentation. Thus, the final model created in this study was a nonlinear version of the Standard Linear Model for biological tissues with both spring and dashpot elements being nonlinear. This model was approximated by a piecewise linear model due to the complexity of nonlinear modeling. Curve fitting model responses against normalized experimental data with local minimization of error between the two was used

in estimating parameters of indentor specific models for each of five subjects. The experimental force responses were normalized with respect to the highest steady state, static force measured. The individual subject models were surprisingly good ($R^2 > 0.95$) at predicting the output responses of its subject. And, mean indentor specific models, based on the average of the set of individual subject parameters were nearly as good at predicting this data.

A substantial amount of characteristic data has been collected on the fingertip force response to indentation on five subjects, but there are still future directions for analysis and applications to take. Once normalization of indentation response data with respect to steady state force values (see Figure 6-7 (e)). Although the models developed were quite accurate at predicting this normalized data requiring an initial force measurement for the model to be usable is not desirable in forming a universal fingerpad model. In Figure 6-7 (b-c) of steady state force data vs. indentation depth, attempts were made with less success to normalize static data with respect to fingerpad dimensions. In fact, it was noted that two subjects, #2 and #4, had fingers of very similar geometry but very different force characteristics. A "quick" measure of stiffness of the fingerpad though (i.e. a steady state force value at a specified indentation depth) is perhaps the only method to distinguish between two such fingerpads. There is clearly more to investigate in this area. Additionally, there are avenues to explore in direct nonlinear modeling and perhaps a method of implementing Fung's (1990) infinite parallel spring-dashpot model. Similarly, if the number of spring-dashpot links is increased sufficiently and ordered spatially, it may be possible to create one model to predict the response to any indentor shape. At present, the piecewise linear Kelvin block model seems to perform well for the data taken, and it is suggested that this be utilized first, as linear modeling simplifies data processing and parameter estimation.

In short, this thesis provides an extensive set of initial data for fingertip mechanics research as well as one modeling approach and verification of its performance. There are still unanswered questions that must be addressed if improved models are needed.

Appendix A

Stimulator Code

```
/*******************************************************
* Program: STRIS.C                                     *
*                                                      *
* Usage:  Two-Link Stimulator Control for Indentations *
*         name initial(1) trial number(1) indentor(p/c/f) *
* This program is developed to control the stimulator in *
* two link mode with JDRTIMER as the timing control.   *
* Inverse kinematics are used to control position, as  *
* can be traced through in the code                    *
*                                                      *
* Rogeve J. Gulati  Last Modification: 04/23/94        *
*                                                      *
*******************************************************/

#include <stdio.h>
#include <conio.h>
#include <dos.h>
#include <math.h>
#include <string.h>
#include <alloc.h>

/* DT2811-PGH A/D BOARD ADDRESSES----------------------------------*/
#define  BASE_ADDRESS      0x218
#define  MODE_ZERO         0x0
#define  INIT_VALUE        0x0

/* MAXIMUM OUTPUT OF DA AND INPUT TO MOTORS------------------------*/
#define      MAX_V                    4090    /* +5 Volts    */
#define      MIN_V                    5       /* -5 Volts    */

/* A/D BOARD CHANNEL DEFINITIONS----------------------------------*/
#define      PHI_CHANNEL       6       /* Top Link */
#define      THETA_CHANNEL     7       /* Bottom Link  */
#define      FN_CHANNEL        4
#define      FT_CHANNEL        5

/* HOME POSITION OF STIMULATOR-------------------------------------
        (this must be calibrated with squares and levels on the device)    */
```

```c
#define        PHI_HOME           2090.0          /* Home Position for Top Link */
#define        THETA_HOME         1800.0          /* Bottom Link (as of 6/29)   */

/* COUNTS PER RADIAN---------------------------------------------------*/
#define        CPTHETA            33747.2 /* counts per theta (bottom link) */
#define        CPPHI              35408.8 /* counts per phi (top link) */

/* CONSTANTS FOR FORCE FROM COUNTS------------------------------------*/
#define        KA                 50.5    /* see analysis of force sensor and  */
#define        KB                 15.0    /*        calibration notes           */
#define        KC                 17.25
#define        LN                 24.0
#define        LT                 28.5    /* avg value (shear is not important yet) */

/* ADDRESSES FOR TIMER BOARD------------------------------------------*/
#define TIMER_0                   0x254 /* see JDRTIMER.C for reference */
#define        TIMER_1            0x255
#define        TIMER_2            0x256
#define        TIMER_CTRL         0x257

/* COUNTS PER VELOCITY MEASUREMENT-------------------------------------
            (velocity is determined by counts angle change per cycle, but due
            to noise, several cycles must be read to gain a truer reading--this
            value affects control law gains and stability)            */
#define CVM                       10

/* SIZE OF MEMORY ALLOCATION FOR EACH ARRAY-----------------------------
        (22 seconds maximum * 500 Hz = 11000)                        */
#define ARSIZE                    11000


/* FUNCTION DECLARATIONS-----------------------------------------------*/
void    motor_1(int);
void    motor_2(int);
void    move_theta(float);
void    move_phi(float);
int     read_channel(int);
void    initad(void);
void    calc_angles (float, float);
void    ramp_hold_x (float, float);
void    hold (void);
void    sinusoid (float, float, float, float);
FILE    *outfile;

/* STRUCTURE OF MATLAB BINARY FILE HEADER------------------------------*/
typedef struct {
        long type;
        long mrows;
        long ncols;
        long imagf;
        long namlen;
} Fmatrix;

/* GLOBAL VARIABLES----------------------------------------------------*/
int            prev_phi[11], v_phi, prev_theta[11], v_theta;
```

```
int             theta_pos, phi_pos;
int             torque_phi, torque_theta;
int             offset_phi;
int             offset_theta;
float           theta_cnts;
float           phi_cnts;
int             normal_tmp, tangent_tmp;
int             offset_normal, offset_tangent;
int             normal_f, tangent_f;
int             controlrate;
float           start_x;        /* Used as starting position for ramp/hold and    */
float           start_y;        /* and sinusoids.                                 */
float           x;              /* current position                               */
float           y;
long int        num_sample;     /* # of data samples recorded                     */
int             rh_cnt;         /* counters for time in function loops            */
int             sin_cnt;
int             steady_cnt;
int             function_flag;  /* sets stimulator operation */
int             get_data_flag;
int             save_data_flag;
int             check_flag;     /* when to check control frequency */
char            s1[15];
int             status;         /* flag: idle vs. running trial */

/*--------------------------------------------------------------------*/
/*------------------------------MAIN----------------------------------*/
/*--------------------------------------------------------------------*/

main(int argc, char *argv[])
{
/* SAVE VARIABLES--------------------------------------------------*/
float far               *theta;
float far               *phi;
float far               *normal;
float far               *tangent;
float far               *data_time;

/* MATLAB BINARY FILE HEADER VARIABLES----------------------------*/
char                    *name1;
char                    *name2;
char                    *name3;
char                    *name4;
char                    *name5;
Fmatrix                 header;
int                     size;

/* TIMER VARIABLES------------------------------------------------*/
unsigned int            count_0 = 500;  /* control loop frequency = 2 kHz */
unsigned int            count_1 = 1000; /* see JDRTIMER.C to understand   */
unsigned int            cur_count;
unsigned int            old_count = 0;  /* basically,                     */
int                     flag = 0;       /* count_0 = 1MHz / samp. freq.   */
int                     temp;
```

126

```c
/* EXPERIMENT PARAMETERS----------------------------------------------*/
float                   ramp_vel = 1.0;     /* initial values */
float                   ramp_dep = 0.5;
float                   sin_freq = 0.125;
float                   sin_amp         = 0.25;
float                   sin_start_dep = 1.0;
char                    trial[2] = "a";

/* OTHER VARIABLES----------------------------------------------------*/
char                    answer;
char                    key_stroke;
int                     i;
int                     data_cnt;
int                     force;
long int                cnt;
int                     force_flag = 20;
float                   cnt_time;
float                   theta_tmp, phi_tmp;
float                   tan_dat, norm_dat;
clrscr();

/* CHECK ARGUEMENTS TO MAIN-------------------------------------------*/
if (argc < 3) {
        printf("Usage: program_name  initial(1)  indentor_type (p/c/f)\n");
        return 0;
        }
if (strlen(argv[1]) > 1) {
        printf("Usage: program_name  initial(1)  indentor_type (p/c/f)\n");
        printf("\nInitial can only be one character long!\n");
        return 0;
        }
if (strlen(argv[2]) > 1) {
        printf("Usage: program_name  initial(1)  indentor_type (p/c/f)\n");
        printf("\nTrial_designation can only be one character long!\n");
        return 0;
        }
printf("Welcome to Stris.C, a program written to operate the Tactile\n");
printf("Stimulator. Make sure the power to the Pots and to the Linear\n");
printf("Amplifiers is on and that the Ethernet connection is unplugged\n");
printf("before running any experiments.  Also, make sure that the end\n");
printf("of the stimulator is free of obstruction.  It is likely to spring\n");
printf("to its holding position rapidly.  \n\n");
printf("Make sure the force sensor is on, as well!\n\n");
printf("Once ready to begin, answer the following question and simply\n");
printf("enter the desired operation on the menu that appears.  You do\n");
printf("need to hit return and should not enter commands too rapidly.\n");
printf("When the stimulator is performing an experiment, it will register\n");
printf("a Status: 1.  It saves data in matlab binary format to a filename\n");
printf("based on the parameters entered to describe the experiment.  You can \n");
printf("run numerous experiments without quitting the program, and they will\n");
printf("be saved to different files, as long as some parameter is changed\n");
printf("However, you must exit and reenter to start a new trial with a new\n");
printf("trial designation.\n\n");
printf("Is '%s%s' the correct experiment designation?  ",argv[1], argv[2]);
answer = getch();
```

```c
if(answer != 'y') return 0;
clrscr();

/* INITIALIZE IMPORTANT VARIABLES---------------------------------------*/
controlrate = 2000;  /* 1 MHz / count_0 (see JDRTIMER.C) */
offset_phi = 0;
offset_theta = 0;
rh_cnt = 0;
sin_cnt = 0;
steady_cnt = 0;
function_flag = 0;
get_data_flag = 0;
save_data_flag = 0;
status = 0;

/* SET HOME POSITION-------------------------------------------------*/
x = 76.2;          /* home position (lengths of links) origin at      */
y = 76.2;          /* bottom link pivot point.                */
calc_angles(x,y);          /* convert to home angles in cnts          */

/* MEMORY ALLOCATION----------------------------------------------*/
if((theta = (float far *)farmalloc(ARSIZE*sizeof(float))) == NULL) {
        printf("Not enough memory available for theta\n");
        return 0;
        }
if((phi = (float far *)farmalloc(ARSIZE*sizeof(float))) == NULL) {
        printf("Not enough memory available for phi\n");
        return 0;
        }
if((normal = (float far *)farmalloc(ARSIZE*sizeof(float))) == NULL) {
        printf("Not enough memory available for normal\n");
        return 0;
        }
if((tangent = (float far *)farmalloc(ARSIZE*sizeof(float))) == NULL) {
        printf("Not enough memory available for tangent\n");
        return 0;
        }
if((data_time = (float far *)farmalloc(ARSIZE*sizeof(float))) == NULL) {
        printf("Not enough memory available for data_time\n");
        return 0;
        }

/* INITIALIZE DT2811-PGH A/D BOARD-----------------------------------*/
initad();

/* TIMER BOARD INITIALIZATION (see JDRTIMER.C)------------------------*/
outportb(TIMER_CTRL, 0x34);
outportb(TIMER_0, count_0 % 256);
outportb(TIMER_0, count_0 / 256);
outportb(TIMER_CTRL, 0x74);
outportb(TIMER_1, count_1 % 256);
outportb(TIMER_1, count_1 / 256);

/* DISPLAY MENU----------------------------------------------------*/
printf("\n1\t=\tforward x-axis\t\t\t2\t=\tbackward x-axis\n");
```

```c
printf("8\t=\tfine forward x\t\t\t9\t=\tfine backward x\n");
printf("3\t=\tdownward y-axis\t\t\t4\t=\tupward y-axis\n");
printf("5\t=\tramp/hold\t\t\t6\t=\tsinusoid\n");
printf("\nr\t=\tinc ramp depth\t\t\te\t=\tdecrease\n");
printf("w\t=\tinc ramp velocity\t\tq\t=\tdecrease\n");
printf("s\t=\tinc sine frequency\t\ta\t=\tdecrease\n");
printf("f\t=\tinc sine amplitude\t\td\t=\tdecrease\n");
printf("h\t=\tinc sine start depth\t\tg\t=\tdecrease\n");
printf("b\t=\thome position\t\t\tspace\t=\tend program\n");
printf("\n\t\t\tRamp Depth:\n");
printf("\t\t\tVelocity:\n");
printf("\t\t\tSinusoid Freq:\n");
printf("\t\t\tAmplitude:\n");
printf("\t\t\tStart Depth:\n");
printf("\t\t\tTrial Letter:\n");
printf("\t\t\tNormal Force:\n");
printf("\t\t\tShear Force:\n");
printf("\t\t\tX-Coordinate:\n");
printf("\t\t\tY-Coordinate:\n");
printf("\t\t\tStatus:\n");

/* OUTER SHELL OF CONTROL LOOP----------------------------------------*/
while(flag==0){

/* CALCULATE CURRENT FORCE--------------------------------------------*/
tan_dat = (-tangent_f + offset_tangent) / (LT*KA);
norm_dat = (1/(KB*LN))*((-normal_f + offset_normal) + (KC/KA)*(-tangent + offset_tangent));

/* DISPLAY PARAMETERS-------------------------------------------------*/
gotoxy(43,14);
printf("%3.2f ", ramp_dep);
gotoxy(43,15);
printf("%3.2f ", ramp_vel);
gotoxy(43,16);
printf("%3.3f ", sin_freq);
gotoxy(43,17);
printf("%3.2f ", sin_amp);
gotoxy(43,18);
printf("%3.2f ", sin_start_dep);
gotoxy(43,19);
printf("%s",trial);
gotoxy(43,20);
printf("%3.1f      ", norm_dat);
gotoxy(43,21);
printf("%3.1f       ", tan_dat);
gotoxy(43,22);
printf("%3.3f     ",x);
gotoxy(43,23);
printf("%3.3f     ",y);
gotoxy(43,24);
printf("%d    %s", status, argv[2]);

/* INITIAL TIMER BOARD READING----------------------------------------*/
outportb(TIMER_CTRL, 0x40);
old_count = inportb(TIMER_1) + inportb(TIMER_1) * 256;
```

```c
cur_count = old_count;

/* CHECK_FLAG = 2-------------------------------------------------------
   (system time is required for starting a while loop; see below)      */
check_flag = 10;

/* RUN CONTROL LOOP UNTIL FLAG OR KEY_STROKE--------------------------*/
while((!kbhit()) && (flag==0))
{

/* CHECK CONTROL FREQUENCY-----------------------------------------
   (make sure only one cycle at control frequency has passed this check is bypassed
   when check_flag != 0 to give time for frequency to stabalize;  this occurs after a
   key stroke or save operation or after initial startup of while loop--these have been
   found to take system time)              */

        while(cur_count == old_count)
        {
                outportb(TIMER_CTRL, 0x40);
                cur_count = inportb(TIMER_1) + inportb(TIMER_1) * 256;
        }

        /* CHECK NUMBER OF CYCLES PASSED----------------------------*/
        temp = old_count - cur_count;
        if (cur_count > old_count) temp =0;
        if ((temp > 1) && (check_flag==0) && (!kbhit())) {
                flag = 1;
                printf("Control Frequency too High!  Interrupt = %d cycles",
                        temp);
        }

        /* INCREMENT CHECK_FLAG TO 0-----------------------*/
        else if (check_flag != 0) check_flag = check_flag - 1;

/* HOLD FUNCTION and OFFSET VALUE--------------------------------------
   (if check_flag != 0, control freq not stablized, so no function
    is called)                                                    */

        if(function_flag == 0 && check_flag == 0) {
                hold();
                /* take force data or offset according to flag */
                if(force_flag > 0) {
                        /* averages offset over #=force_flag readings */
                        if (force_flag == 20) {
                            offset_normal = read_channel(FN_CHANNEL);
                            offset_tangent = read_channel(FT_CHANNEL);
                            force_flag--;
                            }
                        else{
                            offset_normal = (offset_normal + read_channel(FN_CHANNEL))/2;
                            offset_tangent = (offset_tangent + read_channel(FT_CHANNEL))/2;
                            force_flag--;
                                }
                        }
                else if (force_flag <= 0 && save_data_flag == 0) {
```

```
                        normal_f = read_channel(FN_CHANNEL);
                        tangent_f = read_channel(FT_CHANNEL);
                        }
                }

/* CALL OTHER FUNCTIONS----------------------------------------------*/

        else if(function_flag == 1 && check_flag == 0)
                ramp_hold_x (ramp_vel, ramp_dep);
        else if(function_flag == 2 && check_flag == 0)
                sinusoid (sin_start_dep, sin_amp, sin_freq, 1.5708);

/* COLLECT DATA IN SAVE VARIABLES----------------------------------------
   (when call is received; during experiment)                        */
        if(get_data_flag == 1 && check_flag == 0) {
                num_sample++;   /* increment at every call */

                /* save data every 4th cycle; sample f = 500 Hz */
                data_cnt = (int) (num_sample / 4);

                /* FORCE READINGS----------------------------------------
                   (alternate to minimize control loop time;  tangent
                   data is hence phase shifted slightly in ouput)     */
                if(num_sample%2==0)
                        normal_tmp = read_channel(FN_CHANNEL);
                else
                        tangent_tmp = read_channel(FT_CHANNEL);
                normal[data_cnt] = (float)normal_tmp;
                tangent[data_cnt] = (float)tangent_tmp;
                theta[data_cnt] = (float)theta_pos;
                phi[data_cnt] = (float)phi_pos;
        }

/* SAVE DATA-----------------------------------------------------------
   (stimulator is allowed to hold stabalize first)                   */

        if(save_data_flag > 0) {
                        save_data_flag++;
                        }
        if(save_data_flag == 50) {
                motor_1(1170);  /* holding torques found experimentally */
                motor_2(2100);  /* stim will hang at roughly home pos  */

                /* this takes a 'long' time; stim is resting; no control */
                if((outfile = fopen(s1,"wb"))==NULL);
                else {
                for(cnt=0; cnt < (int)(num_sample/4); cnt ++)
                {
                data_time[cnt] = cnt * (4.0/controlrate);

                /* FORWARD KINEMATICS------------------------------- */
                /* theta and phi converted to angles */
                theta_tmp = 1.5708 + ((theta[cnt] - THETA_HOME)/CPTHETA);
                phi_tmp = (-phi[cnt] + PHI_HOME) / CPPHI;
```

```c
/* theta and phi are now x and y, respectively; the
            deflection of the force sensor has been accounted for
            in x (as 0.01 mm / 70 normal counts; calibrated----*/

theta[cnt] = 76.2 * cos(theta_tmp) + 76.2 * cos(phi_tmp)
            - ((-1.0*normal[cnt] + offset_normal) * 0.01 / 70.0);
phi[cnt] = 76.2 * sin(theta_tmp) + 76.2 * sin(phi_tmp);

/* FORCE CALCULATION----------------------------------
            (kt and kn were found through calibration)          */
normal[cnt] = (1/(KB*LN))*((-normal[cnt] + offset_normal) + (KC/KA)*(-tangent[cnt]
            + offset_tangent));
tangent[cnt] = (-tangent[cnt]+ offset_tangent) / (LT*KA);


/* SAVE DATA TO MATLAB BINARY FILE------------------ */
size = (int)(num_sample/4);
name1 = "t";
name2 = "x";
name3 = "normal";
name4 = "y";
name5 = "tangent";
header.type = 10;
header.mrows = size;
header.ncols = 1;
header.imagf = 0;            /* no imaginary part */
header.namlen = strlen(name1) + 1;
fwrite(&header, sizeof(Fmatrix), 1, outfile);
fwrite(name1, sizeof(char), (int)header.namlen, outfile);
fwrite(data_time, sizeof(data_time), size, outfile);
header.namlen = strlen(name2) + 1;
fwrite(&header, sizeof(Fmatrix), 1, outfile);
fwrite(name2, sizeof(char), (int)header.namlen, outfile);
fwrite(theta, sizeof(theta), size, outfile);
header.namlen = strlen(name3) + 1;
fwrite(&header, sizeof(Fmatrix), 1, outfile);
fwrite(name3, sizeof(char), (int)header.namlen, outfile);
fwrite(normal, sizeof(normal), size, outfile);
header.namlen = strlen(name4) + 1;
fwrite(&header, sizeof(Fmatrix), 1, outfile);
fwrite(name4, sizeof(char), (int)header.namlen, outfile);
fwrite(phi, sizeof(phi), size, outfile);
header.namlen = strlen(name5) + 1;
fwrite(&header, sizeof(Fmatrix), 1, outfile);
fwrite(name5, sizeof(char), (int)header.namlen, outfile);
fwrite(tangent, sizeof(tangent), size, outfile);

fclose(outfile);
}
status = 0;    /* change status display */
gotoxy(43,24);
printf("%d", status);
save_data_flag = 0;          /* Reset flag */
check_flag = 50;    /* Reset check_flag to indicate that          */
```

```c
                              /* a delay has taken place in control    */
                              /* loop.                  */
              /* NOTE:  DOS does 'stuff' after saving, so control freq */
              /*          takes time to stabalize.  Hence, large check_f */
       }
              old_count = cur_count;   /* see JDRTIMER operation */
}

/* KEY STROKE-------------------------------------------------------*/
key_stroke = getch();

/* these parameters are described by menu ;
   only respond to a key_stroke if stim is stabalized and ready */
if(check_flag==0 && function_flag==0) {
if (key_stroke==' ') flag = 1;

/* MOVE STIMULATOR----------------------------------------------------*/
else if (key_stroke=='1')  x = x + 0.1;
else if (key_stroke=='2')  x = x - 0.1;
else if (key_stroke=='8')  x = x + 0.025;
else if (key_stroke=='9')  x = x - 0.025;
else if (key_stroke=='3')  y = y - 0.1;
else if (key_stroke=='4')  y = y + 0.1;

/* HOME POSITION-----------------------------------------------------*/
else if (key_stroke=='b') {
       x = 76.2;
       y = 76.2;
       }

/* RAMP/HOLD PARAMETERS SET-------------------------------------------*/
else if (key_stroke=='5') {
       status = 5;
       start_x = x;   /* set starting position */
       start_y = y;
       function_flag = 1;         /* ramp & hold */
       num_sample = 0;        /* reset counter for get_data */

       /* create name of file to save data */
       sprintf(s1,"%s%s%s%dr%d%s",argv[1],trial,argv[2], (int)(ramp_vel), (int)(ramp_dep*4),".mat");
       }

/* SINUSOID PARAMETERS SET--------------------------------------------*/
else if (key_stroke=='6') {
       status = 6;
       start_x = x;   /* set starting position */
       start_y = y;
       function_flag = 2;         /* sinusoid */
       num_sample = 0;        /* reset counter for get_data */
       if (sin_freq > 0.9)
       sprintf(s1,"%s%s%d%s%d%d%s",argv[1],trial,(int)(sin_start_dep*4),
              argv[2],(int)(sin_freq),(int)(sin_amp*4),".mat");
       else
       sprintf(s1,"%s%s%d%sf%d%d%s",argv[1],trial,(int)(sin_start_dep*4),
              argv[2],(int)(sin_freq*8),(int)(sin_amp*4),".mat");   }
```

```c
/* EXPERIMENT PARAMETERS CHANGED-----------------------------------*/

else if (key_stroke=='o') {
        force_flag = 20;   /* flag to offset loop */
}
else if (key_stroke=='r' && ramp_dep < 3.00) ramp_dep = ramp_dep + 0.50;
else if (key_stroke=='e' && ramp_dep > 0.50) ramp_dep = ramp_dep - 0.50;
else if (key_stroke=='w' && ramp_vel < 64.0) ramp_vel = ramp_vel * 2.0;
else if (key_stroke=='q' && ramp_vel > 1.0) ramp_vel = ramp_vel / 2.0;
else if (key_stroke=='s' && sin_freq < 16.0) sin_freq = sin_freq * 2.0;
else if (key_stroke=='a' && sin_freq > 0.125) sin_freq = sin_freq / 2.0;
else if (key_stroke=='f' && sin_amp < 0.5) sin_amp = sin_amp + 0.25;
else if (key_stroke=='d' && sin_amp > 0.25) sin_amp = sin_amp - 0.25;
else if (key_stroke=='h' && sin_start_dep < 2.0) sin_start_dep = sin_start_dep + 1.0;
else if (key_stroke=='g' && sin_start_dep > 1.0) sin_start_dep = sin_start_dep - 1.0;
else if (key_stroke=='z' && !strcmp(trial,"a")) strcpy(trial,"b");
else if (key_stroke=='z' && !strcmp(trial,"b")) strcpy(trial,"c");
else if (key_stroke=='z' && !strcmp(trial,"c")) strcpy(trial,"d");
else if (key_stroke=='z' && !strcmp(trial,"d")) strcpy(trial,"a");
}
}

/* ZERO TORQUE TO MOTORS---------------------------------------------*/
motor_1(2048);
motor_2(2048);

/* FREE MEMORY BLOCKS------------------------------------------------*/
farfree(normal);
farfree(tangent);
farfree(phi);
farfree(theta);
farfree(data_time);
clrscr();
return 0;
}

/* A/D BOARD INITIALIZATION FUNCTION---------------------------------*/
void initad(void)
{
        int i;
        outportb(BASE_ADDRESS, INIT_VALUE);
        for(i=1; i<1000; i++);
        inportb(BASE_ADDRESS+2);
        inportb(BASE_ADDRESS+3);
        outportb(BASE_ADDRESS, MODE_ZERO);
}

/* READ CHANNEL ON A/D BOARD FUNCTION--------------------------------*/
int read_channel(int channel_num)
{
        int high_byte, low_byte, q;
        outportb(BASE_ADDRESS + 1, channel_num);
        while (inportb(BASE_ADDRESS) < 128);
        low_byte = inportb(BASE_ADDRESS + 2);
```

```c
        high_byte = inportb(BASE_ADDRESS + 3);
        q = high_byte * 256 + low_byte;
        return q;
}


/* DA OUTPUT TO TOP LINK MOTOR---------------------------------------*/
void motor_1(int dig_value)
{
        outport(BASE_ADDRESS+2, dig_value%256);
        outport(BASE_ADDRESS+3, dig_value/256);
}


/* DA OUTPUT TO BOTTOM LINK MOTOR------------------------------------*/
void motor_2(int dig_value)
{
        outport(BASE_ADDRESS+4, dig_value%256);
        outport(BASE_ADDRESS+5, dig_value/256);
}


/* PD CONTROL OF BOTTOM LINK-----------------------------------------*/
void move_theta(float des_pos)
{
        int             theta_vel;
        float           kp_theta = 5.0;
        float           kv_theta = 8.0;

        /* POSITION READING-----------------------------------------*/
        theta_pos = read_channel(THETA_CHANNEL);

        /* VELOCITY = POSITION / TIME-------------------------------*/
        v_theta++;
        if (v_theta >= CVM) v_theta = 0;
        theta_vel = prev_theta[v_theta] - theta_pos;
        prev_theta[v_theta] = theta_pos;

        /* ADD OFFSET TO CONTROL LAW--------------------------------
           (this is simply a variable kp term, which adds stability
            and it improves holding state/force)                  */

        if ((des_pos - theta_pos) > 20 && offset_theta < 2048) offset_theta = offset_theta + 3;
        if ((des_pos - theta_pos) < -20 && offset_theta > -2048) offset_theta = offset_theta - 3;

        /* PD CONTROL-----------------------------------------------*/
        torque_theta = -kp_theta * (theta_pos - des_pos) +
                        kv_theta * (theta_vel) + offset_theta + 2048;
        if(torque_theta > MAX_V)        torque_theta = MAX_V;
        if(torque_theta < MIN_V)        torque_theta = MIN_V;

        /* OUPUT TO MOTOR-------------------------------------------*/
        motor_2 (torque_theta);
}


/* PD CONTROL OF TOP LINK-------------------------------------------*/
void move_phi(float des_pos)
{
```

```c
int             phi_vel;
float           kp_phi = 3.0;
float           kv_phi = 4.0;

/* POSITION READING-----------------------------------*/
 phi_pos = read_channel(PHI_CHANNEL);

/* VELOCITY = POSITION / TIME-------------------------*/
v_phi++;
if (v_phi >= CVM) v_phi = 0;
phi_vel = prev_phi[v_phi] - phi_pos;
prev_phi[v_phi] = phi_pos;

/* OFFSET TERM----------------------------------------*/
if ((des_pos - phi_pos) > 20 && offset_phi < 2048) offset_phi = offset_phi + 3;
if ((des_pos - phi_pos) < -20 && offset_phi > -2048) offset_phi = offset_phi - 3;

/* PD CONTROL-----------------------------------------*/
torque_phi = -kp_phi * (phi_pos - des_pos) + kv_phi * (phi_vel) + offset_phi + 2048;
if(torque_phi > MAX_V)                  torque_phi = MAX_V;
if(torque_phi < MIN_V)          torque_phi = MIN_V;

/* OUTPUT TORQUE--------------------------------------*/
        motor_1(torque_phi);
}


/* HOLD FUNCTION--------------------------------------*/
void hold (void)
{
        calc_angles(x,y);
        move_theta(theta_cnts);
        move_phi(phi_cnts);
}

/* RAMP/HOLD X-DIR ONLY FUNCTION-----------------------------*/
void ramp_hold_x (float vel, float dep)
{
        int     rh_time = 10 * controlrate;     /* holding time */
        int     steady_time = controlrate / 2;  /* steady time  */
        float           x_due_to_force;

        /* sensor beam deflects; compensate with stimulator */
        x_due_to_force = (offset_normal - normal_tmp) * 0.01 / 70.0;

        /* HOLD AND RECORD STEADY-------------------------*/
        if(steady_cnt < steady_time) {
                get_data_flag = 1;
                steady_cnt++;
                }
        /* RAMP UP----------------------------------------*/
        else if(x < (start_x + dep + x_due_to_force) && rh_cnt < rh_time) {
                x = x + vel / controlrate;
                rh_cnt ++;
                }
        /* HOLD POSITION----------------------------------*/
```

```
                else if (rh_cnt < rh_time) {
                        x = start_x + dep + x_due_to_force;
                        rh_cnt++;
                        }
                /* RAMP OUT----------------------------------------*/
                else if (rh_cnt >= rh_time && x > start_x) {
                        x = x - (vel / controlrate);
                        get_data_flag = 0;
                        }
                /* RETURN TO HOLD STATE----------------------------*/
                else if (rh_cnt >= rh_time && x <= start_x) {
                        x = start_x;
                        function_flag = 0;
                        rh_cnt = 0;        /* reset counter for hold */
                        steady_cnt = 0;
                        check_flag = 5;
                        save_data_flag = 1;        /* indicate that data should be saved */
                        }
                /* MOTION------------------------------------------*/
                calc_angles(x,y);
                move_theta(theta_cnts);
                move_phi(phi_cnts);
}


/* SINUSOID X-DIR ONLY FUNCTION-------------------------------------*/
void sinusoid (float start_dep, float amp, float freq, float phas)
{
                float                t;
                int                  sin_time = 5 * controlrate;
                int                  rh_time = 5 * controlrate;
                float                ramp_vel = 5.0;
                int        steady_time = controlrate / 2;        /* steady time       */
                float                x_due_to_force = 0.0;
                float                cos_term;

                /* CALCULATE SIN_TIME------------------------------------
                   (larger of 5 seconds or two sinusoids)                */
                if (freq < 0.5) sin_time = (int)((2 / freq) * controlrate);

                /* SENSOR DEFLECTION------------------------------------
                        (sensor beam deflects; compensate with stimulator)      */
                x_due_to_force = (offset_normal - normal_tmp) * 0.01 / 70.0;

                /* HOLD AND RECORD STEADY--------------------------------*/
                if(steady_cnt < steady_time) {
                        get_data_flag = 1;
                        steady_cnt++;
                        }

                /* RAMP UP TO STARTING DEPTH----------------------------*/
                else if (x < (start_x + start_dep + x_due_to_force) && rh_cnt < rh_time) {
                        x = x + ramp_vel / controlrate;
                        rh_cnt++;
                        }
```

```c
/* HOLD POSITION UNTIL STEADY STATE----------------------*/
else if (rh_cnt < rh_time) {
        x = start_x + start_dep + x_due_to_force;
        rh_cnt++;
        }


/* SINUSOID---------------------------------------------
  (cos(wt + p);  w = 2*pi*f, where f = frequency
  p = phase shift (radians))                              */

else if (rh_cnt >= rh_time  && sin_cnt < sin_time)
        {
        sin_cnt ++;
        /* convert counts to seconds */
        t = (float)(sin_cnt) / (float)(controlrate);
        cos_term = cos((6.283153*freq*t) + phas);

        /* CALCULATE PRESCRIBED SINE POSITION--------*/
        x = start_x + start_dep + x_due_to_force + amp * cos_term;
        }

/* End at postion you started at */

/* RAMP BACK-----------------------------------------*/
else if (sin_cnt >= sin_time && x > start_x) {
        x = x - 5.0 / controlrate;
        get_data_flag = 0;
        }


/* RETURN TO HOLD STATE-----------------------------*/
else if (sin_cnt >= sin_time && x <= start_x) {
        x = start_x;
        function_flag = 0;
        rh_cnt = 0;     /* reset counters for hold and sine */
        steady_cnt = 0;
        sin_cnt = 0;
        save_data_flag = 1; /* save data */
        }


/* MOTION-------------------------------------------*/
calc_angles(x,y);
move_theta(theta_cnts);
move_phi(phi_cnts);
}

/* XY TO ANGULAR COUNTS FUNCTION-----------------------------------*/
void calc_angles (float x_calc, float y_calc)
{
        float           theta_2;
        float           theta_1;
        float           phi;

/* Convert (x,y) to (theta_1, theta_2) using inverse kinematic equations */
        theta_2 = -acos((pow(x_calc,2) + pow(y_calc,2) - 11612.88) / 11612.88);
        theta_1 = atan(y_calc/x_calc) - atan(76.2*sin(theta_2) / (76.2 + 76.2 * cos(theta_2)));
```

138

```
        phi = theta_1 + theta_2;

/* Convert to counts based on calibrated 90,0 position of stimulator          */
/* as designated by THETA_HOME and PHI_HOME, direction of count increase,      */
/* and calibrated counts/angle for each link/pot                              */

        theta_cnts = THETA_HOME - ((1.5708 - theta_1) * CPTHETA);
        phi_cnts = PHI_HOME - (phi)*CPPHI;
}
```

Appendix B

Sinusoid Response Data

The amount of data collected on the ramp/hold/sinusoid response of the fingerpad to indentation was extensive, and it was undesirable to contain all of it within the main body of the text. Therefore, the remaining 0.5 mm amplitude data with all indentors is given here for reference. The graphs are labeled and given in a sensible order according to the available parameters of frequency, starting depth, subject and indentor.

Input (Point)

Output (Subject #1)

Input (Point)

Output (Subject #1)

Input (Point)

Output (Subject #1)

Input (Point)

Output (Subject #1)

Time (seconds)

Time (seconds)

Input (Point)

Input (Point)

Output (Subject #1)

Output (Subject #1)

Input (Point)

Input (Point)

Output (Subject #1)

Output (Subject #1)

144

Input (Point)

Input (Point)

Output (Subject #2)

Output (Subject #2)

Input (Point)

Input (Point)

Output (Subject #2)

Output (Subject #2)

147

Input (Point) — Depth (mm); Output (Subject #3) — Force (Newtons); Input (Point) — Depth (mm); Output (Subject #3) — Force (Newtons); Time (seconds)

150

Input (Point)

Depth (mm)

Input (Point)

Output (Subject #4)

Force (Newtons)

Output (Subject #4)

Input (Point)

Depth (mm)

Input (Point)

Output (Subject #4)

Force (Newtons)

Time (seconds)

Output (Subject #4)

Time (seconds)

Input (Point)

Input (Point)

Output (Subject #4)

Output (Subject #4)

Input (Point)

Input (Point)

Output (Subject #4)

Output (Subject #4)

Input (Point)

Input (Point)

Output (Subject #5)

Output (Subject #5)

Input (Point)

Input (Point)

Output (Subject #5)

Output (Subject #5)

Input (Point)

Output (Subject #5)

Input (Point)

Output (Subject #5)

160

Input (Circular)

Output (Subject #1)

Input (Circular)

Output (Subject #1)

Input (Circular)

Output (Subject #1)

Input (Circular)

Output (Subject #1)

163

Input (Circular)

Input (Circular)

Output (Subject #2)

Output (Subject #2)

Input (Circular)

Input (Circular)

Output (Subject #2)

Output (Subject #2)

165

Input (Circular)

Input (Circular)

Output (Subject #2)

Output (Subject #2)

Input (Circular)

Input (Circular)

Output (Subject #2)

Output (Subject #2)

Input (Circular)

Input (Circular)

Output (Subject #3)

Output (Subject #3)

Input (Circular)

Input (Circular)

Output (Subject #3)

Output (Subject #3)

Input (Circular)

Input (Circular)

Output (Subject #3)

Output (Subject #3)

Input (Circular)

Input (Circular)

Output (Subject #3)

Output (Subject #3)

Time (seconds)

Time (seconds)

Input (Circular) / Output (Subject #3) / Input (Circular) / Output (Subject #3) / Input (Circular) / Output (Subject #3) / Input (Circular) / Output (Subject #3)

Input (Circular) / Output (Subject #4)

Input (Circular)

Output (Subject #4)

Input (Circular)

Output (Subject #4)

Input (Circular)

Input (Circular)

Output (Subject #5)

Output (Subject #5)

Input (Circular)

Input (Circular)

Output (Subject #5)

Output (Subject #5)

Input (Circular)

Output (Subject #5)

Input (Circular)

Output (Subject #5)

Input (Circular)

Output (Subject #5)

Input (Circular)

Output (Subject #5)

Input (Flat Plate)

Input (Flat Plate)

Output (Subject #1)

Output (Subject #1)

Input (Flat Plate)

Input (Flat Plate)

Output (Subject #1)

Output (Subject #1)

Input (Flat Plate)

Output (Subject #1)

Input (Flat Plate)

Output (Subject #1)

Time (seconds)

Input (Flat Plate) — Depth (mm) vs time (0–20)
Input (Flat Plate) — Depth (mm) vs time (0–12)
Output (Subject #2) — Force (Newtons) vs time (0–20)
Output (Subject #2) — Force (Newtons) vs time (0–12)
Input (Flat Plate) — Depth (mm) vs time (0–10)
Input (Flat Plate) — Depth (mm) vs time (0–10)
Output (Subject #2) — Force (Newtons) vs Time (seconds)
Output (Subject #2) — Force (Newtons) vs Time (seconds)

Input (Flat Plate)

Output (Subject #2)

Input (Flat Plate)

Output (Subject #2)

Input (Flat Plate)

Input (Flat Plate)

Output (Subject #3)

Output (Subject #3)

Input (Flat Plate)

Input (Flat Plate)

Output (Subject #3)

Output (Subject #3)

Time (seconds)

Time (seconds)

Input (Flat Plate)

Output (Subject #3)

Input (Flat Plate)

Output (Subject #3)

190

Input (Flat Plate)

Input (Flat Plate)

Output (Subject #3)

Output (Subject #3)

Input (Flat Plate)

Input (Flat Plate)

Output (Subject #3)

Output (Subject #3)

Input (Flat Plate)

Output (Subject #3)

Input (Flat Plate)

Output (Subject #3)

Input (Flat Plate)

Input (Flat Plate)

Output (Subject #4)

Output (Subject #4)

Input (Flat Plate)

Input (Flat Plate)

Output (Subject #4)

Output (Subject #4)

Time (seconds)

Time (seconds)

Input (Flat Plate)

Output (Subject #4)

Input (Flat Plate)

Output (Subject #4)

Time (seconds)

195

Input (Flat Plate)

Output (Subject #4)

Input (Flat Plate)

Output (Subject #4)

196

Input (Flat Plate)

Output (Subject #5)

Input (Flat Plate)

Output (Subject #5)

197

198

Input (Flat Plate)

Output (Subject #5)

Input (Flat Plate)

Output (Subject #5)

Input (Flat Plate)

Input (Flat Plate)

Output (Subject #5)

Output (Subject #5)

Input (Flat Plate)

Input (Flat Plate)

Output (Subject #5)

Output (Subject #5)

Appendix C

Hysteresis Curves

Again for reasons of conserving space in the main body of the thesis, the hysteresis curves for all subjects is presented here in order of subjects for all indentors but only for 0.125, 0.5, 2 and 4 hz sinusoids.

Subj #1: 0.125 Hz; 0.25 mm

Subj #1: 0.125 Hz; 0.5 mm

Subj #1: 0.5 Hz; 0.25 mm

Subj #1: 0.5 Hz; 0.5 mm

Subj #1: 2 Hz; 0.25 mm

Subj #1: 2 Hz; 0.5 mm

Subj #1: 4 Hz; 0.25 mm

Subj #1: 4 Hz; 0.5 mm

Subj #1: 0.125 Hz; 0.25 mm

Subj #1: 0.125 Hz; 0.5 mm

Subj #1: 0.5 Hz; 0.25 mm

Subj #1: 0.5 Hz; 0.5 mm

Subj #1: 2 Hz; 0.25 mm

Subj #1: 2 Hz; 0.5 mm

Subj #1: 4 Hz; 0.25 mm

Subj #1: 4 Hz; 0.5 mm

Force (N)

Depth w/Circular (mm)

Depth w/Circular (mm)

203

Subj #1: 0.125 Hz; 0.25 mm Subj #1: 0.125 Hz; 0.5 mm

Subj #1: 0.5 Hz; 0.25 mm Subj #1: 0.5 Hz; 0.5 mm

Subj #1: 2 Hz; 0.25 mm Subj #1: 2 Hz; 0.5 mm

Subj #1: 4 Hz; 0.25 mm Subj #1: 4 Hz; 0.5 mm

Depth w/Flat Plate (mm) Depth w/Flat Plate (mm)

Subj #2: 0.125 Hz; 0.25 mm

Subj #2: 0.125 Hz; 0.5 mm

Subj #2: 0.5 Hz; 0.25 mm

Subj #2: 0.5 Hz; 0.5 mm

Subj #2: 2 Hz; 0.25 mm

Subj #2: 2 Hz; 0.5 mm

Subj #2: 4 Hz; 0.25 mm

Subj #2: 4 Hz; 0.5 mm

Depth w/Point (mm)

Force (N)

Subj #2: 0.125 Hz; 0.25 mm

Subj #2: 0.125 Hz; 0.5 mm

Subj #2: 0.5 Hz; 0.25 mm

Subj #2: 0.5 Hz; 0.5 mm

Subj #2: 2 Hz; 0.25 mm

Subj #2: 2 Hz; 0.5 mm

Subj #2: 4 Hz; 0.25 mm

Subj #2: 4 Hz; 0.5 mm

Depth w/Circular (mm)

Depth w/Circular (mm)

Subj #2: 0.125 Hz; 0.25 mm

Subj #2: 0.125 Hz; 0.5 mm

Subj #2: 0.5 Hz; 0.25 mm

Subj #2: 0.5 Hz; 0.5 mm

Subj #2: 2 Hz; 0.25 mm

Subj #2: 2 Hz; 0.5 mm

Subj #2: 4 Hz; 0.25 mm

Subj #2: 4 Hz; 0.5 mm

Depth w/Flat Plate (mm)

Depth w/Flat Plate (mm)

Subj #3: 0.125 Hz; 0.25 mm

Subj #3: 0.125 Hz; 0.5 mm

Subj #3: 0.5 Hz; 0.25 mm

Subj #3: 0.5 Hz; 0.5 mm

Subj #3: 2 Hz; 0.25 mm

Subj #3: 2 Hz; 0.5 mm

Subj #3: 4 Hz; 0.25 mm

Subj #3: 4 Hz; 0.5 mm

Depth w/Point (mm)

Depth w/Point (mm)

Subj #3: 0.125 Hz; 0.25 mm

Subj #3: 0.125 Hz; 0.5 mm

Subj #3: 0.5 Hz; 0.25 mm

Subj #3: 0.5 Hz; 0.5 mm

Subj #3: 2 Hz; 0.25 mm

Subj #3: 2 Hz; 0.5 mm

Subj #3: 4 Hz; 0.25 mm

Subj #3: 4 Hz; 0.5 mm

Depth w/Circular (mm)

Subj #3: 0.125 Hz; 0.25 mm

Subj #3: 0.125 Hz; 0.5 mm

Subj #3: 0.5 Hz; 0.25 mm

Subj #3: 0.5 Hz; 0.5 mm

Subj #3: 2 Hz; 0.25 mm

Subj #3: 2 Hz; 0.5 mm

Subj #3: 4 Hz; 0.25 mm

Subj #3: 4 Hz; 0.5 mm

Depth w/Flat Plate (mm)

Depth w/Flat Plate (mm)

Subj #4: 0.125 Hz; 0.25 mm

Subj #4: 0.125 Hz; 0.5 mm

Subj #4: 0.5 Hz; 0.25 mm

Subj #4: 0.5 Hz; 0.5 mm

Subj #4: 2 Hz; 0.25 mm

Subj #4: 2 Hz; 0.5 mm

Subj #4: 4 Hz; 0.25 mm

Subj #4: 4 Hz; 0.5 mm

Subj #4: 0.125 Hz; 0.25 mm

Subj #4: 0.125 Hz; 0.5 mm

Subj #4: 0.5 Hz; 0.25 mm

Subj #4: 0.5 Hz; 0.5 mm

Subj #4: 2 Hz; 0.25 mm

Subj #4: 2 Hz; 0.5 mm

Subj #4: 4 Hz; 0.25 mm

Subj #4: 4 Hz; 0.5 mm

212

Subj #4: 0.125 Hz; 0.25 mm

Subj #4: 0.125 Hz; 0.5 mm

Subj #4: 0.5 Hz; 0.25 mm

Subj #4: 0.5 Hz; 0.5 mm

Subj #4: 2 Hz; 0.25 mm

Subj #4: 2 Hz; 0.5 mm

Subj #4: 4 Hz; 0.25 mm

Subj #4: 4 Hz; 0.5 mm

Force (N)

Depth w/Flat Plate (mm)

Subj #5: 0.125 Hz; 0.25 mm

Subj #5: 0.125 Hz; 0.5 mm

Subj #5: 0.5 Hz; 0.25 mm

Subj #5: 0.5 Hz; 0.5 mm

Subj #5: 2 Hz; 0.25 mm

Subj #5: 2 Hz; 0.5 mm

Subj #5: 4 Hz; 0.25 mm

Subj #5: 4 Hz; 0.5 mm

Depth w/Point (mm)

Force (N)

Subj #5: 0.125 Hz; 0.25 mm

Subj #5: 0.125 Hz; 0.5 mm

Subj #5: 0.5 Hz; 0.25 mm

Subj #5: 0.5 Hz; 0.5 mm

Subj #5: 2 Hz; 0.25 mm

Subj #5: 2 Hz; 0.5 mm

Subj #5: 4 Hz; 0.25 mm

Subj #5: 4 Hz; 0.5 mm

Depth w/Circular (mm)

Subj #5: 0.125 Hz; 0.25 mm

Subj #5: 0.125 Hz; 0.5 mm

Subj #5: 0.5 Hz; 0.25 mm

Subj #5: 0.5 Hz; 0.5 mm

Subj #5: 2 Hz; 0.25 mm

Subj #5: 2 Hz; 0.5 mm

Subj #5: 4 Hz; 0.25 mm

Subj #5: 4 Hz; 0.5 mm

Depth w/Flat Plate (mm)

Appendix D

Hysteresis Slope and Percentage Area

This appendix displays the slope and percentage area data of the hysteresis curves for the five subjects with the five indentors. Solid lines indicate 0.5 mm amplitude and dashed 0.25 mm.

Subject #1 – 1 mm starting depth

2 mm starting depth

1 mm starting depth

2 mm starting depth

Frequency (hz)

Subject #2 – 1 mm starting depth

2 mm starting depth

1 mm starting depth

2 mm starting depth

Frequency (hz)

Subject #3 – 1 mm starting depth

2 mm starting depth

1 mm starting depth

2 mm starting depth

Frequency (hz)

Subject #4 – 1 mm starting depth

2 mm starting depth

1 mm starting depth

2 mm starting depth

Frequency (hz)

Subject #5 – 1 mm starting depth

2 mm starting depth

1 mm starting depth

2 mm starting depth

Frequency (hz)

Appendix E

Matlab™ Modeling Software

In order to estimate parameters of the final model using real data, software had to be written to perform simulations in Matlab™. These entailed some preexisting notion of the model and hence the form of the response. A function called fmins in Matlab was used to curve fit a response equation to the real data. Given the model and the equations of its response, fmins is a local minimizer which uses a Simplex search method to find the unknown coefficients of a function that "best fit" a vector of data. Following is a pair of programs used to fit to the steady state data and the pair of programs used to fit the final model to the experimental data. The latter were performed twice, the second time with starting paramters equal to the mean of those estimated on the first run to achieve some degree of consistency in estimation across subjects. Additional software was used for processes such as the numerical filtering and averaging of data, processing the results and graphs and parameters, etc., but it is not included in this document.

```
% POLYFITDATA.M

% also uses rpolyfit.m
% SAVE:  results to pnonlink.mat, cnonlink.mat, fnonlink.mat

%2mm/sec INDENTATIONS

%DEFINE FORCES (1              2              3              4              5)
%              ========     ========     =========     ========     ========
%POINT
PFssD = [      0              0              0              0              0;
               0.01615        0.0005819      0.01511        0              0.0292;
               0.05199        0.02829        0.03257        0.02667        0.04459;
               0.08337        0.06624        0.05603        0.1029         0.07759;
               0.1515         0.1315         0.1076         0.1771         0.1192;
               0.2726         0.223          0.1664         0.2759         0.1497;
               0.4016         0.4445         0.2642         0.4497         0.2234];


%CIRCULAR
CFssD = [      0              0              0              0              0;
               0.02488        0.01943        0.01273        0.02349        0.02896;
               0.08464        0.08559        0.06308        0.06827        0.08545;
               0.2093         0.167          0.1282         0.1966         0.1214;
               0.3846         0.3244         0.2227         0.3496         0.247;
               0.7977         0.7233         0.4166         0.5822         0.4386;
               1.461          1.212          0.667          0.9872         0.681];


%FLAT
FFssD = [      0              0              0              0              0;
               0.04103        0.0429         0.02235        0.04212        0.03037;
               0.2238         0.2319         0.109          0.1675         0.1281;
               0.5513         0.6428         0.2243         0.4592         0.3395;
               1.03           1.422          0.5003         0.845          0.6753];

%DEPTH of INDENTATION

Depth = [0.0; 0.5; 1.0; 1.5; 2.0; 2.5; 3.0];

% POLYFIT to get COEFF of NON-LINEAR SPRING
%============================================================================

global Fss D PlotHandle z

for i = 1:5,
        Fss = PFssD(:,i);
        D = Depth;
        clg
        plot(D,Fss,'b')
        hold on
        PlotHandle = plot(D,Fss,'EraseMode','xor');
        lam = [0 0 0 ]';
        trace = 0;
```

```
                    tol = 0.01;
                    options = [trace tol];
                    options(14) = 1000;
                    lambda = fmins('rpolyfit3',lam,options);

                    pnonlink (i,:) = [abs(lambda') 0];
end

save pnonlink pnonlink

for i = 1:5,
                    Fss = CFssD(:,i);
                    D = Depth;
                    clg
                    plot(D,Fss,'b')
                    hold on
                    PlotHandle = plot(D,Fss,'EraseMode','xor');
                    lam = [0 0 0]';
                    trace = 0;
                    tol = 0.01;
                    options = [trace tol];
                    options(14) = 1000;
                    lambda = fmins('rpolyfit3',lam,options);

                    cnonlink (i,:) = [abs(lambda') 0];
end

save cnonlink cnonlink

for i = 1:5,
                    Fss = FFssD(:,i);
                    D = Depth(1:5);
                    clg
                    plot(D,Fss,'b')
                    hold on
                    PlotHandle = plot(D,Fss,'EraseMode','xor');
                    lam = [0 0 0]';
                    trace = 0;
                    tol = 0.01;
                    options = [trace tol];
                    options(14) = 1000;
                    lambda = fmins('rpolyfit3',lam,options);

                    fnonlink (i,:) = [abs(lambda') 0];
end

save fnonlink fnonlink

%========================================================================
```

```
function err = rpolyfit(lambda)

% RPOLYFIT.M
% local minizer curve fit to data of the form of a 3rd order polynomical


global Fss D PlotHandle z

z = (abs(lambda(1)).*D.^3) + (abs(lambda(2)).*D.^2) + (abs(lambda(3)).*D);

set(PlotHandle,'ydata',z);
drawnow

err = sum((z-Fss).^2);
```

```
%========================================================
%
% BKPLMNEW.M        (1/6/95)
%
% Kelvin block nonlinear model approximated in a piecewise linear fashion
% Blocks are in 0.5 mm increments
% Parallel spring coefficients have been predicted once from steady state data
%               (see ssfit.m, rssfit.m)
%
% !! NORMALIZES THE RESPONSE WRT/ STEADY STATE FORCE AT HIGHEST MEASURED
DEPTH
%
%========================================================

% LOAD:  parallel piecewise spring coefficients
% =================================
load pssfit
load cssfit
load fssfit
% =================================

amp = '2';
AMP = 0.5;
depth = '8';
DEPTH = 2;

t0 = clock;

for subloop = 1:5,

        if subloop == 1,
                subj = 'd';
                directory = 'danna';
                Fss = [0.4016 1.461 1.03];
        elseif subloop == 2,
                subj = 'j';
                directory = 'jeremy';
                Fss = [0.4445 1.212 1.422];
        elseif subloop == 3,
                subj = 'r';
                directory = 'rogeve';
                Fss = [0.2642 0.667 0.5003];
        elseif subloop == 4,
                subj = 's';
                directory = 'srini';
                Fss = [0.4497 0.9872 0.845];
        elseif subloop == 5,
                subj = 'w';
                directory = 'walt';
                Fss = [0.2234 0.681 0.6753];
```

```
          end

for indloop = 1:3,

          if indloop == 1,
                    ind = 'p';
          elseif indloop == 2,
                    ind = 'c';
          elseif indloop == 3,
                    ind = 'f';
          end

setpk = ['pk = ',ind,'ssfit(subloop,:);'];
eval(setpk);

for freqloop = 1:8,

          if freqloop == 1,
                    freq = 'f1';
                    FREQ = 0.125;
          elseif freqloop == 2,
                    freq = 'f2';
                    FREQ = 0.25;
          elseif freqloop == 3,
                    freq = 'f4';
                    FREQ = 0.5;
          elseif freqloop == 4,
                    freq = '1';
                    FREQ = 1.0;
          elseif freqloop == 5,
                    freq = '2';
                    FREQ = 2.0;
          elseif freqloop == 6,
                    freq = '4';
                    FREQ = 4.0;
          elseif freqloop == 7,
                    freq = '8';
                    FREQ = 8.0;
          elseif freqloop == 8,
                    freq = '16';
                    FREQ = 16.0;
          end

% TAKE RAMP/HOLD AND 2 WAVES TO FIT
%==================================
timewave = (1/FREQ) * 500;
beginsin = 250;
%endsin = 2750 + 2*timewave;
endsin = 5250;
newinc = 4;

% LOAD RAW RAMP/HOLD/SINUSOID DATA
%==================================
ldfil = ['load ',directory,'/',ind,'/',subj,'4',ind,freq,amp,';'];
eval(ldfil);
```

```
% Decrease sampling rate by a factor of 'newinc'; still allows 8 pts per sine at 16 hz
%---------------------------------------------------------------------------------
sin4x(:,freqloop) = x(250:newinc:endsin);

% Convert force output to Newtons and normalize with respect to steady state force
%---------------------------------------------------------------------------------
sin4f(:,freqloop) = normal(250:newinc:endsin) * 0.00981 / Fss(indloop);

ldfil = ['load ',directory,'/',ind,'/',subj,'8',ind,freq,amp,';'];
eval(ldfil);
sin8x(:,freqloop) = x(250:newinc:endsin);
sin8f(:,freqloop) = normal(250:newinc:endsin) * 0.00981 / Fss(indloop);

end      %freqloop

% SOLVE USING FMINS giving preliminary values for parallel spring coefficients
%=============================================================
global sin4x sin4f sin8x sin8f newinc

tol = 0.1;
trace = 0;
options = [trace tol];

lam = [pk(1) 0.1 0.1 pk(2) 0.1 0.1 pk(3) 0.1 0.1 pk(4) 0.1 0.1 pk(5) 0.1 0.1];

lambda = fmins('sinfitnew',lam,options);

setvar = [ind,'coeff(subloop,:) = abs(lambda)'];
eval(setvar);

savevar = ['save ',ind,'coeff1 ',ind,'coeff'];
eval(savevar);

% display elapsed time for reference
etime(clock,t0)

end      %indloop

end      %subloop
```

```
function err = sinfitnew(lambda)

% SINFITNEW.M
%
% USAGE:  FMINS from BKPLMNEW.M
%
% fmins function to fit ramp/hold/sinusoid data with piecewise linear
% model of series spring and dashpot in parallel with piecewiselinear spring.
%

% Piece from 0 mm
k1a = abs(lambda(1));
k1b = abs(lambda(2));
b1 = abs(lambda(3));

% Piece from 0.5 mm
k2a = abs(lambda(4));
k2b = abs(lambda(5));
b2 = abs(lambda(6));

% Piece from 1 mm
k3a = abs(lambda(7));
k3b = abs(lambda(8));
b3 = abs(lambda(9));

% Piece from 1.5 mm
k4a = abs(lambda(10));
k4b = abs(lambda(11));
b4 = abs(lambda(12));

% Piece from 2 mm
k5a = abs(lambda(13));
k5b = abs(lambda(14));
b5 = abs(lambda(15));

global sin4x sin4f sin8x sin8f newinc

% Sampling period.
% (decreased by a factor of newinc)
Ts = newinc/500;

num = [k1a+k1b k1a*k1b/b1];
den = [1 k1b/b1];
[a,b,c,d] = tf2ss(num,den);
[a1,b1,c1,d1] = c2dm(a,b,c,d,Ts);

num = [k2a+k2b k2a*k2b/b2];
den = [1 k2b/b2];
[a,b,c,d] = tf2ss(num,den);
[a2,b2,c2,d2] = c2dm(a,b,c,d,Ts);
```

230

```
num = [k3a+k3b k3a*k3b/b3];
den = [1 k3b/b3];
[a,b,c,d] = tf2ss(num,den);
[a3,b3,c3,d3] = c2dm(a,b,c,d,Ts);


num = [k4a+k4b k4a*k4b/b4];
den = [1 k4b/b4];
[a,b,c,d] = tf2ss(num,den);
[a4,b4,c4,d4] = c2dm(a,b,c,d,Ts);


num = [k5a+k5b k5a*k5b/b5];
den = [1 k5b/b5];
[a,b,c,d] = tf2ss(num,den);
[a5,b5,c5,d5] = c2dm(a,b,c,d,Ts);


for freqloop = 2:7,

sinx = sin4x(:,freqloop);
x2 = zeros(size(sinx));
x2(find(sinx>0.5)) = sinx(sinx>0.5) - 0.5;
x3 = zeros(size(sinx));
x3(find(sinx>1)) = sinx(sinx>1) - 1;
x4 = zeros(size(sinx));
x4(find(sinx>1.5)) = sinx(sinx>1.5) - 1.5;
x5 = zeros(size(sinx));
x5(find(sinx>2)) = sinx(sinx>2) - 2;

[output1,statevar] = dlsim(a1,b1,c1,d1,sinx);
[output2,statevar] = dlsim(a2,b2,c2,d2,x2);
[output3,statevar] = dlsim(a3,b3,c3,d3,x3);
[output4,statevar] = dlsim(a4,b4,c4,d4,x4);
[output5,statevar] = dlsim(a5,b5,c5,d5,x5);
output=output1+output2+output3+output4+output5;
error4 (freqloop) = sum(abs(output-sin4f(:,freqloop)));

sinx = sin8x(:,freqloop);
x2 = zeros(size(sinx));
x2(find(sinx>0.5)) = sinx(sinx>0.5) - 0.5;
x3 = zeros(size(sinx));
x3(find(sinx>1)) = sinx(sinx>1) - 1;
x4 = zeros(size(sinx));
x4(find(sinx>1.5)) = sinx(sinx>1.5) - 1.5;
x5 = zeros(size(sinx));
x5(find(sinx>2)) = sinx(sinx>2) - 2;

[output1,statevar] = dlsim(a1,b1,c1,d1,sinx);
[output2,statevar] = dlsim(a2,b2,c2,d2,x2);
[output3,statevar] = dlsim(a3,b3,c3,d3,x3);
[output4,statevar] = dlsim(a4,b4,c4,d4,x4);
[output5,statevar] = dlsim(a5,b5,c5,d5,x5);
output=output1+output2+output3+output4+output5;
error8 (freqloop) = sum(abs(output-sin8f(:,freqloop)));
```

```
end      %freqloop

err = sum(error4) + sum(error8);
```

Appendix F

Model vs. Experimental Data

This section of the appendix presents the graphs of the model predictions vs. the experimental data for all frequencies and indentors but only at 2 mm starting depth and 0.5 mm amplitudes.

S1 – 0.5 mm,2 mm (Point)

R^2 = 0.9876

R^2 = 0.9944

R^2 = 0.9955

R^2 = 0.994

R^2 = 0.9941

R^2 = 0.9863

R^2 = 0.9794

R^2 = 0.9564

Force (Newtons)

Time (seconds)

Time(seconds)

S2 – 0.5 mm,2 mm (Point)

235

S3 – 0.5 mm,2 mm (Point)

R^2 = 0.9961

S3 – 0.5 mm,2 mm (Point)

R^2 = 0.9982

S3 – 0.5 mm,2 mm (Point)

R^2 = 0.995

S3 – 0.5 mm,2 mm (Point)

R^2 = 0.9974

S3 – 0.5 mm,2 mm (Point)

R^2 = 0.9956

S3 – 0.5 mm,2 mm (Point)

R^2 = 0.9965

S3 – 0.5 mm,2 mm (Point)

R^2 = 0.9935

S3 – 0.5 mm,2 mm (Point)

R^2 = 0.9761

Force (Newtons)

Time (seconds)

Time(seconds)

S4 – 0.5 mm,2 mm (Point)

238

S1 – 0.5 mm, 2 mm (Circular)

R^2 = 0.9825

S1 – 0.5 mm, 2 mm (Circular)

R^2 = 0.9912

S1 – 0.5 mm, 2 mm (Circular)

R^2 = 0.9935

S1 – 0.5 mm, 2 mm (Circular)

R^2 = 0.9951

S1 – 0.5 mm, 2 mm (Circular)

R^2 = 0.9956

S1 – 0.5 mm, 2 mm (Circular)

R^2 = 0.9934

S1 – 0.5 mm, 2 mm (Circular)

R^2 = 0.9958

S1 – 0.5 mm, 2 mm (Circular)

R^2 = 0.988

240

S4 – 0.5 mm,2 mm (Circular)

242

S5 – 0.5 mm,2 mm (Circular)

$R^2 = 0.9906$

S5 – 0.5 mm,2 mm (Circular)

$R^2 = 0.9985$

S5 – 0.5 mm,2 mm (Circular)

$R^2 = 0.9976$

S5 – 0.5 mm,2 mm (Circular)

$R^2 = 0.9989$

S5 – 0.5 mm,2 mm (Circular)

$R^2 = 0.9979$

S5 – 0.5 mm,2 mm (Circular)

$R^2 = 0.9964$

S5 – 0.5 mm,2 mm (Circular)

$R^2 = 0.9947$

S5 – 0.5 mm,2 mm (Circular)

$R^2 = 0.9853$

Force (Newtons)

Time (seconds)

Time(seconds)

243

S1 – 0.5 mm,2 mm (Flat)

244

S2 – 0.5 mm,2 mm (Flat)

S2 – 0.5 mm,2 mm (Flat)

R^2 = 0.9966

R^2 = 0.999

R^2 = 0.9993

R^2 = 0.9991

R^2 = 0.9996

R^2 = 0.9992

R^2 = 0.999

R^2 = 0.9946

Force (Newtons)

Time (seconds)

Time(seconds)

S4 – 0.5 mm,2 mm (Flat)
S4 – 0.5 mm,2 mm (Flat)

R^2 = 0.9849
R^2 = 0.9835
R^2 = 0.9906
R^2 = 0.993
R^2 = 0.9961
R^2 = 0.99
R^2 = 0.9942
R^2 = 0.996

Force (Newtons)

Time (seconds)
Time(seconds)

Appendix G

General Model vs. Experimental Data

In this section, additional results from tests of a composite model formed from the average of the parameters for the 5 subjects in the case of each indentor. Again, the graphs are presented for all frequencies and indentors but for only 2 mm starting depth and 0.5 mm amplitude.

S1 – 0.5 mm,2 mm (Point)

R^2 = 0.9519

S1 – 0.5 mm,2 mm (Point)

R^2 = 0.8729

S1 – 0.5 mm,2 mm (Point)

R^2 = 0.8801

S1 – 0.5 mm,2 mm (Point)

R^2 = 0.8663

S1 – 0.5 mm,2 mm (Point)

R^2 = 0.8992

S1 – 0.5 mm,2 mm (Point)

R^2 = 0.8879

S1 – 0.5 mm,2 mm (Point)

R^2 = 0.9387

S1 – 0.5 mm,2 mm (Point)

R^2 = 0.9874

Force (Newtons)

Time(seconds)

S2 – 0.5 mm,2 mm (Point)

R^2 = 0.819

R^2 = 0.8316

R^2 = 0.9018

R^2 = 0.9076

R^2 = 0.8639

R^2 = 0.9405

R^2 = 0.9223

R^2 = 0.9718

Force (Newtons)

Time(seconds)

S4 – 0.5 mm,2 mm (Point)

R^2 = 0.9814

S4 – 0.5 mm,2 mm (Point)

R^2 = 0.9858

S4 – 0.5 mm,2 mm (Point)

R^2 = 0.963

S4 – 0.5 mm,2 mm (Point)

R^2 = 0.9833

S4 – 0.5 mm,2 mm (Point)

R^2 = 0.98

S4 – 0.5 mm,2 mm (Point)

R^2 = 0.972

S4 – 0.5 mm,2 mm (Point)

R^2 = 0.9752

S4 – 0.5 mm,2 mm (Point)

R^2 = 0.96

Force (Newtons)

Time(seconds)

255

S3 – 0.5 mm,2 mm (Circular)

S3 – 0.5 mm,2 mm (Circular)

R^2 = 0.9956

R^2 = 0.9901

R^2 = 0.9913

R^2 = 0.9921

R^2 = 0.9868

R^2 = 0.9756

R^2 = 0.9911

R^2 = 0.9876

Force (Newtons)

Time(seconds)

S4 - 0.5 mm,2 mm (Circular)

R^2 = 0.9601

R^2 = 0.9398

R^2 = 0.9704

R^2 = 0.9757

R^2 = 0.975

R^2 = 0.9652

R^2 = 0.9688

R^2 = 0.9828

Force (Newtons)

Time(seconds)

S5 – 0.5 mm,2 mm (Circular)

R^2 = 0.993

S5 – 0.5 mm,2 mm (Circular)

R^2 = 0.9834

S5 – 0.5 mm,2 mm (Circular)

R^2 = 0.9725

S5 – 0.5 mm,2 mm (Circular)

R^2 = 0.9864

S5 – 0.5 mm,2 mm (Circular)

R^2 = 0.9845

S5 – 0.5 mm,2 mm (Circular)

R^2 = 0.9883

S5 – 0.5 mm,2 mm (Circular)

R^2 = 0.9864

S5 – 0.5 mm,2 mm (Circular)

R^2 = 0.9687

Force (Newtons)

Time(seconds)

S2 – 0.5 mm,2 mm (Flat)

References

"Basics of Design Engineering." *Machine Design Annual Article Index.* Vol. 63, 1991.

Bolsinger, P.P. and Mai, N. "A Microcomputer System for the Measurement of Finger Forces." *J. Biomed. Eng.* 7:51-55, 1985.

Brooks, T.L. "Telerobot Response Requirements: A Position Paper on Control Response for the FTS Telerobot." 1990.

Darian-Smith, I. "The Sense of Touch: Performance and Peripheral Neural Processes." *Handbook of Physiology-The Nervouse System III.* pp. 739-788, 1984.

Finlay, B. "Dynamic Mechanical Testing of Human Skin *In Vivo.*" *J. Biomech.* 3:557-568, 1970.

Franke, E.K. "Mechanical Impedence of the Surface of the Human Body." 3:582-590, 1950.

Fung, Y.C. *Biomechanics: Mechanical Properties of Living Tissues, 2nd Ed.* New York: Springer-Verlag, 1993.

Fung, Y.C. "Mechanics of Soft Tissues." *Handbook of Bioengineering.* Eds. R. Skalak and S. Chien, New York: McGraw Hill, 1987.

Horowitz, P. and Hill, W. *The Art of Electronics, 2nd Ed.* Cambridge: Cambridge University Press, 1989.

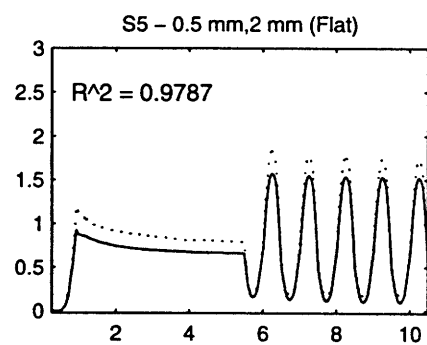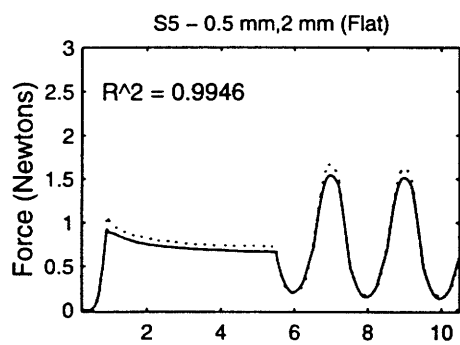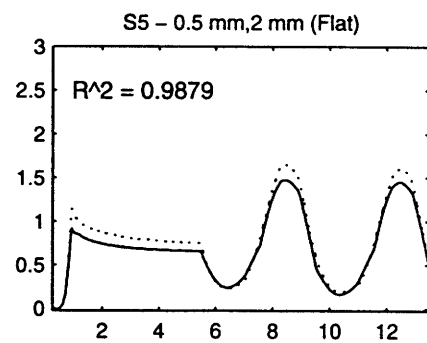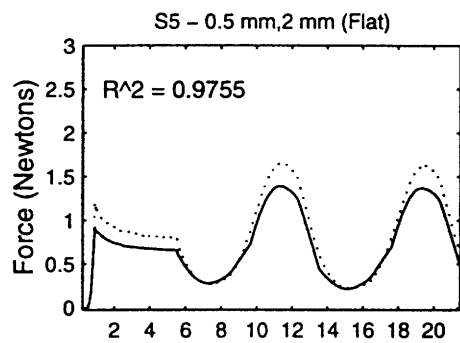Howe, R.D. "A Force-Reflecting Teleoperated Hand System for the Study of Tactile Sensing in Precision Manipulation." Int. Conf. on Robotics and Automation, 1992.

Johnson, K.O. and Hsiao, S.S. "Tactual Form and Texture Perception." *Annual Rev. Neuroscience.* 15:227-250, 1992.

McMahon, T.A. *Mucscles, Reflexes and Locomotion.* Princeton: Princeton University Press, 1984.

Moore, T.J. and Mundie, J.R. "Measurement and Specific Mechanical Impedence of the Skin: Effects of Static Force, Site of Stimulation, Area of Probe, and Presence of a Surround." *J. Acoustical Soc. of Am.* 52: 577-584, 1972.

North, J.F. and Gibson, F. "Volume Compressibility of Human Abdominal Skin." *J. Bioimechanics.* 11: 203-207, 1978.

O'Rahilly, Ronan. "Skin, Hair and Nails." *Anatomy: A Regional Study of Human Structure, 3rd Ed.* W.B. Saunders & Co.

Pereira, J.M., Mansour, J.M. and Daviss, B.R. "Analysis of Shear Wave Propogation in Skin: Application to an Experimental Procedure." *J. Biomechanics.* 23:745-751, 1990.

Pereira, J.M., Mansour, J.M. and Davis, B.R. "Dynamic Measurement of the Viscoelastic Properties of Skin." *J. Biomechanics.* 24:157-162, 1991.

Pereira, J.M., Mansour, J.M. and Davis, B.R. "The Effects of Layer Properties on Shear Disturbance Propogation in Skin." *Transations of the ASME.* 113: 30-35, 1991.

Petit, J. and Galifret, Y. "Sensory Coupling Function and the Mechanical Properties of the Skin." *Active Touch.* Ed. G. Gordon, 1978.

Phillips, J.R., and Johnson, K.O. "Tactile Spatial Resolution. II. Neural Representation of Bars, Edges, and Gratings in Monkey Primary Afferents." *J. Neurophysiology.* 46: 1192-1203, 1981.

Quillam, T.A. "The Structure of Fingerprint Skin." *Active Touch.* Ed. G. Gordon, Oxford: Pergamon, 1978.

Sacks, A.H., O'Neill, H. and Perkash, I. "Skin Blood Flow Changes and Tissue Deformations Produced by Cylindrical Indentors." *J. Rehabilitation R&D.* 22:1-6, 1985.

Srinivasan, M.A. "Surface Deformation of Primate Fingertip Under Line Load." *J. Bioimechanics.* 22: 343-349, 1989.

Srinivasan, M.A., Gulati, R.J. and Dandekar, K. "*In Vivo* Compressibility of the Human Fingertip." *Advances in Bioengineering.* 22: 573-576, 1992.

Srinivasan, M.A. and LaMotte, R.H. "Tactile Discrimination of Shape: Responses of Rapidly Adapting Mechanoreceptive Afferents to a Step Stroked Across the Monkey Fingerpad." *J. Neuroscience.* 7: 1672-1681, 1987.

Srinivasan, M.A. and Salisbury, J.K. "Human and Robot Hands: Mechanics, Sensorimotor Functions and Cognition." Proposal to ONR, 1991.

Thomine, J.M. "The Skin of the Hand." *The Hand.* Vol. 1, Ed. R. Tubiana, W.B. Saunders & Co., 1981.

Veronda, D.R. and Westmann, R.A. "Mechanical Characterization of Skin-Finite Deformations." *J. Biomechanics.* 3: 111-124, 1970.

von Gierke, H.E., Oestreicher, H.L., Franke, E.K., Parrack, H.O. and von Wittern, W.W. "Physics of Vibrations in Living Tissues." *J. App. Physiology.* 4: 886-900, 1952.